diffusion , drift , ambipolar diffusion

experiments

Diffusion

Drift

Ambipolar diffusion

$\nu \sim N v \sigma$

Úvod do fyziky plazmatu
ČSAV, Academia Praha
Francis F. Chen

DIFÚZE , DRIFT

$\nu_1 \sim N v \sigma$

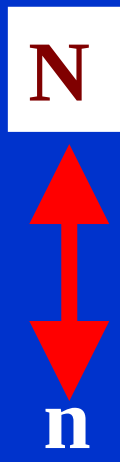

grad(**n**)

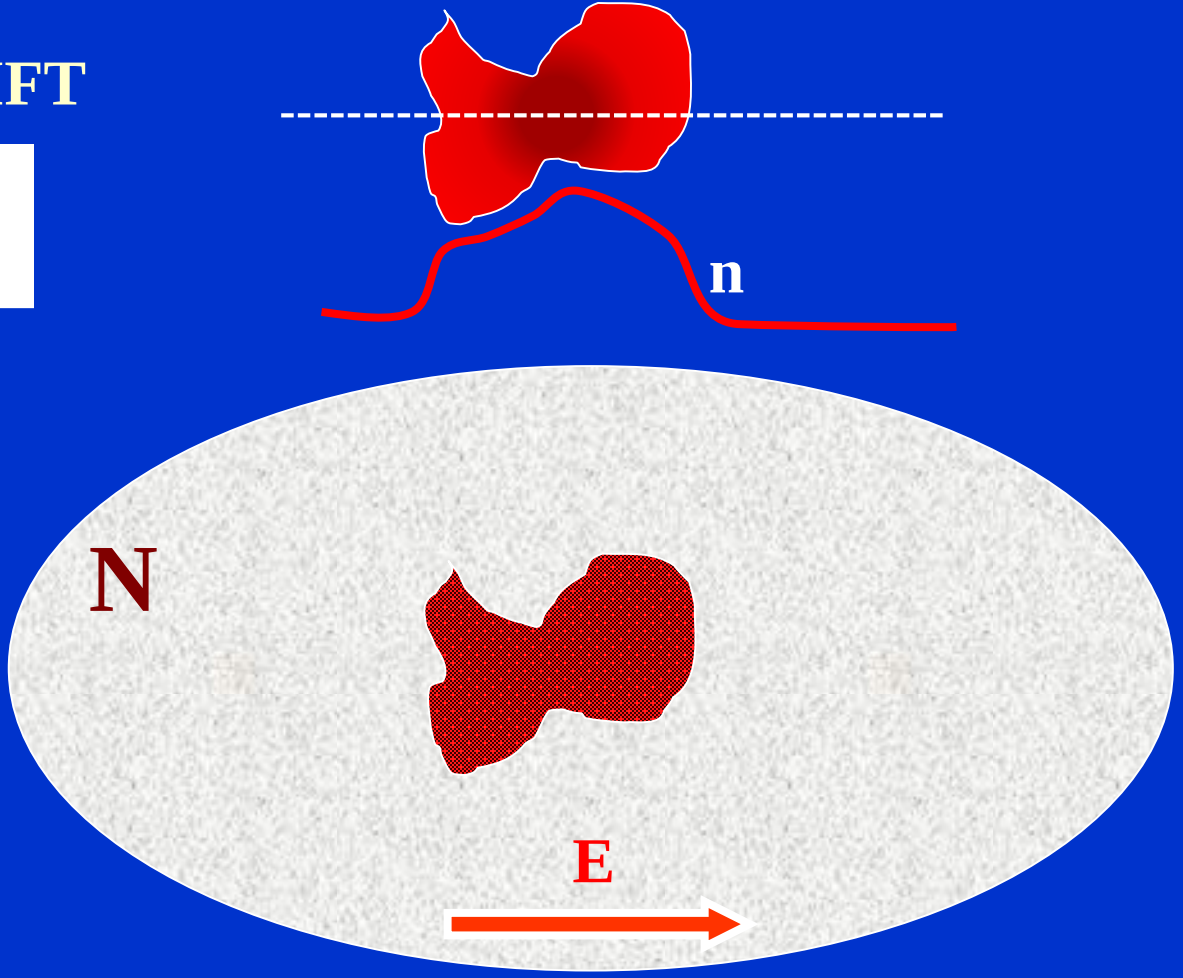

Difúze

$$\vec{v} = -D\frac{\nabla_r n}{n}$$

Drift

$$\vec{v} = \pm\mu\vec{E}$$

Drift elektronů v He, Ne, Ar…

- He, Ar

$$\vec{v} = \pm \mu \vec{E}$$

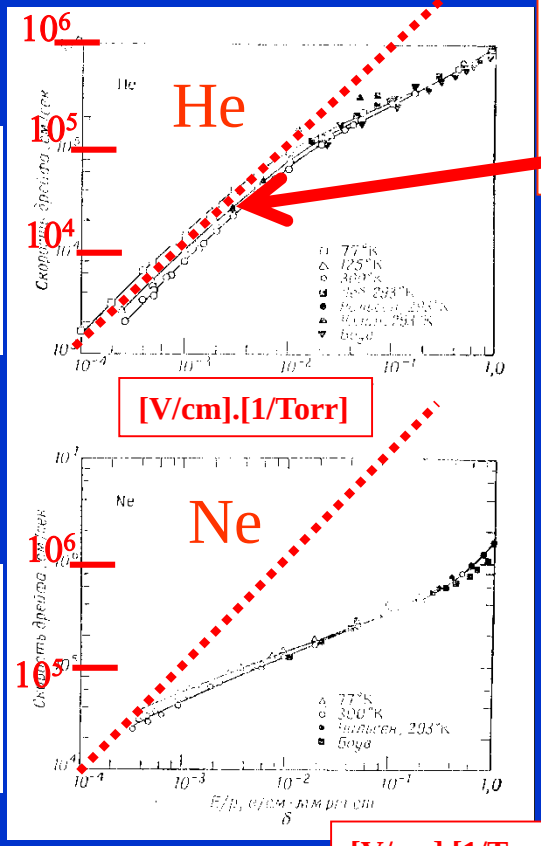

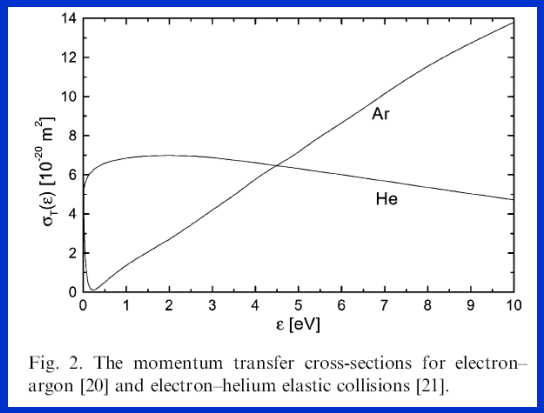

Fig. 2. The momentum transfer cross-sections for electron–argon [20] and electron–helium elastic collisions [21].

Pro daný plyn

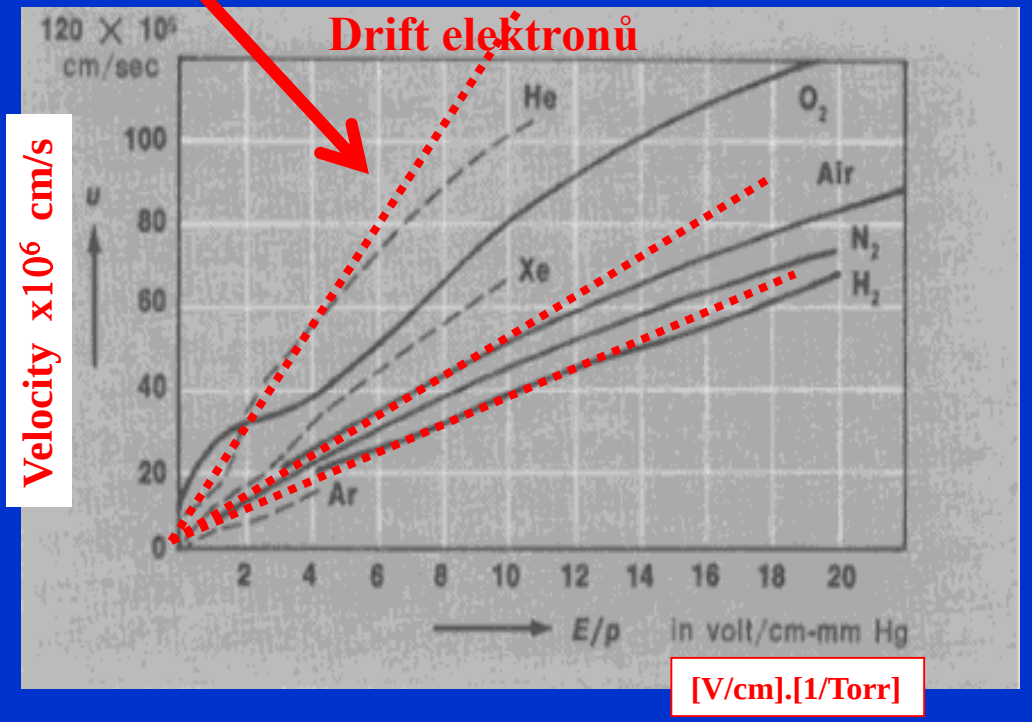

$$v = function \quad of\left(\frac{E}{p}\right)$$

$$\mu = function \quad of\left(\frac{E}{p}\right)$$

Dependence of u on the ratio E/p for different gases: (u) velocity of the directed motion of electrons under the action of the electric field E, (p) gas pressure referred to the equivalent pressure at 0° C

DIFÚZE , DRIFT

Difúze

$$\vec{\bar{v}} = -D\frac{\nabla_r n}{n}$$

Drift

$$\vec{\bar{v}} = \pm\mu\vec{E}$$

Koeficient difúze

$$D = \frac{kT}{m\nu_1}$$

$\nu \sim N v \sigma$

POHYBLIVOST

$$\mu = \frac{e}{m\nu_1}$$

DIFÚZE , DRIFT

- Difúze

$$\vec{\bar{v}} = \pm\frac{e}{m\nu_1}\vec{E} - \frac{kT}{m\nu_1}\frac{\nabla_r n}{n} = \pm\mu\vec{E} - D\frac{\nabla_r n}{n}$$

POHYBLIVOST

Koeficient difúze

pozor na závislost na v

$$\nu_1 = 2\pi N v \int_0^{\pi}(1-\cos\chi)\,\sigma(\chi, v)\sin\chi\,\mathrm{d}\chi$$

$$\mu = \frac{e}{m\nu_1}$$

$$D = \frac{kT}{m\nu_1}$$

$$\vec{\bar{v}} = \pm\mu\vec{E} - D\frac{\nabla_r n}{n}$$

Difúze

$$\vec{\bar{v}} = -D\frac{\nabla_r n}{n}$$

Drift

$$\vec{\bar{v}} = \pm\mu\vec{E}$$

$\nu \sim N v \sigma$

Einsteinův vztah

- Difúze

$$\mu = \frac{e}{m\nu_1} \qquad D = \frac{kT}{m\nu_1}$$

$$\nu_1 = 2\pi N v \int_0^{\pi} (1 - \cos\chi)\,\sigma(\chi, v)\sin\chi\,d\chi$$

$\nu \sim N v \sigma$

$$\frac{\mu}{D} = \frac{e}{kT}$$

Einsteinův vztah

Difúze

$$\vec{\bar{v}} = -D\frac{\nabla_r n}{n}$$

Fickův zákon

$$\vec{\Gamma} = -D\nabla_r n$$

Tok částic

Drift

$$\vec{\bar{v}} = \pm\mu\vec{E}$$

Závislost difúze na tlaku a na teplotě

$$D = \frac{kT}{m\nu_1}$$

$$D \sim \frac{1}{p}$$

$$\nu \sim N v \sigma$$

$$Dp \sim const. \Rightarrow Dp = D_0 p_0$$

$$D = \frac{kT}{m\nu_1} \sim \frac{kT}{mNv\sigma} \sim \frac{(kT)^2}{mkTN\sqrt{T}\sigma} \sim \frac{1}{p}$$

Drift nabitých částic v elektrickém poli

$$\vec{v} = \pm \mu \vec{E}$$

$$\mu = \frac{e}{m \nu_1}$$

$$\nu \sim N v \sigma$$

$$D \sim \frac{1}{p} \qquad \frac{\mu}{D} = \frac{e}{kT}$$

$$\mu \sim \frac{1}{p}$$

$$\mu = \text{function} \quad of\left(\frac{E}{p}\right)$$

Low E

$$\mu_0 = \mu \cdot \frac{p}{760} \cdot \frac{273}{T}$$

Vodivost

- Pohyb elektronů v elektrickém poli

$$\vec{v} = \pm \mu \vec{E}$$

$$\mu = \frac{e}{m \nu_1}$$

$$\vec{J}_e = e n_e \vec{v}_e = (e^2 n_e / \nu_1 m_e) \cdot \vec{E} = \sigma_{COND} \vec{E}$$

vodivost

$$\nu_1 \sim N v \sigma$$

$$\mu p = \mu_0 p_0$$

The reduced mobility μ_0 $m^2\ s^{-1}\ V^{-1}$ is the value at a gas number density of $2.69 \times 10^{25}\ m^{-3}$.

$$\sigma_{cond.} = \frac{e^2 n_e}{m_e \nu_{1e}}$$

vodivost

Interpretace transportní rovnice pro plazma

- Pohyb elektronů v elektrickém poli

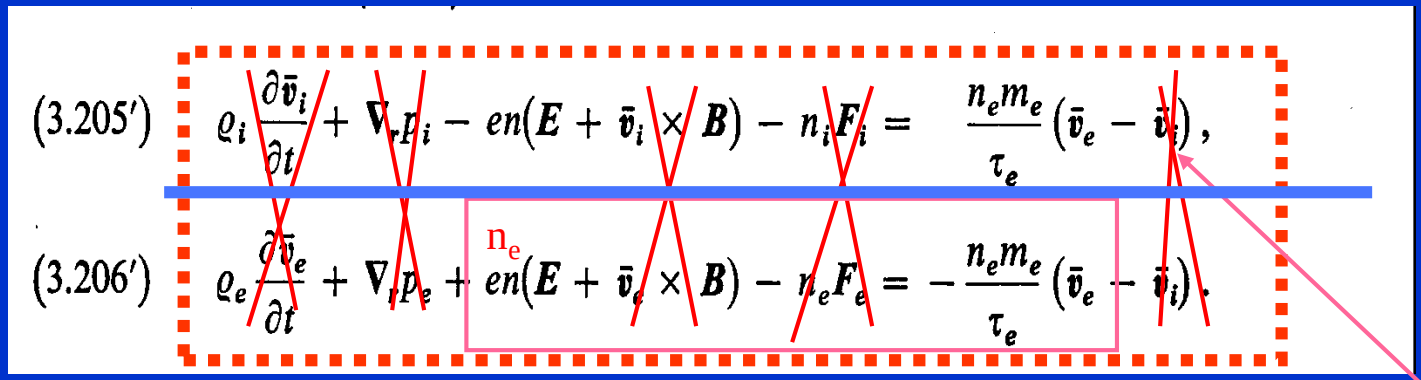

$$(3.205') \quad \varrho_i \frac{\partial \bar{v}_i}{\partial t} + \nabla_r p_i - en(E + \bar{v}_i \times B) - n_i F_i = \frac{n_e m_e}{\tau_e}(\bar{v}_e - \bar{v}_i),$$

$$(3.206') \quad \varrho_e \frac{\partial \bar{v}_e}{\partial t} + \nabla_r p_e + en(E + \bar{v}_e \times B) - n_e F_e = -\frac{n_e m_e}{\tau_e}(\bar{v}_e - \bar{v}_i).$$

n_e

$$en_eE = n_e m_e \underline{v}_e/\tau_e$$

Neglected ion velocity

Electron-ion

$$\underline{J_e} = en_e\underline{v_e} = (e^2 n_e \tau_e/m_e) \cdot \underline{E}$$

Electron/ion plasma

Electron/ion/neutral plasma

vodivost

Doležité bolo, že jedné sú ťažké a elektrony ľahké ….

Treba postupovať veľmi opatrne z hľadiska zameny iont ← → neutrálna častica

Transportní rovnice pro plazma – vodivost – zobecněný Ohmův zákon

b) Pro systém nabitých částic (plazma jako celek):

1) Rovnici kontinuity

$$\frac{\partial \varrho}{\partial t} + \nabla_r \cdot (\varrho \boldsymbol{v}_0) = 0 , \tag{3.209}$$

zákon zachování náboje

$$\frac{\partial \sigma_e}{\partial t} + \nabla_r \cdot \boldsymbol{j} = 0 . \tag{3.210}$$

2) Pohybovou rovnici (zákon zachování impulsu)

$$\varrho \frac{\partial \boldsymbol{v}_0}{\partial t} = -\nabla_r p + \boldsymbol{j} \times \boldsymbol{B} + \sum_k n_k \boldsymbol{F}_k . \tag{3.211}$$

3) Rovnici pro proudovou hustotu $\boldsymbol{j}$

$$\frac{\partial \boldsymbol{j}}{\partial t} - \frac{e^2 n_e}{m_e}(\boldsymbol{E} + \boldsymbol{v}_0 \times \boldsymbol{B}) + \frac{e}{m_e}\boldsymbol{j} \times \boldsymbol{B} - \frac{e}{m_e}\nabla_r p_e - \sum_k \frac{Z_k e}{m_k} n_k \boldsymbol{F}_k = \tag{3.212}$$

$$= \frac{Z_i e n_i}{m_i}\delta_e(m_i \overline{V}_i) - \frac{e n_e}{m_e}\delta_i(m_e \overline{V}_e) ,$$

protože podle (3.199) a (3.201) platí

$$\sum_k \frac{Z_k^2 e^2 n_k}{m_k}\bar{\boldsymbol{v}}_k = \frac{e^2}{m_e}\left[n_e \bar{\boldsymbol{v}}_e + \frac{Z_i^2 n_i m_e}{m_i}\bar{\boldsymbol{v}}_i\right] \cong \tag{3.213}$$

$$\cong \frac{e^2}{m_e}\left[-\frac{\boldsymbol{j}}{e} + \boldsymbol{v}_0 Z_i n_i\left(1 + \frac{Z_i m_e}{m_i}\right)\right] \cong \frac{e^2}{m_e}\left(n_e \boldsymbol{v}_0 - \frac{\boldsymbol{j}}{e}\right).$$

Pravou stranu (3.212) můžeme ještě dále upravit, protože (3.208) můžeme psát jako

$$n_e \delta_i(m_e \overline{V}_e) = -n_i \delta_e(m_i \overline{V}_i) = -\frac{n_e m_e}{\tau_e}(\overline{V}_e - \overline{V}_i) \cong +\frac{m_e}{\tau_e e}\boldsymbol{j} . \tag{3.214}$$

Potom ale můžeme psát, že

$$\frac{Z_i e n_i}{m_i}\delta_e(m_i \overline{V}_i) - \frac{e n_e}{m_e}\delta_i(m_e \overline{V}_e) = -\frac{e n_e}{m_e}\left(1 + \frac{Z_i m_e}{m_i}\right)\delta_i(m_e \overline{V}_e) \cong \tag{3.215}$$

$$\cong -\frac{e n_e}{m_e}\delta_i(m_e \overline{V}_e) \cong -\frac{\boldsymbol{j}}{\tau_e}$$

a rovnice pro proudovou hustotu $\boldsymbol{j}$ (zobecněný Ohmův zákon) má nyní tvar

$$\frac{\partial \boldsymbol{j}}{\partial t} - \frac{e^2 n_e}{m_e}(\boldsymbol{E} + \boldsymbol{v}_0 \times \boldsymbol{B}) + \frac{e}{m_e}\boldsymbol{j} \times \boldsymbol{B} - \frac{e}{m_e}\nabla_r p_e - \tag{3.216}$$

$$- \sum_{(k)} \frac{Z_k^2 e^2 n_k}{m_k}\boldsymbol{F}_k = -\frac{\boldsymbol{j}}{\tau_e} .$$

Zde je ovšem nutno poznamenat, že zobecněný Ohmův zákon (3.216) je použitelný pro plně ionizované plazma opět pouze v prvním přiblížení. Obecně totiž může pravá strana této rovnice záviset na magnetickém poli uvnitř plazmatu a gradientu teploty elektronů. Jestliže zanedbáme $\nabla_r T_e$, pak je pravá strana (3.216) stále ještě složena ze dvou členů; jestliže systém není daleko rovnováhy, pak přesnější tvar pravé strany rovnice (3.216) je

$$-\frac{1}{\tau_e}\left(\frac{\boldsymbol{j}_\parallel}{1{,}96} + \boldsymbol{j}_\perp\right) \tag{3.217}$$

V magnetickém poli

kde $\boldsymbol{j}_\parallel$ je složka proudové hustoty ve směru magnetického pole a $\boldsymbol{j}_\perp$ je složka proudové hustoty ve směru kolmém na magnetické pole.

Rozdíl mezi (3.217) a (3.215) resp. pravou stranou (3.216), si ukážeme názorně na příkladu. Předpokládejme stacionární stav, tj. $\partial \boldsymbol{j}/\partial t = 0$ a nechť $\boldsymbol{F}_k = 0$. Z rovnice (3.216) pak dostaneme

$$\boldsymbol{E}' = \frac{\boldsymbol{j}}{\sigma} + \frac{1}{n_e e}\boldsymbol{j} \times \boldsymbol{B} , \tag{3.218}$$

kde

$$\boldsymbol{E}' = \boldsymbol{E} + (\boldsymbol{v}_0 \times \boldsymbol{B}) + \frac{1}{n_e e}\nabla_r p_e \tag{3.219}$$

a

$$\sigma = \frac{e^2 n_e \tau_e}{m_e} \tag{3.220}$$

VODIVOST

je vodivost plazmatu. Vyjádříme-li z (3.218) $\boldsymbol{j}$, dostaneme po menších úpravách, že

$$\boldsymbol{j} = \sigma \boldsymbol{E}'_\parallel + \frac{\sigma}{1 + \omega_{ce}^2 \tau_e^2}\{\boldsymbol{E}'_\perp + \omega_{ce}\tau_e(\boldsymbol{h} \times \boldsymbol{E}')\} , \tag{3.221}$$

kde

$$\boldsymbol{h} = \frac{\boldsymbol{B}}{B} \quad \text{a} \quad \omega_{ce} = \frac{eB}{m_e} \tag{3.222}$$

je elektronová cyklotronová frekvence.

Transportní rovnice pro plazma - vodivost

a rovnice pro proudovou hustotu $\boldsymbol{j}$ (zobecněný Ohmův zákon) má nyní tvar

(3.216) $$\frac{\partial \boldsymbol{j}}{\partial t} - \frac{e^2 n_e}{m_e}(\boldsymbol{E} + \boldsymbol{v}_0 \times \boldsymbol{B}) + \frac{e}{m_e}\boldsymbol{j} \times \boldsymbol{B} - \frac{e}{m_e}\nabla_r p_e - \\ - \sum_{(k)} \frac{Z_k^2 e^2 n_k}{m_k} \boldsymbol{F}_k = -\frac{\boldsymbol{j}}{\tau_e}.$$

Zde je ovšem nutno poznamenat, že zobecněný Ohmův zákon (3.216) je použitelný pro plně ionizované plazma opět pouze v prvním přiblížení. Obecně totiž může pravá strana této rovnice záviset na magnetickém poli uvnitř plazmatu a gradientu teploty elektronů. Jestliže zanedbáme $\nabla_r T_e$, pak je pravá strana (3.216) stále ještě složena ze dvou členů; jestliže systém není daleko rovnováhy, pak přesnější tvar pravé strany rovnice (3.216) je

(3.217) $$-\frac{1}{\tau_e}\left(\frac{\boldsymbol{j}_\parallel}{1{,}96} + \boldsymbol{j}_\perp\right),$$

kde $\boldsymbol{j}_\parallel$ je složka proudové hustoty ve směru magnetického pole a $\boldsymbol{j}_\perp$ je složka proudové hustoty ve směru kolmém na magnetické pole.

Rozdíl mezi (3.217) a (3.215) resp. pravou stranou (3.216), si ukážeme názorně na příkladu. Předpokládejme stacionární stav, tj. $\partial \boldsymbol{j}/\partial t = 0$ a nechť $\boldsymbol{F}_k = 0$. Z rovnice (3.216) pak dostaneme

(3.218) $$\boldsymbol{E}' = \frac{\boldsymbol{j}}{\sigma} + \frac{1}{n_e e}\boldsymbol{j} \times \boldsymbol{B},$$

kde

(3.219) $$\boldsymbol{E}' = \boldsymbol{E} + (\boldsymbol{v}_0 \times \boldsymbol{B}) + \frac{1}{n_e e}\nabla_r p_e$$

a

(3.220) $$\sigma = \frac{e^2 n_e \tau_e}{m_e}$$

je vodivost plazmatu. Vyjádříme-li z (3.218) $\boldsymbol{j}$, dostaneme po jistých úpravách, že

(3.221) $$\boldsymbol{j} = \sigma \boldsymbol{E}'_\parallel + \frac{\sigma}{1 + \omega_{ce}^2 \tau_e^2}\{\boldsymbol{E}'_\perp + \omega_{ce}\tau_e(\boldsymbol{h} \times \boldsymbol{E}')\},$$

kde

(3.222) $$\boldsymbol{h} = \frac{\boldsymbol{B}}{B} \quad \text{a} \quad \omega_{ce} = \frac{eB}{m_e}$$

je elektronová cyklotronová frekvence.

$$\sigma = \frac{e^2 n_e \tau_e}{m_e}$$

vodivost

$$\omega_{ce} = \frac{eB}{m_e}$$

cyklotronová frekvence

Jestliže nyní použijeme na pravé straně (3.216) výrazu (3.217), dostaneme, že

(3.223) $$\boldsymbol{E}' = \frac{\boldsymbol{j}_\parallel}{\sigma_\parallel} + \frac{\boldsymbol{j}_\perp}{\sigma_\perp} + \frac{1}{n_e e}(\boldsymbol{j} \times \boldsymbol{B}),$$

kde

(3.224) $$\sigma_\parallel = 1{,}96\sigma \quad \text{a} \quad \sigma_\perp = \sigma;$$

vyloučením $\boldsymbol{j}$ pak dostaneme

(3.225) $$\boldsymbol{j} = \sigma_\parallel \boldsymbol{E}'_\parallel + \frac{\sigma_\perp}{1 + \omega_{ce}^2 \tau_e^2}\{\boldsymbol{E}'_\perp + \omega_{ce}\tau_e(\boldsymbol{h} \times \boldsymbol{E}')\}.$$

Odtud již vidíme, že i v tak jednoduchém případě, kdy $\nabla_r T_e = 0$ a systém je blízko rovnováhy, je vodivost plazmatu závislá na směru magnetického pole.

V obecném případě má vodivost plazmatu tenzorový charakter.*)

Vodivost a ani netušíme EEDF..? Je to vobec možné…? A čo σ(v) ??

Ja tomu neverí, …. Ale tie podmienky sú asi iné než plazma v našej leborke….

A čo σ(v) ??

$$\omega_{ce} = \frac{eB}{m_e}$$

cyklotronová frekvence

$$\sigma = \frac{e^2 n_e \tau_e}{m_e}$$

vodivost

Srážky a cyklotronová frekvence

$$(3.208)\quad n_e\,\delta_i(m_e\bar{V}_e) = -\,n_i\,\delta_e(m_i\bar{V}_i) = \frac{n_e m_e}{\tau_e}(\bar{V}_e - \bar{V}_i) = -\frac{n_e m_e}{\tau_e}(\bar{v}_e - \bar{v}_i)\,,$$

kde τ_e je střední doba mezi srážkami mezi elektrony a ionty resp. mezi částicemi různých druhů; $\tau_e^{-1} = \nu$ je pak srážková frekvence.

Jestliže nyní použijeme na pravé straně (3.216) výrazu (3.217), dostaneme, že

$$(3.223)\quad E' = \frac{j_\parallel}{\sigma_\parallel} + \frac{j_\perp}{\sigma_\perp} + \frac{1}{n_e e}(j \times B)\,,$$

kde

$$(3.224)\quad \sigma_\parallel = 1{,}96\sigma \quad \text{a} \quad \sigma_\perp = \sigma\,;$$

vyloučením j pak dostaneme

$$(3.225)\quad j = \sigma_\parallel E'_\parallel + \frac{\sigma_\perp}{1 + \omega_{ce}^2\tau_e^2}\{E'_\perp + \omega_{ce}\tau_e(h \times E')\}\,.$$

Odtud již vidíme, že i v tak jednoduchém případě, kdy $\nabla T_e = 0$ a systém je blízko rovnováhy, je vodivost plazmatu závislá na směru magnetického pole.

V obecném případě má vodivost plazmatu tenzorový charakter.*)

rovnice pro DRIFT

$$\vec{\bar{v}} = -\frac{e}{m\nu_1}\vec{E} = \mu\vec{E}$$

$$\nu_1 = 2\pi N v \int_0^\pi (1 - \cos\chi)\,\sigma(\chi, v)\sin\chi\,d\chi$$

Treba postupovať veľmi opatrne
z hľadiska zameny iont ← → neutrálna častica

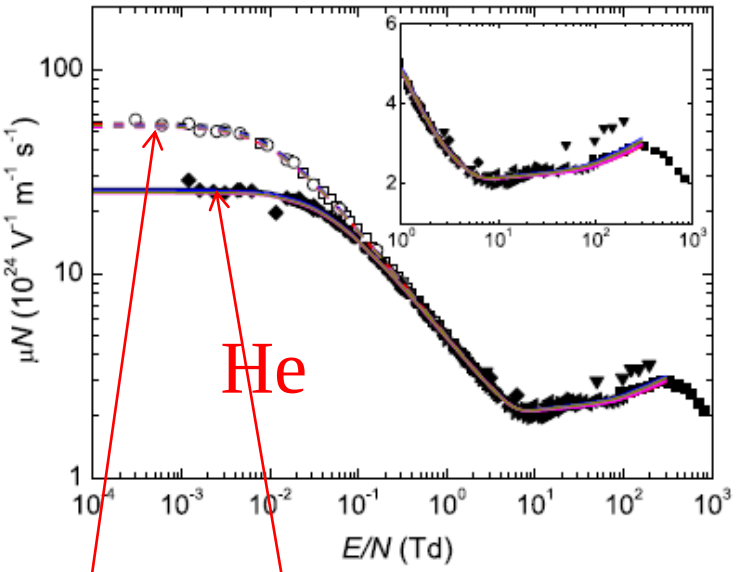

Figure 9. Reduced mobility in helium, as a function of the reduced electric field. The lines are calculations at $T_g = 300$ K (solid) and 77 K (dashed), obtained using a two-term Boltzmann solver with the cross sections from the following databases: BIAGI-v8.9 (——), BIAGI-v7.1 (——), IST-LISBON (——), MORGAN (——), PHELPS (——). The points are measurements from the following authors: Stern (1963) (■), Crompton *et al* (1967) (293 K, ●), Milloy and Crompton (1977) (293 K, ▲), Kücükarpaci *et al* (1981) (▼), Pack *et al* (1992) (300 K, ♦), Dall'Armi *et al* (1992) (◄), Šašić *et al* (2005) (►), Crompton *et al* (1970) (77 K, □), Pack *et al* (1992) (77 K, ○). The inset is a zoom in the 1–1000 Td region.

The reduced mobility μ_0 $m^2\ s^{-1}\ V^{-1}$ is the value at a gas number density of $2.69 \times 10^{25}\ m^{-3}$.

elektrony

$$\mu p = \mu_0 p_0$$

Drift

$$\vec{v} = \pm \mu \vec{E}$$

?

Loschmidovo číslo ~2,687x10^{19}cm^{-3}

at 1 Torr … N=3.53 10^{-16}cm^{-3}

$$1\ \mathrm{Td} = 10^{-21}\ \mathrm{V \cdot m^2} = 10^{-17}\ \mathrm{V \cdot cm^2}.$$

Energia elektronů

- Energia, rychlost, Einsteinův vztah

$$1\,\mathrm{Td} = 10^{-21}\,\mathrm{V}\cdot\mathrm{m}^2 = 10^{-17}\,\mathrm{V}\cdot\mathrm{cm}^2.$$

$$D = \frac{1}{3}\left(\frac{\overline{\nu^2}}{\nu_1}\right)$$

$$\mu = \frac{e}{m\nu_1}$$

$$\frac{D}{\mu} = \frac{m}{3}\left(\frac{\overline{\nu^2}}{e}\right) = \frac{2\bar{\varepsilon}}{3e} \sim \frac{kT}{e}$$

$$\frac{D}{\mu} = \frac{kT}{e}$$

která je to T

limita

At 300K ➔kT~.025eV

elektrony

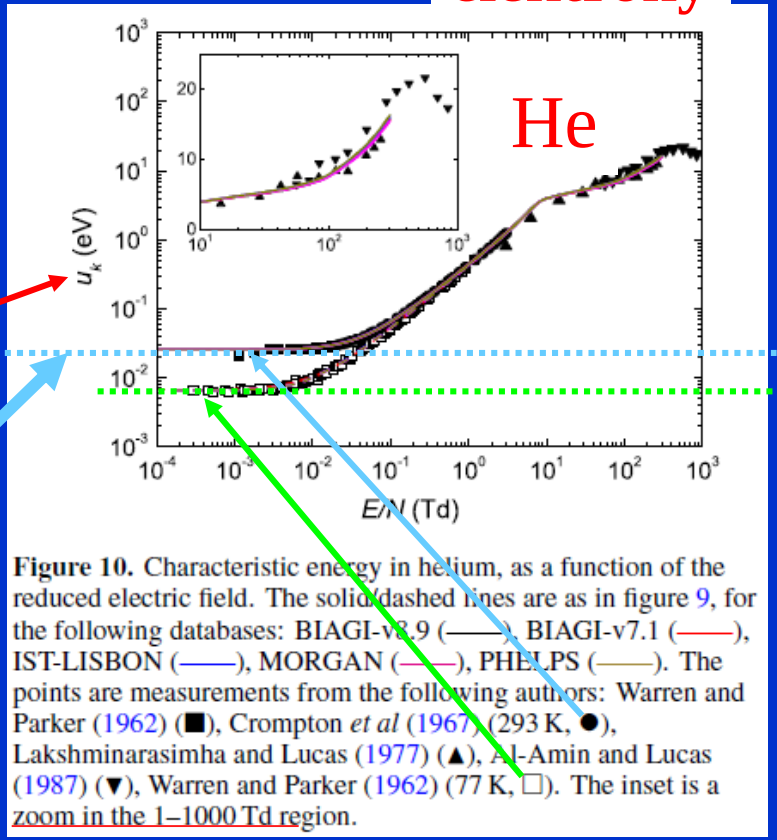

Figure 10. Characteristic energy in helium, as a function of the reduced electric field. The solid/dashed lines are as in figure 9, for the following databases: BIAGI-v8.9 (——), BIAGI-v7.1 (——), IST-LISBON (——), MORGAN (——), PHELPS (——). The points are measurements from the following authors: Warren and Parker (1962) (■), Crompton *et al* (1967) (293 K, ●), Lakshminarasimha and Lucas (1977) (▲), Al-Amin and Lucas (1987) (▼), Warren and Parker (1962) (77 K, □). The inset is a zoom in the 1–1000 Td region.

elektrony

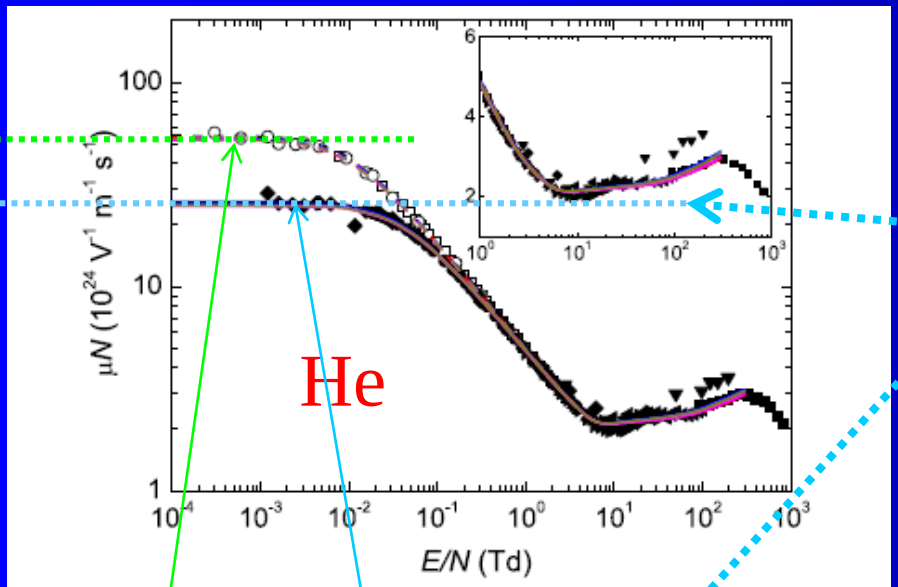

Figure 9. Reduced mobility in helium, as a function of the reduced electric field. The lines are calculations at $T_g = 300$ K (solid) and 77 K (dashed), obtained using a two-term Boltzmann solver with the cross sections from the following databases: BIAGI-v8.9 (——), BIAGI-v7.1 (——), IST-LISBON (——), MORGAN (——), PHELPS (——). The points are measurements from the following authors: Stern (1963) (■), Crompton *et al* (1967) (293 K, ●), Milloy and Crompton (1977) (293 K, ▲), Kücükarpaci *et al* (1981) (▼), Pack *et al* (1992) (300 K, ♦), Dall'Armi *et al* (1992) (◄), Šašić *et al* (2005) (►), Crompton *et al* (1970) (77 K, □), Pack *et al* (1992) (77 K, ○). The inset is a zoom in the 1–1000 Td region.

300 K

Drift

?

$$\vec{v} = \pm \mu \vec{E}$$

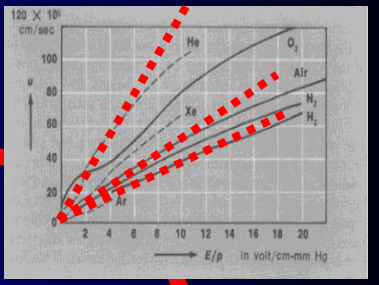

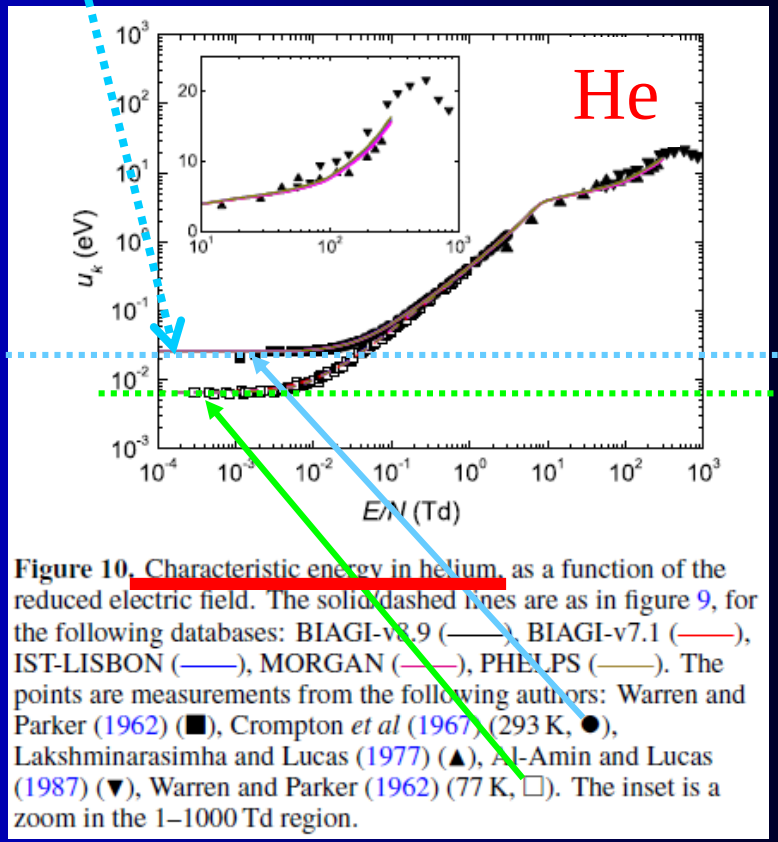

Figure 10. Characteristic energy in helium, as a function of the reduced electric field. The solid/dashed lines are as in figure 9, for the following databases: BIAGI-v8.9 (——), BIAGI-v7.1 (——), IST-LISBON (——), MORGAN (——), PHELPS (——). The points are measurements from the following authors: Warren and Parker (1962) (■), Crompton *et al* (1967) (293 K, ●), Lakshminarasimha and Lucas (1977) (▲), Al-Amin and Lucas (1987) (▼), Warren and Parker (1962) (77 K, □). The inset is a zoom in the 1–1000 Td region.

Energia elektronů

$$1\,\mathrm{Td} = 10^{-21}\,\mathrm{V}\cdot\mathrm{m}^2 = 10^{-17}\,\mathrm{V}\cdot\mathrm{cm}^2.$$

$$D = \frac{1}{3}\left(\frac{\overline{\nu^2}}{\nu_1}\right)$$

$$\mu = \frac{e}{m\nu_1}$$

$$\frac{D}{\mu} = \frac{m}{3}\left(\frac{\overline{\nu^2}}{e}\right) = \frac{2\bar{\varepsilon}}{3e} \sim \frac{kT}{e}$$

která je to T

elektrony

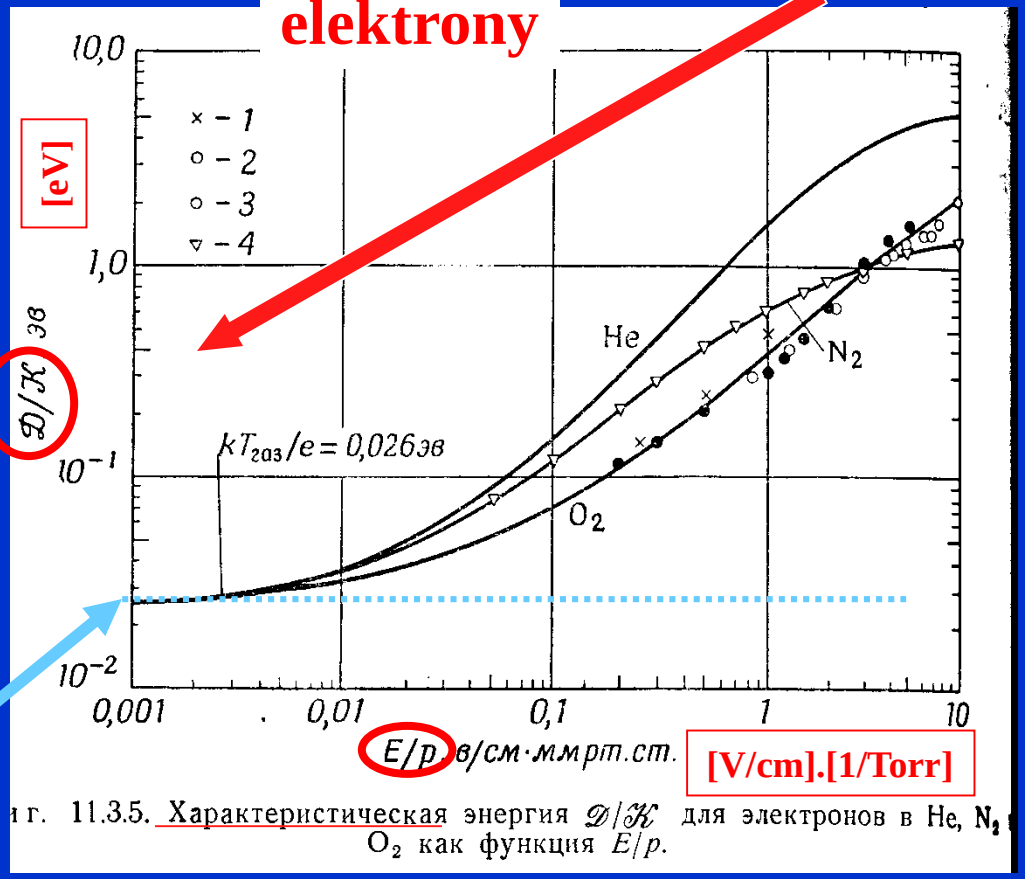

г. 11.3.5. Характеристическая энергия $\mathscr{D}/\mathscr{K}$ для электронов в He, N_2, O_2 как функция E/p.

$$\frac{D}{\mu} = \frac{kT}{e}$$

která je to T

limita

At 300K ➔kT~.025eV

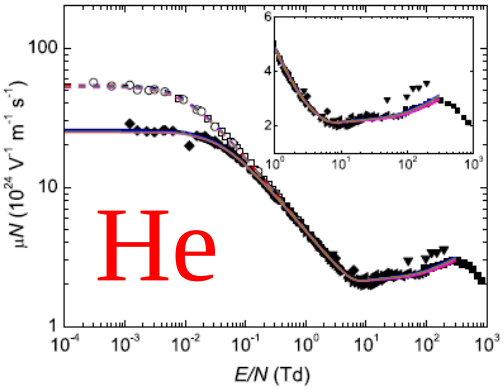

Figure 9. Reduced mobility in helium, as a function of the reduced electric field. The lines are calculations at $T_g = 300$ K (solid) and 77 K (dashed), obtained using a two-term Boltzmann solver with the cross sections from the following databases: BIAGI-v8.9 (——), BIAGI-v7.1 (——), IST-LISBON (——), MORGAN (——), PHELPS (——). The points are measurements from the following authors: Stern (1963) (■), Crompton *et al* (1967) (293 K, ●), Milloy and Crompton (1977) (293 K, ▲), Kücükarpaci *et al* (1981) (▼), Pack *et al* (1992) (300 K, ◆), Dall'Armi *et al* (1992) (◄), Šašić *et al* (2005) (►), Crompton *et al* (1970) (77 K, □), Pack *et al* (1992) (77 K, ◯). The inset is a zoom in the 1–1000 Td region.

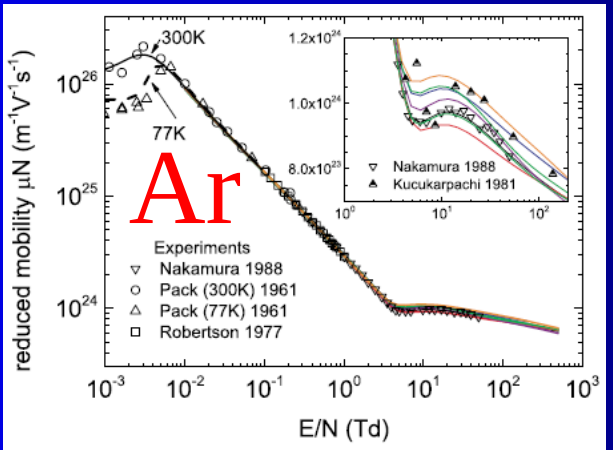

Figure 5. Reduced electron mobility versus E/N. The symbols are experimental data and the solid lines are calculations using the two-term Boltzmann solver, BOLSIG+. The inset is a zoom to illustrate the differences in the calculated results in the region of the knee at $E/N \sim 5$ Td. The colour code is BIAGI-v8.9 (——); BSR (——); HAYASHI (——); IST-LISBON (——); MORGAN (——); PHELPS (——); PUECH (——). The legend refers to the first author and year of publication of references reporting measurements shown in the figure.

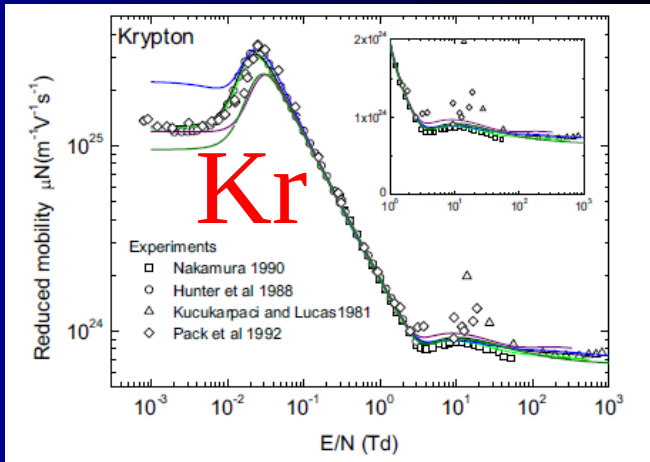

Figure 7. Measured and calculated reduced electron mobility versus E/N in krypton. The symbols are experimental data referenced in the table 5 and the solid lines are calculations using a two-term Boltzmann solver. The inset is a zoom to illustrate the differences in the results in the 1 to 1000 Td region. The color code is: BIAGI-v8.9 (——); BIAGI-v7.1 (——); BSR+ (——); SIGLO (——); MORGAN (——).

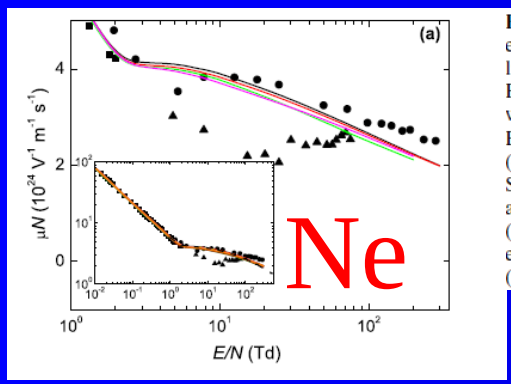

Figure 13. Reduced mobility in neon, as a function of the reduced electric field in the most relevant region of $E/N = 1$–500 Td. The lines are calculations at $T_g = 300$ K, obtained using a two-term Boltzmann solver (solid lines) or Monte Carlo simulations (dashed with the cross sections from the following databases: (a) BIAGI-v8.9 (——), BIAGI-v7.1 (——), BSR (——), MORGAN (——); (b) BIAGI-v8.9 (——), PHELPS (——), PUECH (——), SIGLO (——). The points are measurements from the following authors: Robertson (1972) (293 K, ■), Kücükarpaci *et al* (1981) (●), Dall'Armi *et al* (1992) (▲). The inset in (*a*) is a plot over the entire E/N region analysed here. The BIAGI-v8.9 results (Boltzmann) are repeated in (*a*) and (*b*) for comparison purposes.

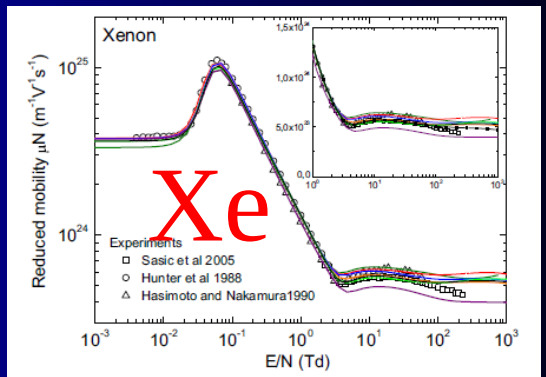

Figure 8. Measured and calculated reduced electron mobility versus E/N in xenon. The symbols are experimental data referenced in the text (table 5) and the solid lines are calculations using a two-term Boltzmann solver. The inset is a zoom to illustrate the differences in the results in the [1–1000 Td] E/N region for which PT calculations with BIAGI-v8.9 (-■-) are added. The color code is: BIAGI-v8.9 (——); BIAGI-v7.1 (——); BSR+ (——); HAYASHI (——); SIGLO (——); MORGAN (——); PUECH (——).

$$\nu_1 = 2\pi N v \int_0^{\pi} (1 - \cos\chi)\, \sigma(\chi, v) \sin\chi \, d\chi$$

$$\vec{\bar{v}} = -\frac{e}{m\nu_1}\vec{E} = \mu\vec{E}$$

$$\vec{\bar{v}} = -\frac{4\pi}{3}\frac{e}{nm}\vec{E}\int \frac{v^3}{\nu_1}\frac{\partial f_0}{\partial v}dv = \vec{E}\left(-\frac{4\pi}{3}\frac{e}{nm}\int \frac{v^3}{\nu_1}\frac{\partial f_0}{\partial v}dv\right)$$

$$\mu_1 = f\left(\frac{E}{\nu_1}\right) = f\left(\frac{E}{N}\right)$$

Electron swarm experiments in dense rare gases: a review.

A. F. Borghesani*

elektrony

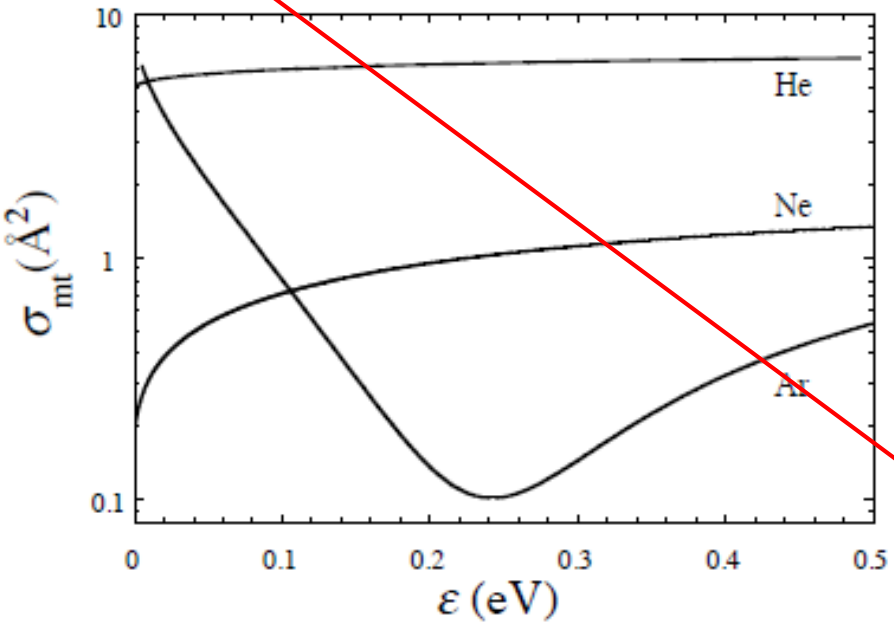

FIG. 2. σ_{mt} vs ϵ for He [16], Ne [17], and Ar [18].

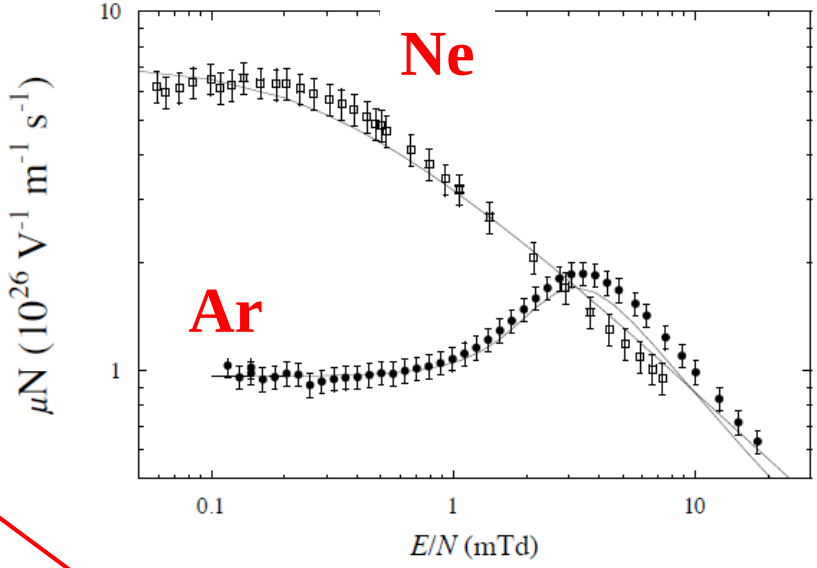

FIG. 4. μN vs E/N at high density. Squares: Neon at $T = 46.5\,\mathrm{K}$ and $N = 1.89\,\mathrm{nm}^{-3}$ [7]. Circles: Argon at $T = 152.15\,\mathrm{K}$ and $N = 5.14\,\mathrm{nm}^{-3}$ [8]. Lines: heuristic model.

Classical kinetic theory

Electron swarm experiments in dense rare gases: a review.

A. F. Borghesani*

elektrony

Ar

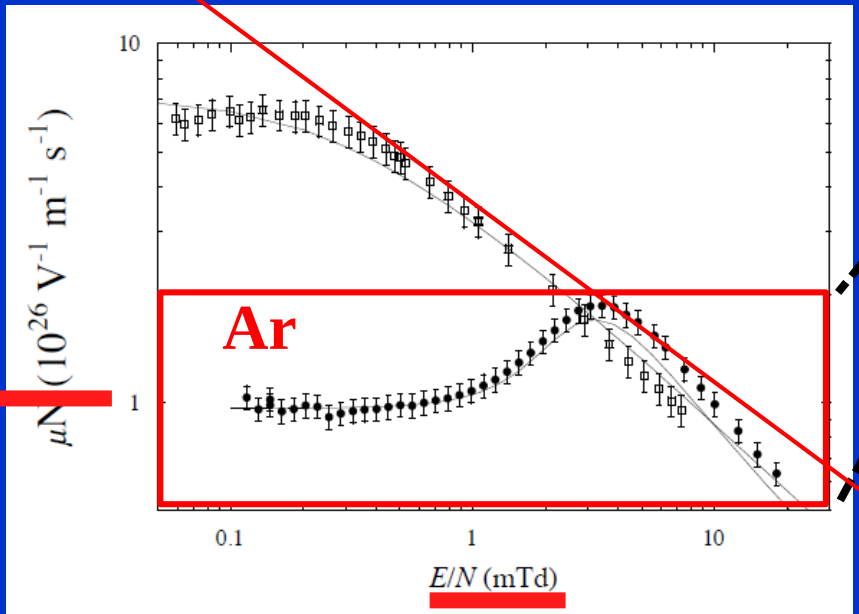

FIG. 4. μN vs E/N at high density. Squares: Neon at $T = 46.5\,\mathrm{K}$ and $N = 1.89\,\mathrm{nm}^{-3}$ [7]. Circles: Argon at $T = 152.15\,\mathrm{K}$ and $N = 5.14\,\mathrm{nm}^{-3}$ [8]. Lines: heuristic model.

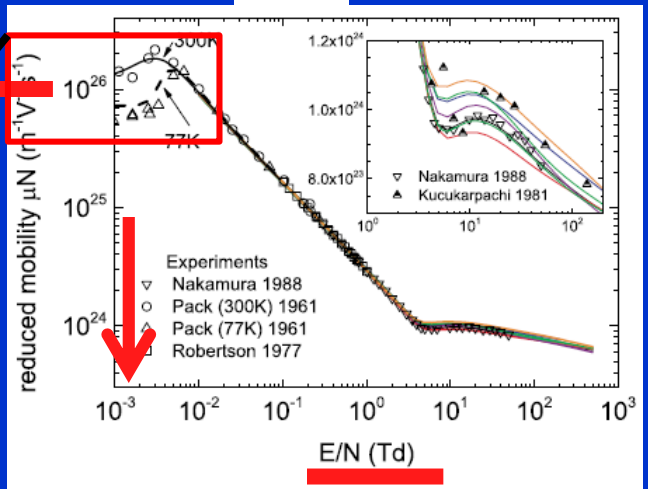

Figure 5. Reduced electron mobility versus E/N. The symbols are experimental data and the solid lines are calculations using the two-term Boltzmann solver, BOLSIG+. The inset is a zoom to illustrate the differences in the calculated results in the region of the knee at $E/N \sim 5\,\mathrm{Td}$. The colour code is BIAGI-v8.9 (——); BSR (——); HAYASHI (——); IST-LISBON (——); MORGAN (——); PHELPS (——); PUECH (——). The legend refers to the first author and year of publication of references reporting measurements shown in the figure.

Classical kinetic theory

Electron swarm experiments in dense rare gases: a review.

A. F. Borghesani*

elektrony

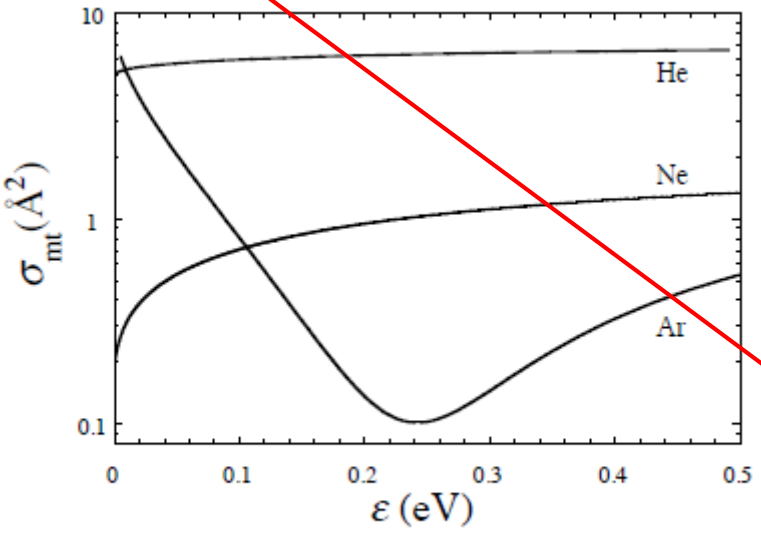

FIG. 2. σ_{mt} vs ϵ for He [16], Ne [17], and Ar [18].

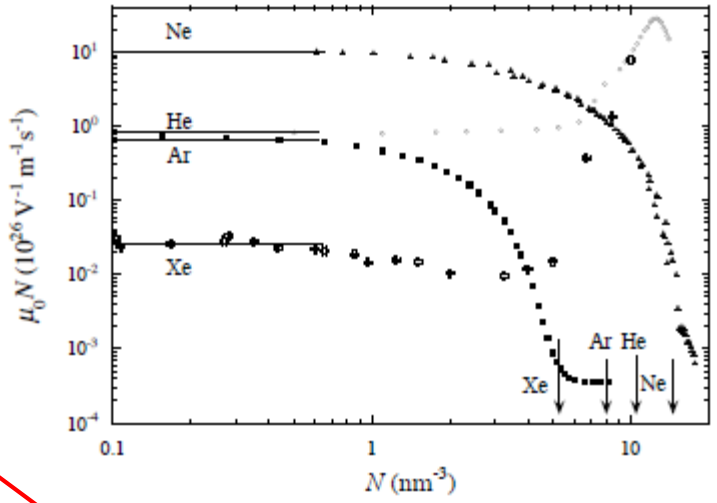

FIG. 1. $\mu_0 N$ vs N. Triangles: Ne at $T = 45$ K [7]. Circles: Ar at $T = 152.2$ K [8]. Squares: He at $T = 26$ K [9]. Crosses: Xe at SVP [10]. Solid lines: prediction of cKT. Arrows: critical densities.

Classical kinetic theory

Trochu teorie

Řešení B. rovnice

$$\frac{\partial f_i}{\partial t} + \vec{v}_i \cdot \nabla_r f_i + \frac{\vec{F}_i}{m_i} \cdot \nabla_{v_i} f_i = \frac{\delta f_i}{\delta t}$$

$$f(\vec{v}, \vec{r}, t)$$

$$f(\vec{v}, \vec{r}, t) = f_0(v, \vec{r}, t) + \frac{\vec{v}}{v} \cdot \vec{f}_1(v, \vec{r}, t)$$

Řešení B. rovnice

- Malý a Velký Kracík.

Lorentzovské přiblížení pro dvousložkový systém tvořený jednak neutrálními částicemi a jednak částicemi, které mají elektrický náboj….

$$\frac{\partial f_i}{\partial t} + \vec{v}_i \cdot \nabla_r f_i + \frac{\vec{F}_i}{m_i} \cdot \nabla_{v_i} f_i = \frac{\delta f_i}{\delta t}$$

Závislost na rychlosti

Hledáme řešení ve tvaru

$$f(\vec{v},\vec{r},t) = f_0(v,\vec{r},t) + \frac{\vec{v}}{v} \cdot \vec{f}_1(v,\vec{r},t)$$

aby jsme vyjádřili toky částic

$$\frac{\partial\left(f_0(v,\vec{r},t) + \frac{\vec{v}}{v} \cdot \vec{f}_1(v,\vec{r},t)_i\right)}{\partial t} + \vec{v}_i \cdot \nabla_r \left(f_0(v,\vec{r},t) + \frac{\vec{v}}{v} \cdot \vec{f}_1(v,\vec{r},t)\right) + \frac{\vec{F}_i}{m_i} \cdot \nabla_{v_i} \left(f_0(v,\vec{r},t) + \frac{\vec{v}}{v} \cdot \vec{f}_1(v,\vec{r},t)\right) = \frac{\delta f_i}{\delta t}$$

Řešení B. rozklad do dvou rovnic

- Velký Kracík
- Rovnice (A) a (B)

(5.14) $$\nu_1 = 2\pi N v \int_0^\pi (1 - \cos\chi)\,\sigma(\chi, v)\sin\chi\,d\chi$$

Držíme se Velkého Kracíka proto:

$$f(\vec{v},\vec{r},t) = f_0(v,\vec{r},t) + \vec{v}\cdot\vec{f}_1(v,\vec{r},t)$$

Veličinu $\nu_l(v)$ definovanou rovnicí (5.11) resp. (5.12) můžeme interpretovat jako relaxační frekvenci l-tého řádu pro různé anisotropie plynu lehkých částic. Speciálně

(5.14) $$\nu_1 = 2\pi N v \int_0^\pi (1 - \cos\chi)\,\sigma(\chi, v)\sin\chi\,d\chi$$

N

$$\Gamma = \frac{Ze}{m}E, \quad \omega_c = -\frac{Ze}{m}B,$$

(5.95) $$\mathbf{f}_{(k)} = 0 \quad \text{pro} \quad k \geqq 2,$$

redukuje se rozklad (5.55) resp. (5.55′) na

(5.96) $$f(v, r, t) = f_0(v, r, t) + v\,.\,f_1(v, r, t)$$

a rovnice pro funkce f_0 a f_1 mají tvar

(5.97′) $$\frac{\partial f_0}{\partial t} + \frac{v^2}{3}\nabla_r\,.\,f_1 + \frac{1}{3v^2}\frac{\partial}{\partial v}(v^3\Gamma\,.\,f_1) = J_{\text{I.L.}}(f_0),$$

nebo rozepíšeme-li pravou stranu podle (5.40)

(5.97) $$\frac{\partial f_0}{\partial t} + \frac{v^2}{3}\nabla_r\,.\,f_1 + \frac{1}{3v^2}\frac{\partial}{\partial v}(v^3\Gamma\,.\,f_1) = \frac{1}{2v^2}\frac{\partial}{\partial v}\left[\frac{2m}{M}\nu_1 v^3\left(f_0 + \frac{2kT}{m}\frac{\partial f_0}{\partial(v^2)}\right)\right]$$

A

a

(5.98) $$\frac{\partial f_1}{\partial t} + \nabla_r f_0 + \frac{\Gamma}{v}\frac{\partial f_0}{\partial v} - (\omega_c \times f_1) = -\nu_1 f_1\,.$$

B

interpretace

(5.131) $$f_0 = C \exp\left\{ - \int \frac{v\,dv}{\frac{kT}{m} + \frac{\mathscr{G}(v_1)}{3\gamma v_1^2}} \right\},$$

a) Nechť vnější elektrické pole je nulové, tj. $\Gamma = 0$. Potom

(5.133) $$\mathscr{G}(v_1) = 0$$

B může byt nenulové

a pro $f_0(v)$ máme Maxwellovu rozdělovací funkci

(5.134) $$f_0 = C \exp\left(- \frac{mv^2}{2kT} \right),$$

kde

(5.135) $$C = n \left(\frac{m}{2\pi kT} \right)^{3/2}.$$

b) Nechť vnější magnetické pole je nulové, tj. $\omega_c = 0$. Potom

(5.136) $$\mathscr{G}(v_1) = \Gamma^2$$

a (5.131) můžeme upravit na tvar

(5.137) $$f_0 = C \exp\left\{ - \int \frac{m}{kT} \left(\frac{v v_1^2}{v_1^2 + \left(\frac{\Gamma^2 m}{3\gamma kT} \right)} \right) dv \right\}.$$

Bude-li nyní srážková frekvence v_1 nezávislá na rychlosti, tj.

(5.138) $$v_1 = v = \text{konst},$$

pak f_0 bude opět maxwellovské rozdělení

(5.139) $$f_0 = C \exp\left[- \frac{mv^2}{2k\left(T + \frac{\Gamma^2 m}{3\gamma k} v^{-2} \right)} \right] = C \exp\left(- \frac{mv^2}{2kT^*} \right)$$

ale s teplotou

(5.140) $$T^* = T + \frac{m}{3\gamma k} \left(\frac{\Gamma}{v} \right)^2 = T + \frac{M}{3k} \left(\frac{ZeE}{mv} \right)^2.$$

To ale znamená, že při $v_1 = \text{konst}$ je kinetická teplota lehkých nabitých částic (elektronů) vyšší ve srovnání s teplotou neutrálních částic.

Předpoklad, že srážková frekvence elektronů s neutrálními částicemi je konstantní, nezávislá na rychlosti, je příliš ostrý. V obecném případě totiž platí, že v_1 na rychlosti elektronů závisí. Předpokládejme, že

(5.141) $$v_1(v) = Av^l,$$

kde l je libovolné číslo*) a A je konstanta (pro $l = 1$ máme

(5.141′) $$v_1 = Av$$

a tedy $A^{-1} = \lambda$, kde λ je střední volná dráha elektronů).

Rovnice pro f_0 (5.137) má nyní tvar

(5.142) $$f_0 = C \exp\left\{ - \int \frac{m}{kT} \frac{v^{2l+1}}{v^{2l} + \frac{\Gamma^2 m}{3\gamma A^2 kT}} dv \right\}.$$

Pro $l = 1$, tj. případ modelu dokonale pružných koulí (viz kapitolu 2), kdy

(5.143) $$v_1 = Av,$$

je integrál v (5.142) snadno spočitatelný a f_0 má tvar

(5.144′) $$f_0 = C \left[1 + \frac{3A^2}{\Gamma^2} \frac{kT}{m} v^2 \right]^{(m\Gamma/AkT)^2 \cdot (1/6\gamma)} \cdot \exp\left(- \frac{mv^2}{2kT} \right).$$

Po kratších úpravách pak dostaneme

(5.144) $$f_0 = C \left[v^2 + \frac{M}{3} \left(\frac{ZeE}{mA} \right)^2 \frac{1}{kT} \right]^{(mM/6k^2T^2) \cdot (ZeE/mA)^2} \cdot \exp\left(- \frac{mv^2}{2kT} \right),$$

což je rozdělovací funkce, kterou jako první odvodil Davydov.**) Pro silné elektrické pole, kdy

(5.145) $$\frac{\Gamma^2 m}{3\gamma AkT} = \frac{M}{3kT} \left(\frac{ZeE}{mA} \right)^2 \gg v^2,$$

přechází Davydovova rozdělovací funkce na známou rozdělovací funkci Druyvesteyna (o tom je možno se přesvědčit z (5.142), kde položíme $l = 1$ a provedeme příslušné zanedbání), která má tvar

(5.146) $$f_0 = C \exp\left(- \frac{3}{4} \gamma \left(\frac{A}{\Gamma} \right)^2 v^4 \right) = C \exp\left[- \frac{3}{4} \frac{m}{M} \left(\frac{mA}{ZeE} \right)^2 v^4 \right].$$

*) Závislost (5.141) pro $l = 0$ vystihuje s dobrou přesností srážky elektronů s atomy He a H_2, pro $l = 1$ pak srážky v Ne a dále pro $l = 3$, 3,5 a 4 pak srážky pomalých elektronů v Ar, Kr a Xe; viz D. Darbiere: Phys. Rev. *84* (1951), 653; S. C. Brown: Handbuch der Physik, ed. S. Flüge, Vol. 22 (Berlin 1956), 531; G. L. Braglia: Phys. Lett. *17* (1965), 260.

**) B. Davydov, ŽETF *6* (5) (1936), 463; viz též B. Davydov, Uspěchi fiz. nauk *93* (1967), 401.

Odvození difúzní rovnice z B. rovnice

Rovnice (A)

$$f(\vec{v},\vec{r},t) = f_0(v,\vec{r},t) + \vec{v}\cdot\vec{f}_1(v,\vec{r},t)$$

$$\frac{\partial f_1}{\partial t} + \nabla_r f_0 + \frac{\boldsymbol{\Gamma}}{v}\frac{\partial f_0}{\partial v} - (\omega_c \times f_1) = -\nu_1 f_1$$

Rovnice B

$$\nabla_r f_0 = -\nu_1 \vec{f}_1$$

$$\varphi = v\varphi'(v, \boldsymbol{r}, t)$$

$$\bar{\varphi} = \frac{1}{n}\int (f_0 + \boldsymbol{v}\,.\boldsymbol{f}_1)\, v\varphi'\, \mathrm{d}\boldsymbol{v} = \frac{1}{n}\int (\boldsymbol{v}\,.\boldsymbol{f}_1)\, v\varphi'\, \mathrm{d}\boldsymbol{v} = \frac{4\pi}{3}\frac{1}{n}\int_0^\infty v^4 f_1 \varphi'\, \mathrm{d}v$$

$$\bar{\varphi} = \frac{4\pi}{n}\int_0^\infty v^2 f_0 \varphi\, \mathrm{d}v$$

$$\vec{\varphi} = \vec{v}.1$$

$$\bar{\vec{v}} = \frac{4\pi}{3}\frac{1}{n}\int v^4 f_1 dv = -\frac{4\pi}{3}\frac{1}{n}\int v^4 \frac{\nabla f_0}{\nu_1} dv = \ldots \sim \ldots = -\frac{1}{3}\frac{4\pi}{n}\int \frac{v^2}{\nu_1} v^2 \nabla f_0 dv = \ldots = -\frac{1}{3}\nabla\left(\left(\frac{\overline{v^2}}{\nu_1}\right).n\right)$$

$$\bar{\vec{v}} = -\frac{1}{3}\frac{1}{n}\nabla\left(\left(\frac{\overline{v^2}}{\nu_1}\right).n\right) \Rightarrow \bar{\vec{v}} = -\frac{1}{3}\frac{1}{n}\nabla\left(\left(\frac{\overline{v^2}}{\nu_1}\right).n\right) = -D\frac{\nabla n}{n} \Rightarrow D = \frac{1}{3}\left(\frac{\overline{v^2}}{\nu_1}\right)$$

Odvození rovnice pro drift z B. rovnice

Rovnice B

$$\frac{\partial f_1}{\partial t} + \nabla_r f_0 + \frac{\Gamma}{v}\frac{\partial f_0}{\partial v} - (\omega_c \times f_1) = -\nu_1 f_1$$

$\frac{\partial}{\partial t} = 0$ $\quad \nabla_r = 0$ $\quad \vec{E} \neq 0$ $\quad B = 0$

$$\frac{\Gamma}{v}\frac{\partial f_0}{\partial v} = -\nu_1 \vec{f}_1$$

$$\vec{\Gamma} = \frac{e\vec{E}}{m}$$

$$\vec{f}_1 = -\frac{1}{\nu_1}\frac{\Gamma}{v}\frac{\partial f_0}{\partial v}$$

Per-partes
+ conditions of limits for *f*

$$\vec{\bar{v}} = \frac{4\pi}{3}\frac{1}{n}\int v^4 \vec{f}_1 dv = -\frac{4\pi}{3}\frac{1}{n}\int v^4 \frac{1}{\nu_1}\frac{\vec{\Gamma}}{v}\frac{\partial f_0}{\partial v} dv = \ldots = -\frac{4\pi}{3}\frac{1}{nm\nu_1} e\vec{E}\int v^3 \frac{\partial f_0}{\partial v} dv = -\frac{4\pi}{3}\frac{3}{nm\nu_1} e\vec{E}\int v^2 f_0 dv$$

ν_1~const

$\nu_1 \sim N v \sigma$

$$\mu_1 = f\left(\frac{E}{\nu_1}\right) = f\left(\frac{E}{N}\right)$$

$$\bar{\varphi} = \frac{4\pi}{n}\int_0^\infty v^2 f_0 \varphi \, dv$$

ν_1~const

$$\vec{\bar{v}} = -\frac{4\pi}{3}\frac{3}{nm\nu_1} e\vec{E}\int v^2 f_0 dv = -\frac{e}{m\nu_1}\vec{E}\frac{4\pi}{n}\int v^2 f_0 dv = -\frac{e}{m\nu_1}\vec{E}.1$$

$$\varphi = 1$$

ν_1~function of v

$$\vec{\bar{v}} = -\frac{4\pi}{3}\frac{e}{nm}\vec{E}\int \frac{v^3}{\nu_1}\frac{\partial f_0}{\partial v} dv = \vec{E}\left(-\frac{4\pi}{3}\frac{e}{nm}\int \frac{v^3}{\nu_1}\frac{\partial f_0}{\partial v} dv\right)$$

$$\vec{\bar{v}} = -\frac{e}{m\nu_1}\vec{E} = \mu\vec{E}$$

Drift elektronů v He, Ne, Ar…

- He, Ar

$$\vec{v} = \pm \mu \vec{E}$$

$\mu = function \quad of(\frac{E}{p})$

Pro daný plyn

$v = function \quad of(\frac{E}{p})$

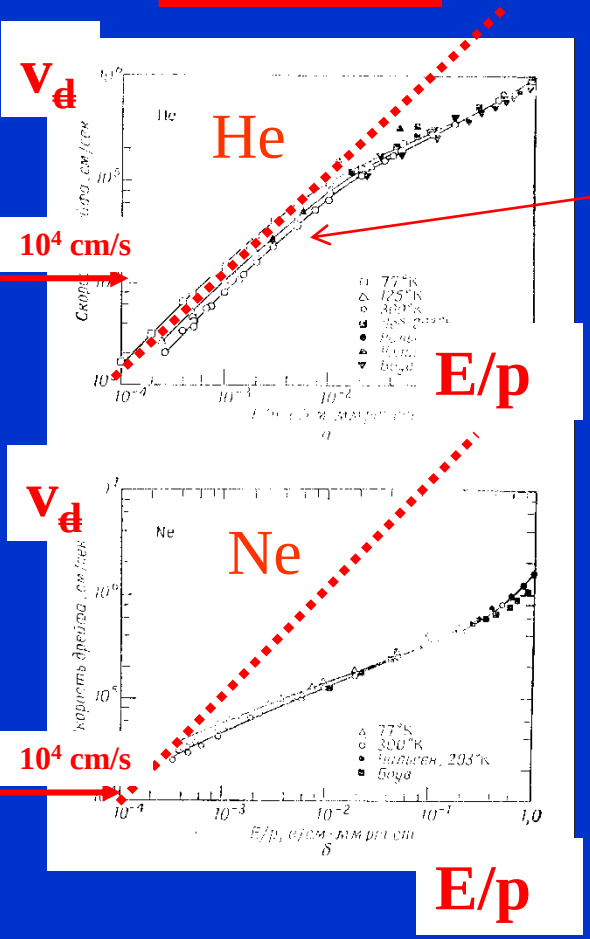

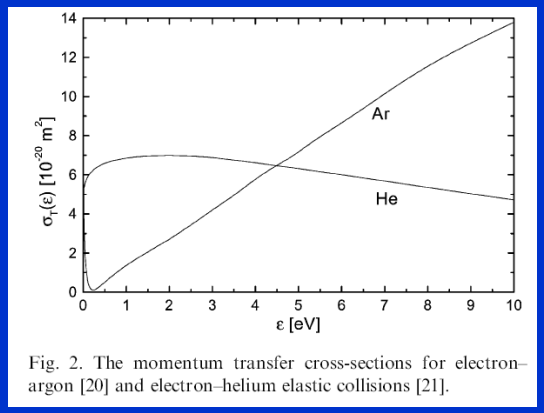

Fig. 2. The momentum transfer cross-sections for electron–argon [20] and electron–helium elastic collisions [21].

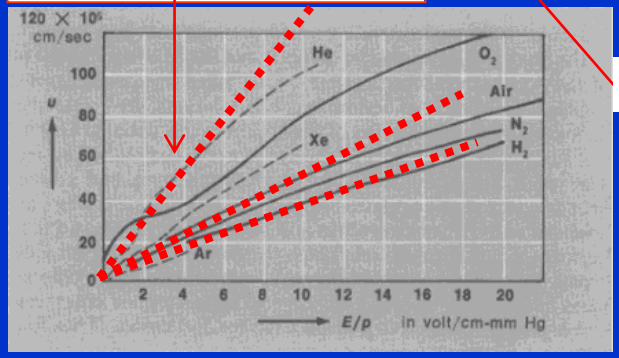

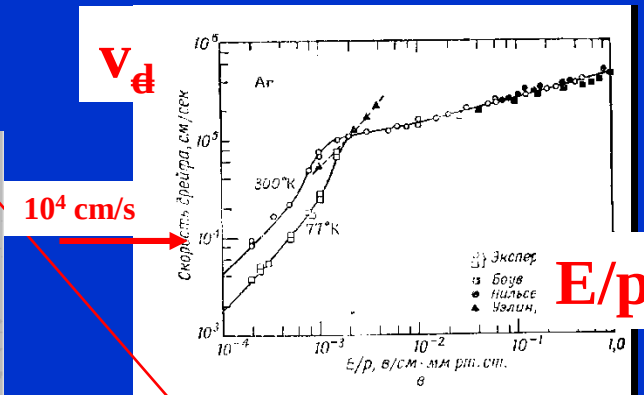

[V/cm].[1/Torr]

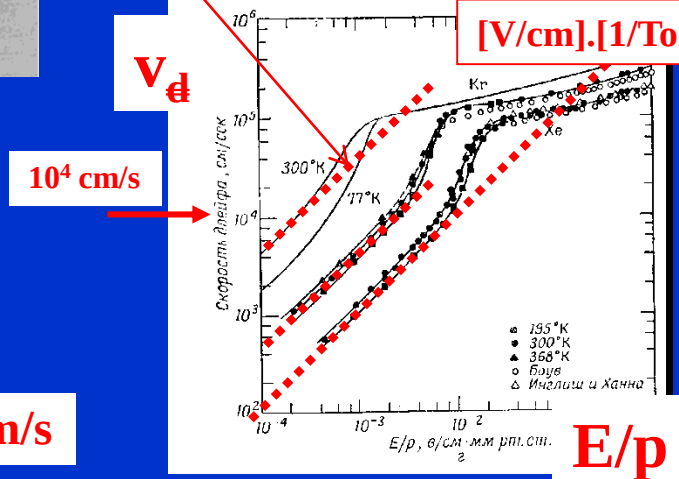

Dependence of *u* on the ratio *E/p* for different gases: (*u*) velocity of the directed motion of electrons under the action of the electric field *E*, (*p*) gas pressure referred to the equivalent pressure at 0° C

Velocity 10^4 cm/s

Drift iontů - experiment

ionty

- rychlost

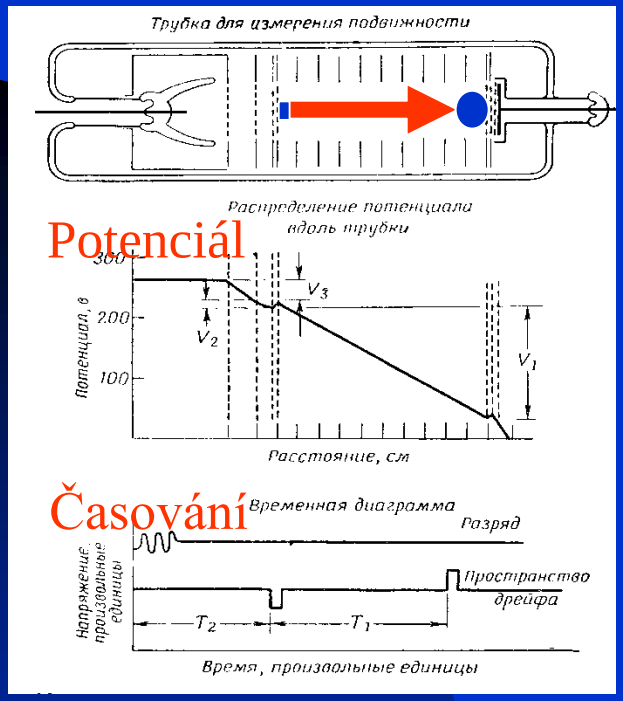

Velocity 10^4 cm/s

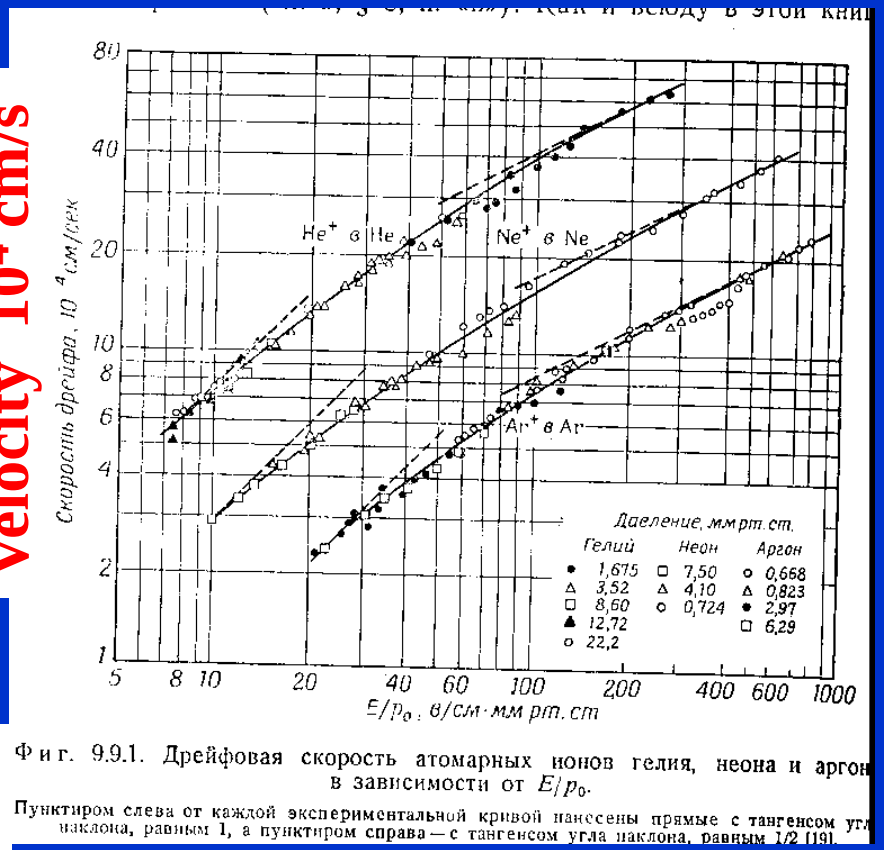

Фиг. 9.9.1. Дрейфовая скорость атомарных ионов гелия, неона и аргона в зависимости от E/p_0.

Пунктиром слева от каждой экспериментальной кривой нанесены прямые с тангенсом угла наклона, равным 1, а пунктиром справа — с тангенсом угла наклона, равным 1/2 [19].

[V/cm].[1/Torr]

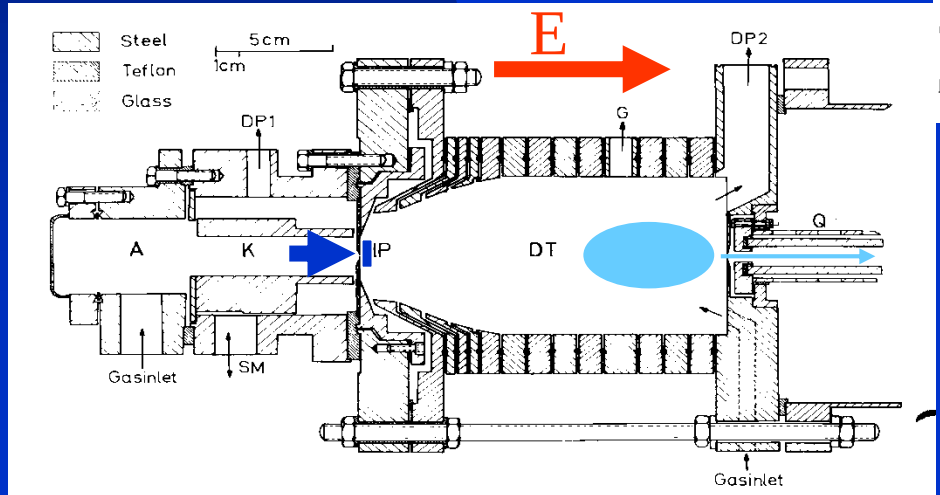

Fig. 1. Section through the main part of the apparatus. A, anode; K, cathode; DP, diffusion pump; SM, shift mechanism (not used in this work); HP, hole probe; DT, drift tube; G, pressure gauge; Q, quadrupole.

Drift iontů

$$v_d = \mu \cdot E$$

$$\mu_0 = \mu \cdot \frac{p}{760} \cdot \frac{273}{T}$$

$$\mu = \mu_0 \cdot \frac{760}{p} \cdot \frac{T}{273}$$

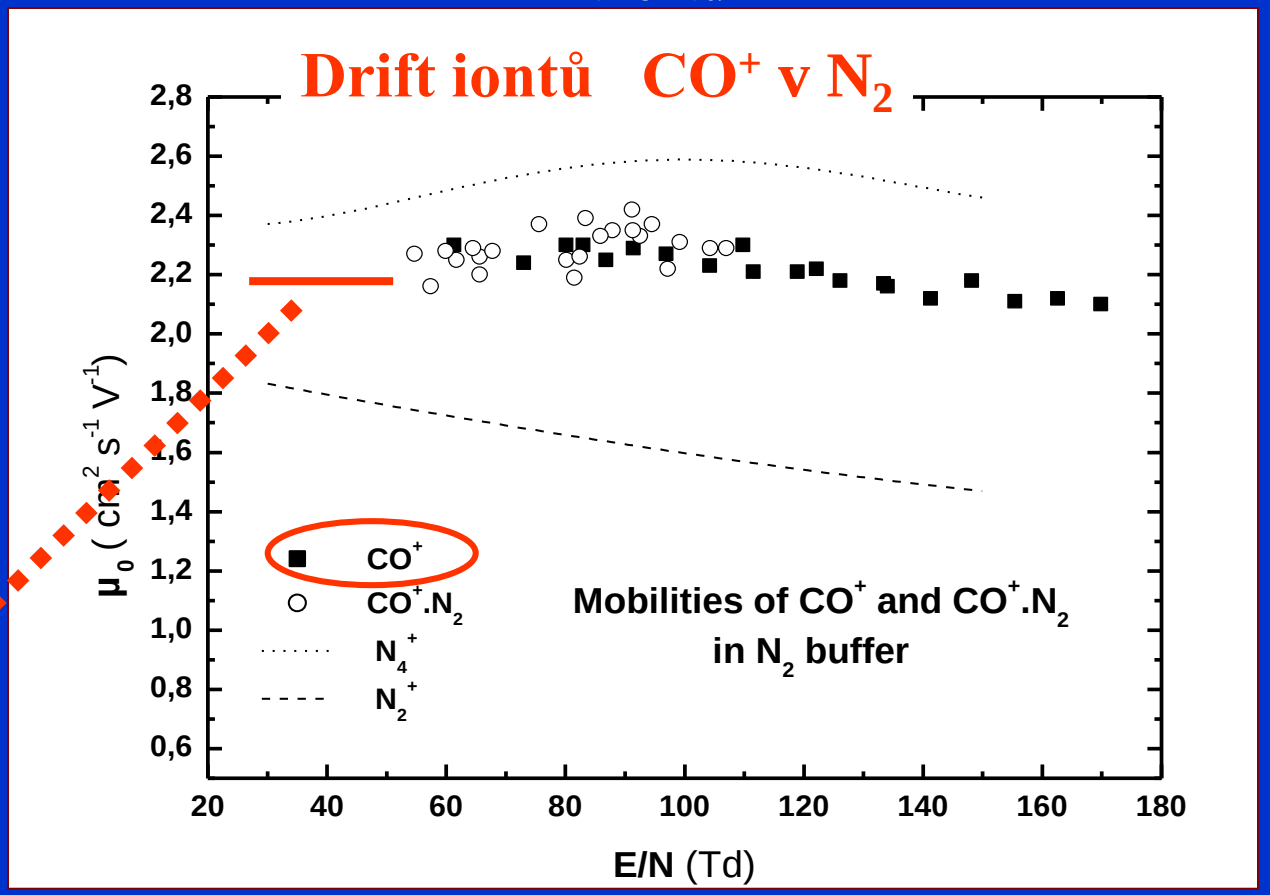

$$\mu = 2.2 \cdot \frac{760}{1} \cdot 1 \sim 1700 cm^2 s^{-1} V^{-1}$$

$$v_d = \mu \cdot E = 1700 cm/s = 17 m/s$$

CO^+ in N_2

$$E = 1V/cm = 100V/1m$$

Drift iontů - experiment

PHYSICAL REVIEW VOLUME 106, NUMBER 3 MAY 1, 1957

Temperature Dependence of Ion Mobilities in Helium, Neon, and Argon

LORNE M. CHANIN AND MANFRED A. BIONDI
Westinghouse Research Laboratories, Pittsburgh, Pennsylvania

(Received January 25, 1957)

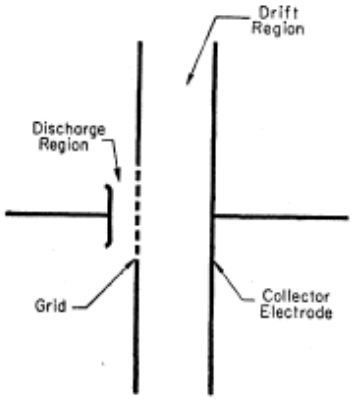

FIG. 1. Schematic arrangement of the electrodes in the mobility tube.

- A

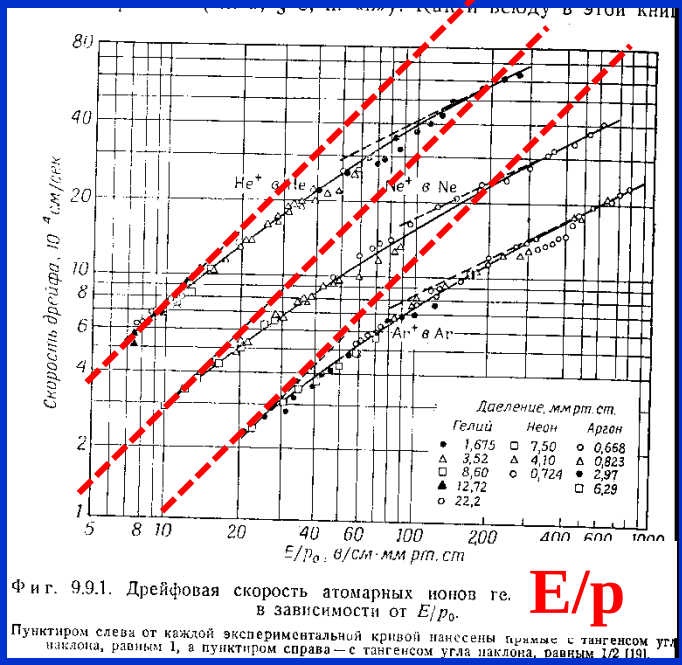

Фиг. 9.9.1. Дрейфовая скорость атомарных ионов гелия в зависимости от E/p_0.

Пунктиром слева от каждой экспериментальной кривой нанесены прямые с тангенсом угла наклона, равным 1, а пунктиром справа — с тангенсом угла наклона, равным 1/2 [19].

E/p

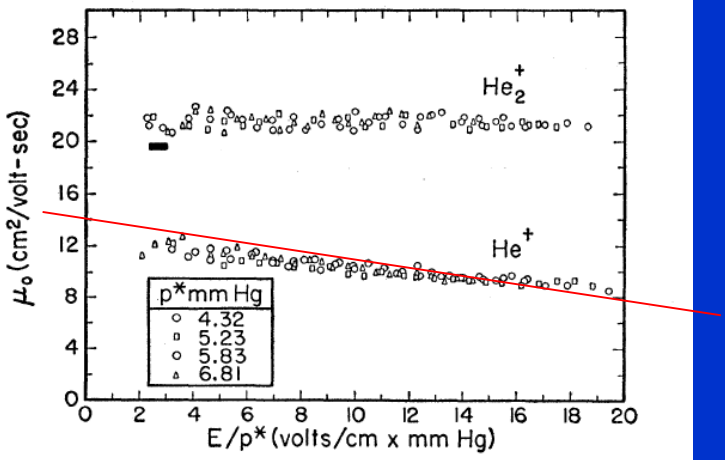

FIG. 2. Mobilities of He^+ and He_2^+ in helium at 195°K. Tyndall and Pearce's measurements are indicated by the short heavy bar. A pressure $p^*=1$ mm Hg refers to a gas density of 3.22×10^{16} atoms/cc.

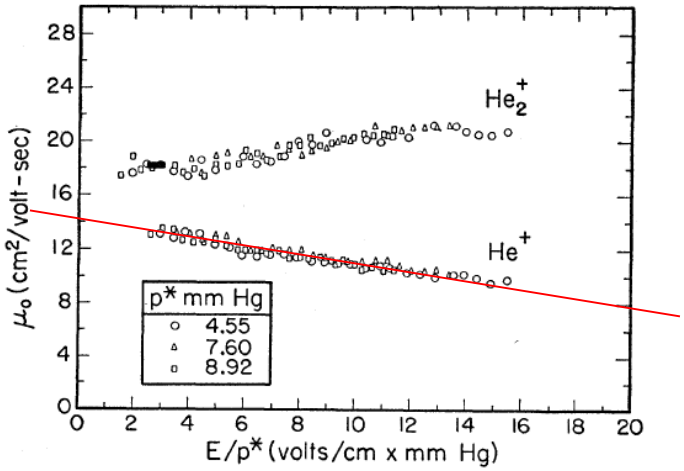

FIG. 3. Mobilities of He^+ and He_2^+ in helium at 77°K. Tyndall and Pearce's measurements are indicated by the short heavy bar.

Drift iontů - experiment

- A

PHYSICAL REVIEW VOLUME 106, NUMBER 3 MAY 1, 1957

Temperature Dependence of Ion Mobilities in Helium, Neon, and Argon

LORNE M. CHANIN AND MANFRED A. BIONDI
Westinghouse Research Laboratories, Pittsburgh, Pennsylvania

(Received January 25, 1957)

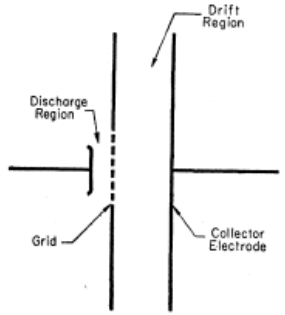

FIG. 1. Schematic arrangement of the electrodes in the mobility tube.

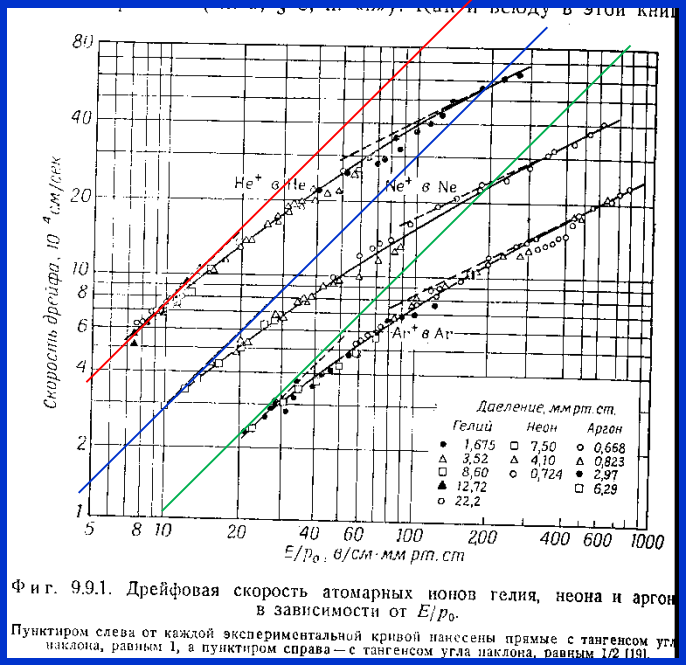

Фиг. 9.9.1. Дрейфовая скорость атомарных ионов гелия, неона и аргона в зависимости от E/p_0.

Пунктиром слева от каждой экспериментальной кривой нанесены прямые с тангенсом угла наклона, равным 1, а пунктиром справа — с тангенсом угла наклона, равным 1/2 [19].

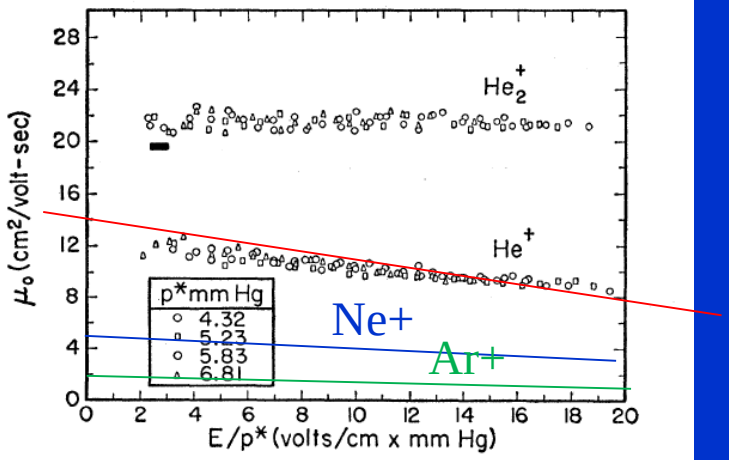

FIG. 2. Mobilities of He^+ and He_2^+ in helium at 195°K. Tyndall and Pearce's measurements are indicated by the short heavy bar. A pressure $p^*=1$ mm Hg refers to a gas density of 3.22×10^{16} atoms/cc.

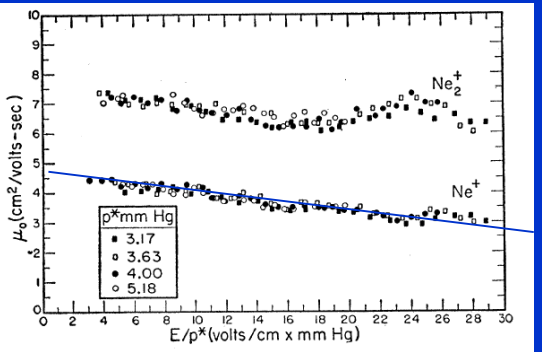

FIG. 4. Mobilities of Ne^+ and Ne_2^+ in neon at 195°K.

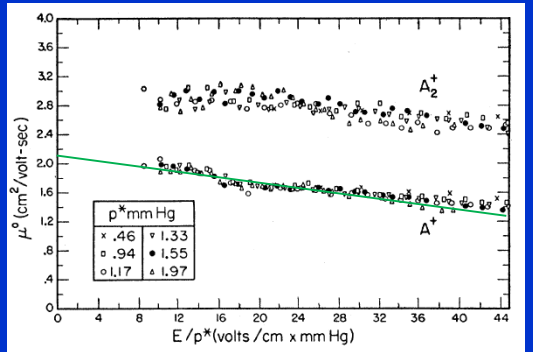

FIG. 6. Mobilities of A^+ and A_2^+ in argon at 195°K.

Drift iontů - experiment

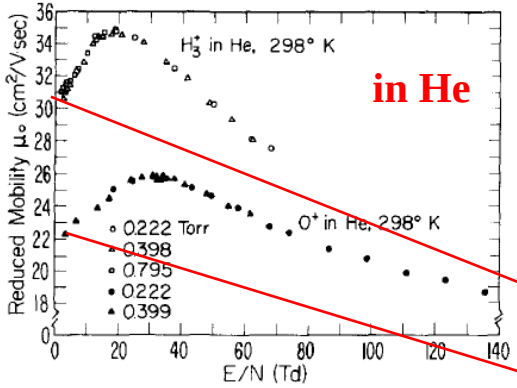

FIG. 1. Reduced mobilities of H_3^+ and O^+ in helium.

The Journal of Chemical Physics, Vol. 62, No. 9, 1 May 1975

1975

Mobilities of various mass-identified positive ions in helium and argon

W. Lindinger* and D. L. Albritton

Aeronomy Laboratory, NOAA Environmental Research Laboratories, Boulder, Colorado 80302
(Received 7 January 1975)

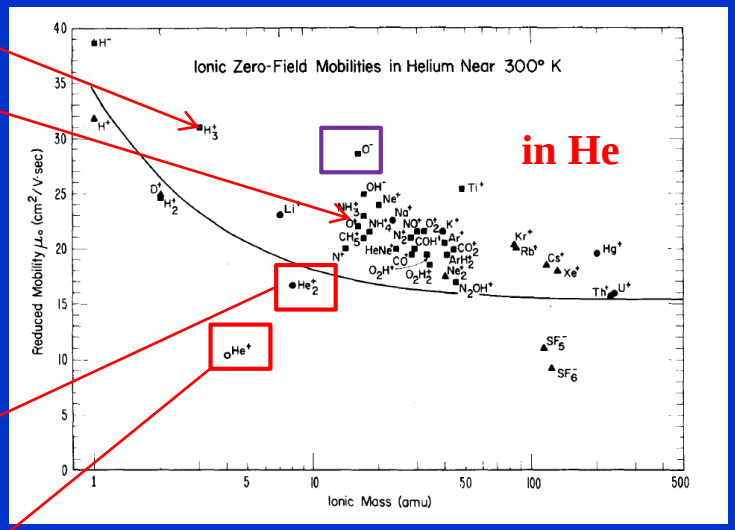

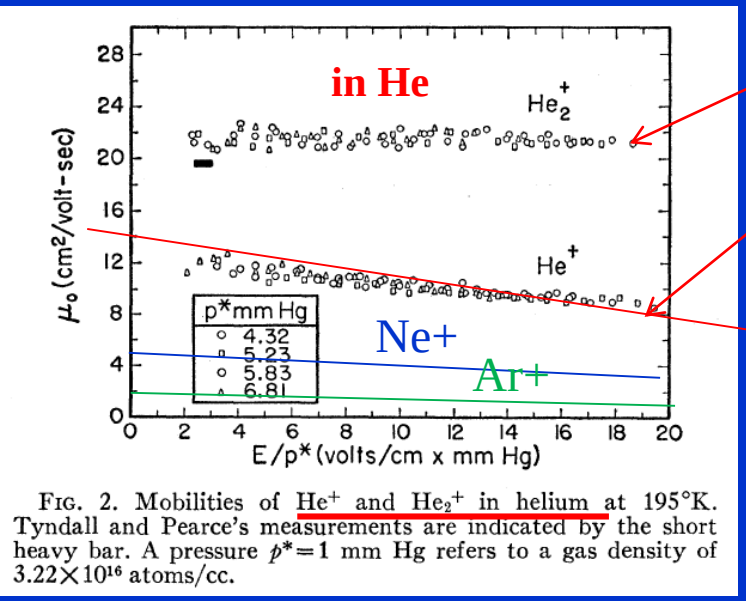

FIG. 2. Mobilities of He^+ and He_2^+ in helium at 195°K. Tyndall and Pearce's measurements are indicated by the short heavy bar. A pressure $p^*=1$ mm Hg refers to a gas density of 3.22×10^{16} atoms/cc.

TABLE II. Reduced zero-field mobilities μ_0 and free and ambipolar diffusion coefficients, D and D_a, times buffer gas pressure and number density, p and N, at 300°K, for a variety of ions in helium and in argon.

Ion	Buffer	μ_0 (cm^2/V·sec)	Dp (cm^2·Torr/sec)	DN (10^{19} cm^{-1}·sec^{-1})	D_ap (cm^2·Torr/sec)	D_aN (10^{19} cm^{-1}·sec^{-1})
H_3^+	Helium	30.5±2.4	658	2.12	1320	4.24
O^+	Helium	22.0±1.8	475	1.53	949	3.06
CO^+	Helium	19.5±1.6	421	1.35	842	2.71
COH^+	Helium	19.5±1.6	421	1.35	842	2.71
Ar^+	Helium	20.5±1.6	442	1.42	885	2.85
ArH^+	Helium	19.4±1.6	419	1.35	837	2.69
O_2^+	Helium	21.8±1.7	470	1.51	941	3.03
O_2H^+	Helium	19.5±1.6	421	1.35	842	2.71
$O_2H_2^+$	Helium	18.5±1.5	399	1.28	798	2.57
NH_3^+	Helium	23.0±1.8	496	1.60	993	3.20
NH_4^+	Helium	21.8±1.7	470	1.51	941	3.03
CH_5^+	Helium	21.0±1.7	453	1.46	906	2.92
CO_2^+	Helium	20.0±1.6	432	1.39	863	2.78
NO^+	Helium	21.5±1.7	464	1.49	928	2.99
N_2OH^+	Helium	17.2±1.4	371	1.19	742	2.39
COH^+	Argon	2.50±0.20	53.9	0.173	108	0.347
CO_2^+	Argon	2.15±0.17	46.4	0.149	92.8	0.299
N_2OH^+	Argon	2.14±0.17	46.2	0.149	92.4	0.297

Drift iontů - experiment

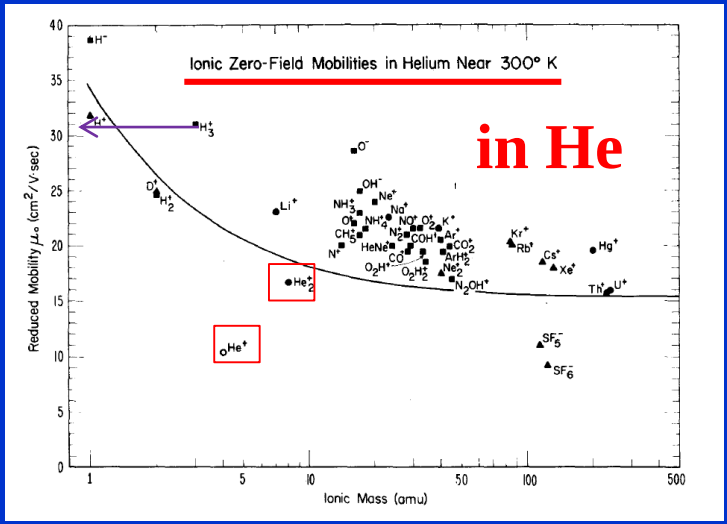

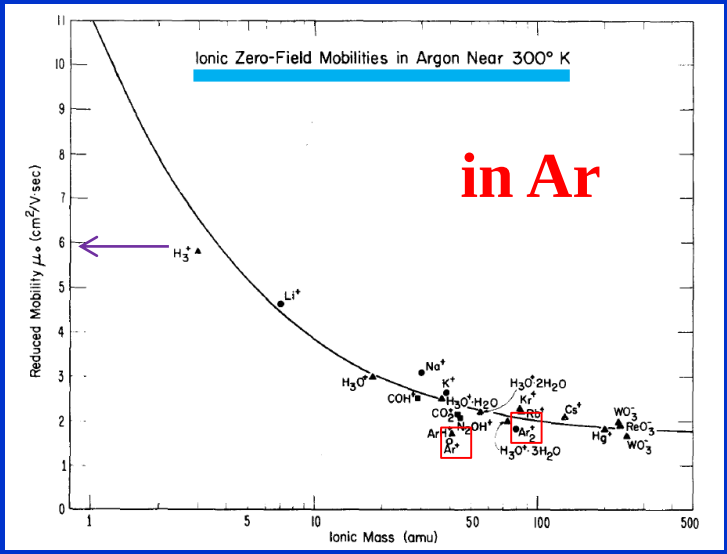

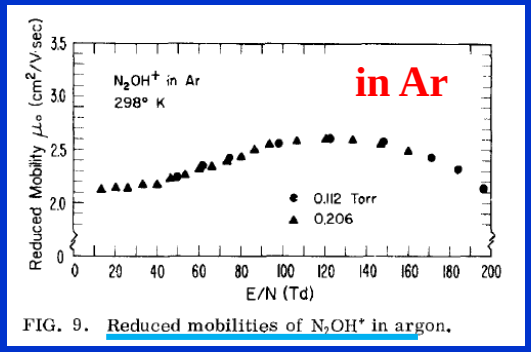

FIG. 9. Reduced mobilities of N_2OH^+ in argon.

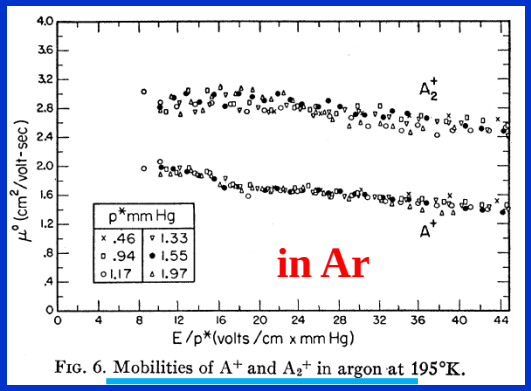

FIG. 6. Mobilities of A^+ and A_2^+ in argon at 195°K.

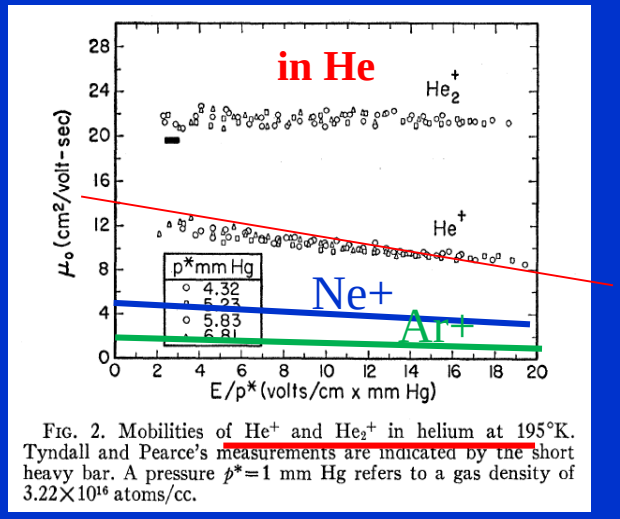

FIG. 2. Mobilities of He^+ and He_2^+ in helium at 195°K. Tyndall and Pearce's measurements are indicated by the short heavy bar. A pressure $p^*=1$ mm Hg refers to a gas density of 3.22×10^{16} atoms/cc.

For polarizable neutrals, the point-charge, induced-dipole attraction always contributes to the ion–neutral interaction. The reduced zero-field mobility for the polarization force alone is given by (Ref. 12, p. 146)

$$\mu_0(\text{Langevin}) = 13.876/(\alpha m_r)^{1/2}\ \text{cm}^2/\text{V}\cdot\text{sec}, \qquad (6)$$

where α is the polarizability in Å^3 and m_r is the reduced mass in g/mole. Since the polarization force is often the strongest long-range interaction and therefore may be the dominant contribution to the mobility at low E/N, it is instructive to test how well the polarization, i.e., Langevin, mobilities agree with the experimental zero-field values, for use when only an approximate value is needed.

Závislost na hmotě plynů a hmotě iontů

$$\mu = \frac{e}{m\nu_1}$$

$$\sigma_0 = \pi\rho_0^2 = \frac{2\pi e}{\nu_0(4\pi\varepsilon_0)}\sqrt{\frac{\alpha}{\mu}}$$

$$\sigma_{coll} = \sigma_L = const\,\frac{1}{v}\sqrt{\frac{\alpha}{\mu}} \sim \sigma_0\frac{v_0}{v}\,cm^2$$

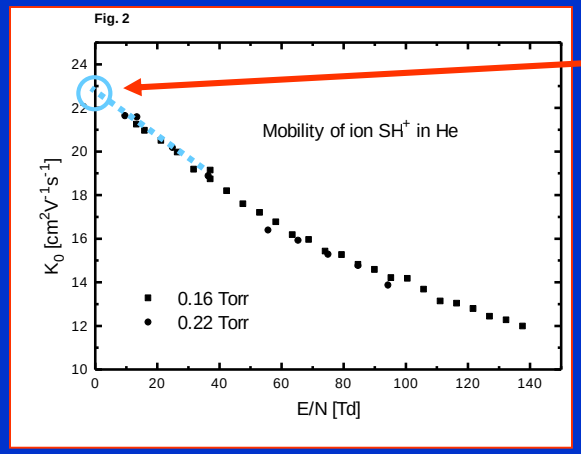

Low E region

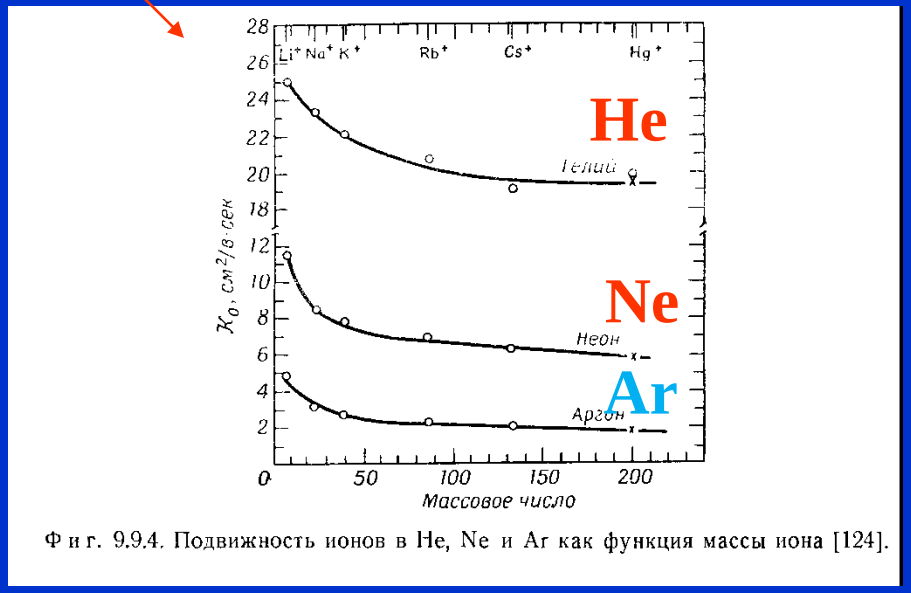

Фиг. 9.9.4. Подвижность ионов в He, Ne и Ar как функция массы иона [124].

experiments

Drift tube

- Innsbruck Drift Tube

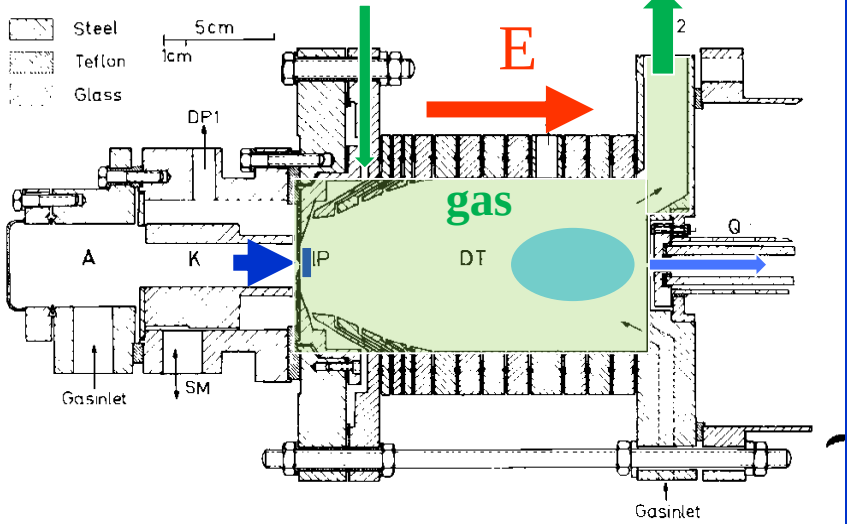

Fig. 1. Section through the main part of the apparatus. A, anode; K, cathode; DP, diffusion pump; SM, shift mechanism (not used in this work); HP, hole probe; DT, drift tube; G, pressure gauge; Q, quadrupole.

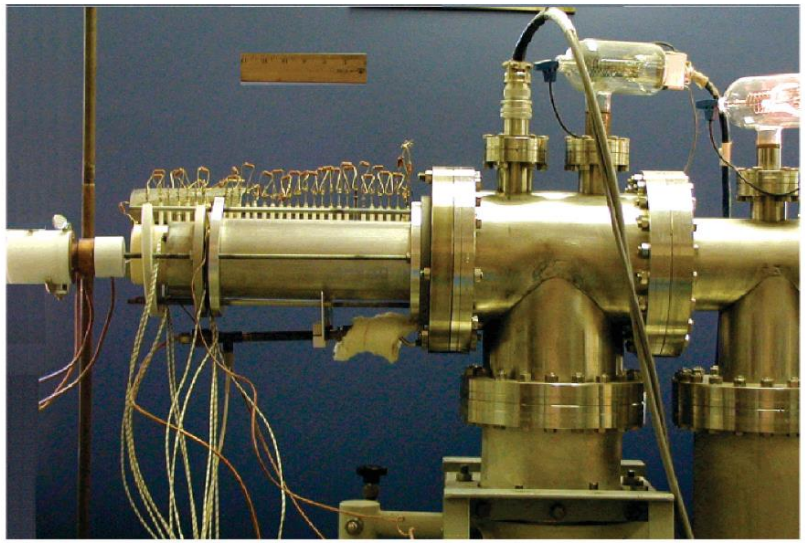

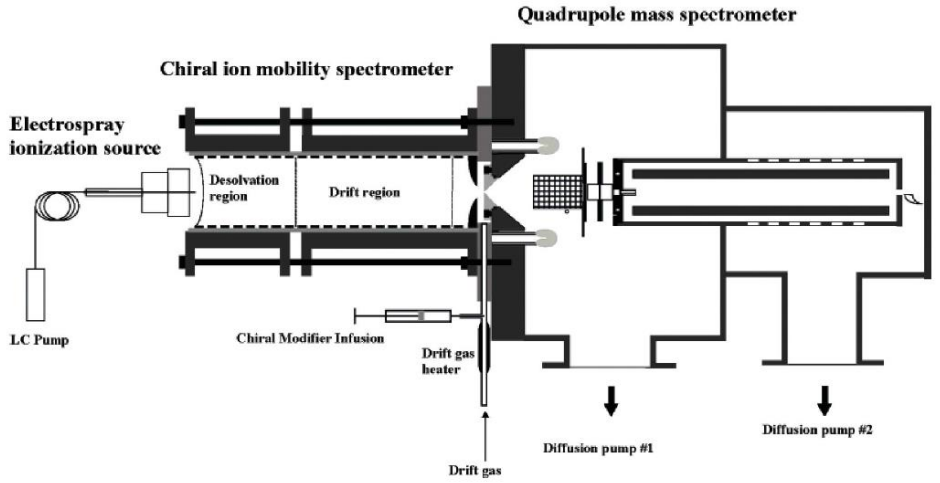

Ambipolar diffusion

EEDF from Boltzmann equation

a) Nechť vnější elektrické pole je nulové, tj. $\Gamma = 0$. Potom

(5.133) $$\mathcal{G}(v_1) = 0$$

a pro $f_0(v)$ máme Maxwellovu rozdělovací funkci

(5.134) $$f_0 = C \exp\left(-\frac{mv^2}{2kT}\right),$$

kde

(5.135) $$C = n\left(\frac{m}{2\pi kT}\right)^{3/2}.$$

b) Nechť vnější magnetické pole je nulové, tj. $\omega_c = 0$. Potom

(5.136) $$\mathcal{G}(v_1) = \Gamma^2$$

a (5.131) můžeme upravit na tvar

(5.137) $$f_0 = C \exp\left\{-\int \frac{m}{kT}\left(\frac{v v_1^2}{v_1^2 + \left(\frac{\Gamma^2 m}{3\gamma kT}\right)}\right) \mathrm{d}v\right\}.$$

Bude-li nyní srážková frekvence v_1 nezávislá na rychlosti, tj.

(5.138) $$v_1 = v = \text{konst},$$

pak f_0 bude opět maxwellovské rozdělení

(5.139) $$f_0 = C \exp\left[-\frac{mv^2}{2k\left(T + \frac{\Gamma^2 m}{3\gamma k} v^{-2}\right)}\right] = C \exp\left(-\frac{mv^2}{2kT^*}\right)$$

ale s teplotou

(5.140) $$T^* = T + \frac{m}{3\gamma k}\left(\frac{\Gamma}{v}\right)^2 = T + \frac{M}{3k}\left(\frac{ZeE}{mv}\right)^2.$$

To ale znamená, že při $v_1 = \text{konst}$ je kinetická teplota lehkých nabitých částic (elektronů) vyšší ve srovnání s teplotou neutrálních částic.

Předpoklad, že srážková frekvence elektronů s neutrálními částicemi je konstantní, nezávislá na rychlosti, je příliš ostrý. V obecném případě totiž platí, že v_1 na rychlosti elektronů závisí. Předpokládejme, že

(5.141) $$v_1(v) = Av^l,$$

kde l je libovolné číslo*) a A je konstanta (pro $l = 1$ máme

(5.141′) $$v_1 = Av$$

a tedy $A^{-1} = \lambda$, kde λ je střední volná dráha elektronů).

Rovnice pro f_0 (5.137) má nyní tvar

(5.142) $$f_0 = C \exp\left\{-\int \frac{m}{kT} \frac{v^{2l+1}}{v^{2l} + \frac{\Gamma^2 m}{3\gamma A^2 kT}} \mathrm{d}v\right\}.$$

Pro $l = 1$, tj. případ modelu dokonale pružných koulí (viz kapitolu 2), kdy

(5.143) $$v_1 = Av,$$

je integrál v (5.142) snadno spočitatelný a f_0 má tvar

(5.144′) $$f_0 = C\left[1 + \frac{3A^2}{\Gamma^2}\frac{kT}{m}v^2\right]^{(m\Gamma/AkT)^2 \cdot (1/6\gamma)} \cdot \exp\left(-\frac{mv^2}{2kT}\right).$$

Po kratších úpravách pak dostaneme

(5.144) $$f_0 = C\left[v^2 + \frac{M}{3}\left(\frac{ZeE}{mA}\right)^2 \frac{1}{kT}\right]^{(mM/6k^2T^2)\cdot(ZeE/mA)^2} \cdot \exp\left(-\frac{mv^2}{2kT}\right),$$

což je rozdělovací funkce, kterou jako první odvodil Davydov.**) Pro silné elektrické pole, kdy

(5.145) $$\frac{\Gamma^2 m}{3\gamma AkT} = \frac{M}{3kT}\left(\frac{ZeE}{mA}\right)^2 \gg v^2,$$

přechází Davydovova rozdělovací funkce na známou rozdělovací funkci Druyvesteyna (o tom je možno se přesvědčit z (5.142), kde položíme $l = 1$ a provedeme příslušné zanedbání), která má tvar

(5.146) $$f_0 = C \exp\left(-\frac{3}{4}\gamma\left(\frac{A}{\Gamma}\right)^2 v^4\right) = C \exp\left[-\frac{3}{4}\frac{m}{M}\left(\frac{mA}{ZeE}\right)^2 v^4\right].$$

---

*) Závislost (5.141) pro $l = 0$ vystihuje s dobrou přesností srážky elektronů s atomy He a H_2, pro $l = 1$ pak srážky v Ne a dále pro $l = 3$, 3.5 a 4 pak srážky pomalých elektronů v Ar, Kr a Xe; viz D. Darbiere: Phys. Rev. *84* (1951), 653; S. C. Brown: Handbuch der Physik, ed. S. Flüge, Vol. 22 (Berlin 1956), 531; G. L. Braglia: Phys. Lett. *17* (1965), 260.

**) B. Davydov, ŽETF *6* (5) (1936), 463; viz též B. Davydov, Uspěchi fiz. nauk *93* (1967), 401.

Srovnaní driftů iontů a elektronů

- Drift iontů
- Drift elektronů

$$E = 1V/cm = 100V/1m$$

$$p = 1Torr$$

CO^+ v N_2

$$v_d = \mu \cdot E = 1700cm/s = 17m/s$$

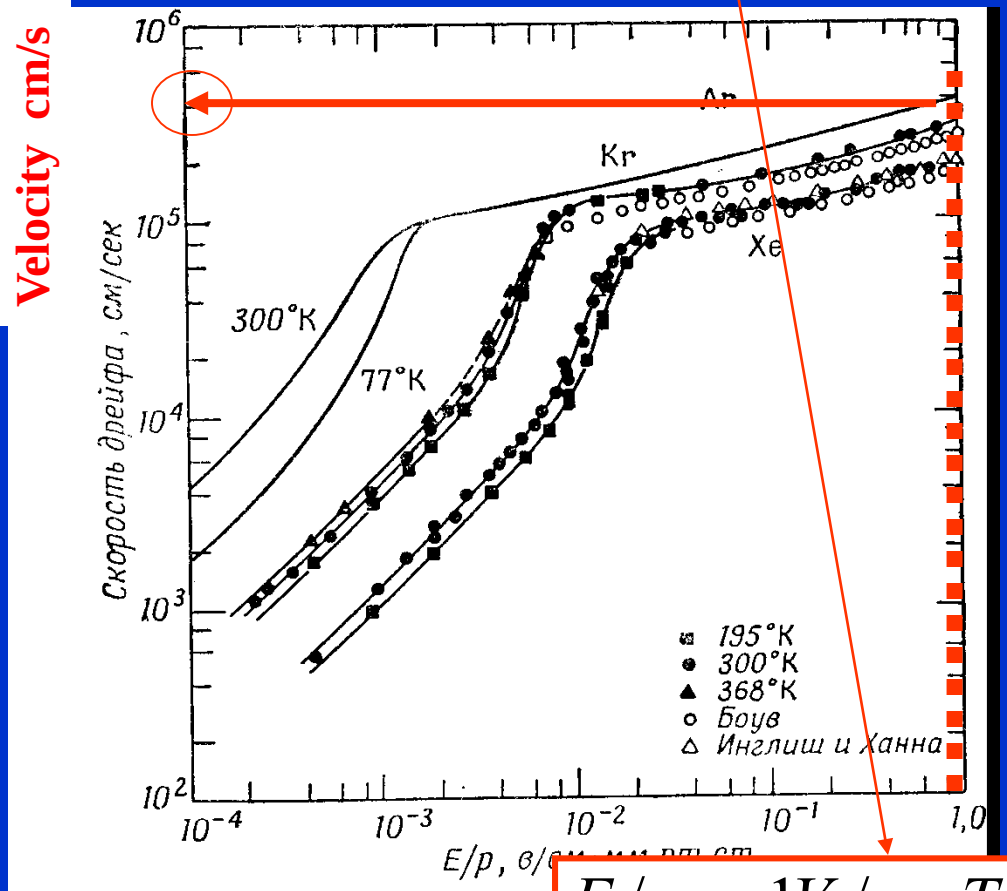

Drift elektronů

e^- v Ar

235x

$$v_{dELECTRON} = 4000m/s$$

$$\mu_e >> \mu_i$$

A co bude dělat plazma v E ??!!

$$E/p = 1V/cmTorr$$

Difúze v plazmatu

- Ambipolární difúze

$$\vec{v} = \frac{1}{nm\nu_1}(\pm ne\vec{E} - kT\nabla_r n) = \pm\frac{e}{m\nu_1}\vec{E} - \frac{kT}{m\nu_1}\frac{\nabla_r n}{n}$$

$$n_e = n_i = n_{PLAZMA} = n$$

$$\frac{\partial n}{\partial t} + \nabla . \Gamma_j = 0$$

$$\Gamma_e = \Gamma_i = \Gamma$$

Potřebné elektrické pole E nalezneme z podmínky $\Gamma_i = \Gamma_e = \Gamma$

$$\Gamma = \mu_i n E - D_i \nabla n = -\mu_e n E - D_e \nabla n$$

$$E = \frac{D_i - D_e}{\mu_i + \mu_e}\frac{\nabla n}{n}$$

$$\Gamma = \mu_i \frac{D_i - D_e}{\mu_i + \mu_e}\nabla n - D_i \nabla n =$$

$$= \frac{\mu_i D_i - \mu_i D_e - \mu_i D_i - \mu_e D_i}{\mu_i + \mu_e}\nabla n =$$

$$= -\frac{\mu_i D_e + \mu_e D_i}{\mu_i + \mu_e}\nabla n .$$

$$D_a \equiv \frac{\mu_i D_e + \mu_e D_i}{\mu_i + \mu_e}$$

$$\partial n/\partial t = D_a \nabla^2 n$$

Ambipolární difúze

- A

$$\partial n/\partial t = D_a \nabla^2 n$$

$$D_a \equiv \frac{\mu_i D_e + \mu_e D_i}{\mu_i + \mu_e}$$

$$\mu = \frac{e}{m\nu_1} \qquad D = \frac{kT}{m\nu_1}$$

$$\frac{\mu}{D} = \frac{e}{kT}$$

Velikost D_a můžeme odhadnout, vezmeme-li $\mu_e \gg \mu_i$. Že tomu tak je, můžeme vidět z rov. [5-7]. Poněvadž ν je úměrné tepelné rychlosti, která je zase úměrná $m^{-1/2}$, je μ úměrné $m^{-1/2}$. Rovnice [5-16] a [5-9] potom dávají

$$D_a \approx D_i + \frac{\mu_i}{\mu_e} D_e = D_i + \frac{T_e}{T_i} D_i \qquad [5\text{-}18]$$

Pro $T_e = T_i$ dostáváme

$$D_a \approx 2D_i . \qquad [5\text{-}19]$$

Pole v plazmatu, odhad

- Ambipolární difúze

$$E = \frac{D_i - D_e}{\mu_i - \mu_e}\frac{\nabla n}{n}$$

$$\frac{D}{\mu} = \frac{kT}{e}$$

$$E \sim \frac{D_e}{\mu_e}\frac{\nabla n}{n} \sim \frac{kT}{e}\frac{\nabla n}{n} \sim V^{kT}\!\!\diagup_{R} \cdot \frac{n}{n} \sim V^{kT}\!\!\diagup_{R}$$

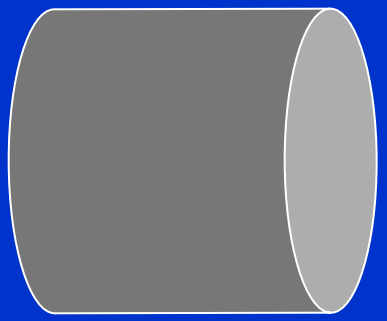

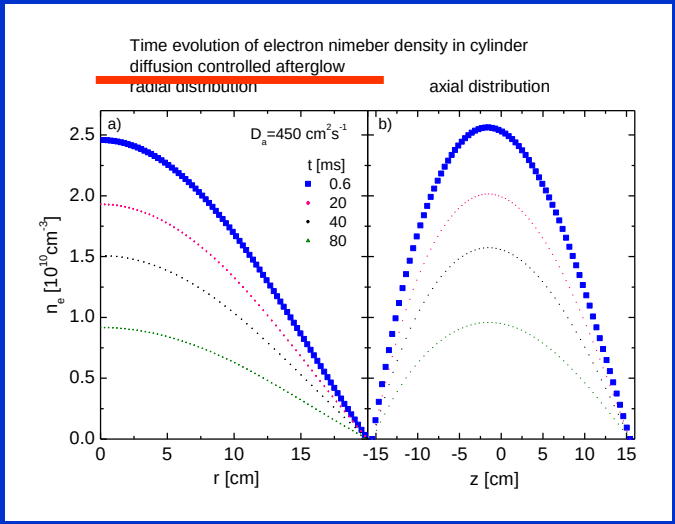

Rovnice kontinuity a difúze

- A

$$\frac{\partial n}{\partial t} + \vec{\nabla}.(n.\vec{\bar{v}}) = 0$$

$$\vec{\bar{v}} = -D\frac{\nabla_r n}{n}$$

$$\frac{\partial n}{\partial t} = -\vec{\nabla}.(n.\vec{\bar{v}}) = \vec{\nabla}.\left(nD\frac{\nabla_r n}{n}\right) = \vec{\nabla}.(D\nabla_r n) = D\vec{\nabla}.(\nabla_r n) = D\Delta n$$

Druhý Fickuv zákon

$$\frac{\partial n}{\partial t} = D\Delta n$$

Řešení rovnice

- Chen etc.
- *Collision phenomena in ionised gases*
  E.W. McDaniel

$$\frac{\partial n}{\partial t} = D\Delta n$$

$$n(\vec{r},t) = T(t).S(\vec{r})$$

$$S\frac{\partial T}{\partial t} = DT\Delta S = DT\nabla^2 S$$

$$\frac{1}{T}\frac{\partial T}{\partial t} = \frac{D}{S}\nabla^2 S$$

$$\frac{1}{T}\frac{\partial T}{\partial t} = -\frac{1}{\tau} = \frac{D}{S}\nabla^2 S \quad \rightarrow \quad \nabla^2 S = -\frac{S}{D\tau} = -\frac{S}{\lambda^2}$$

$$\frac{1}{T}\frac{\partial T}{\partial t} = -\frac{1}{\tau} \quad \rightarrow \quad T = T_0 e^{-t/\tau}$$

Difúze v rovinní geometrii

- Rovina
- Separace proměnných

$$\nabla^2 S = -\frac{S}{D\tau} = -\frac{S}{\lambda^2}$$

$$\nabla^2 S = \frac{\partial^2 S}{\partial x^2} = -\frac{S}{\lambda^2}$$

$$S = A\cos\frac{x}{\lambda} + B\sin\frac{x}{\lambda}$$

$$S = A\cos\frac{x}{\lambda} + B\sin\frac{x}{\lambda}$$

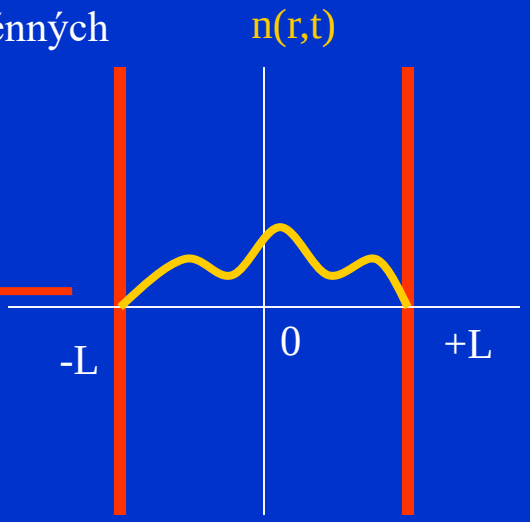

$$T = T_0 e^{-t/\tau}$$

$$n = n_0 e^{-t/\tau} \cos\frac{x}{\sqrt{D\tau}}$$

$$n(L,t) = n_0 e^{-t/\tau} \cos\frac{L}{\sqrt{D\tau}} = 0$$

$$\frac{L}{\sqrt{D\tau}} = \frac{\pi}{2} \quad \rightarrow \tau = \left(\frac{2L}{\pi}\right)^2 \frac{1}{D}$$

$$\tau = \left(\frac{2L}{\pi}\right)^2 \frac{1}{D}$$

$$\lambda^2 = \tau D = \left(\frac{2L}{\pi}\right)^2$$

$$\lambda = \left(\frac{2L}{\pi}\right)$$

$$T = T_0 e^{-t/\tau} = T_0 e^{-\left(\frac{2L}{\pi}\right)^2 Dt}$$

$$n = n_0 e^{-\frac{D}{\lambda^2}t} \cos\frac{x}{\lambda}$$

Charakteristická difúzní délka

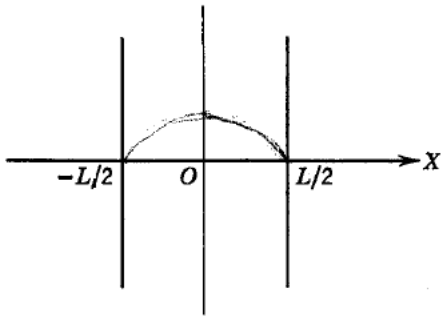

FIG. 10-8-1. A one-dimensional cavity with plane parallel walls.

independent of position in order that $\mathscr{D}$ may be constant. The extrapolation distance is neglected, and N_0 is required to vanish at the geometrical boundaries of the containers.

A. INFINITE PARALLEL PLATES. As the first example of the solution of the time-independent diffusion equation, consider the case of a one-dimensional cavity whose walls are the infinite plane parallel plates shown in Fig. 10-8-1. In this simple case the diffusion equation (10-6-6) becomes

$$\frac{d^2N_0(x)}{dx^2} + \frac{N_0(x)}{\mathscr{D}\tau} = 0 \tag{10-8-1}$$

Since $\mathscr{D}\tau$ is positive, the solution of (10-8-1) is

$$N_0(x) = A\cos\frac{x}{\sqrt{\mathscr{D}\tau}} + B\sin\frac{x}{\sqrt{\mathscr{D}\tau}} \tag{10-8-2}$$

where A and B are constants of integration which must be determined from the boundary conditions and from the requirement that we shall impose for symmetry about the midplane. If the width of the cavity is L and the origin of the coordinate system is located at the midplane, the boundary conditions are $N_0(x) = 0$ when $x = \pm L/2$.

The symmetry requirement makes $B = 0$, and the boundary conditions force τ to assume one of the infinite number of values τ_k $(k = 1, 2, 3, \ldots)$ which satisfy the equation

$$\cos\frac{L}{2\sqrt{\mathscr{D}\tau_k}} = 0 \quad \text{or} \quad \frac{L}{2\sqrt{\mathscr{D}\tau_k}} = (2k-1)\frac{\pi}{2} \tag{10-8-3}$$

Now define a quantity Λ_k which represents the *characteristic diffusion length for the* kth *mode of diffusion*:

$$\Lambda_k^2 = \mathscr{D}\tau_k = \left(\frac{1}{2k-1}\frac{L}{\pi}\right)^2 \tag{10-8-4}$$

The diffusion length is useful in describing the shape of a cavity in the diffusion process. The solution for the kth mode can then be written

$$N_0(x)_k = A_k\cos\frac{x}{\Lambda_k} \tag{10-8-5}$$

The function $\cos x/\Lambda_k$ assumes negative values in certain regions within the cavity for all modes of diffusion except the lowest, or fundamental, mode corresponding to $k = 1$. Therefore, if we consider each solution singly, we must discard all but the fundamental mode on physical grounds, since the particle number density can never be negative. However, since the diffusion equation is linear, the total solution of the diffusion problem consists of an infinite number of modes, many of which may be excited simultaneously. Any sum of these modes is then a possible solution, provided the constants A_k have values which prevent the number density from becoming negative. The use of an ionization source that provides uniform ionization throughout the cavity will ensure that the fundamental mode predominates.

After the ionization source is abruptly turned off at $t = 0$ each diffusion mode decays out with its own characteristic time constant τ_k. The total solution of the time-dependent diffusion problem is thus given by

$$N(x, t) = \sum_{k=1}^{\infty} A_k\cos\frac{x}{\Lambda_k}e^{-t/\tau_k} \tag{10-8-6}$$

- In slab geometry,

$$\frac{d^2S}{dx^2} = -\frac{1}{D_\alpha \tau} S$$

$$S = A\cos\frac{x}{(D_\alpha\tau)^{1/2}} + B\sin\frac{x}{(D_\alpha\tau)^{1/2}}$$

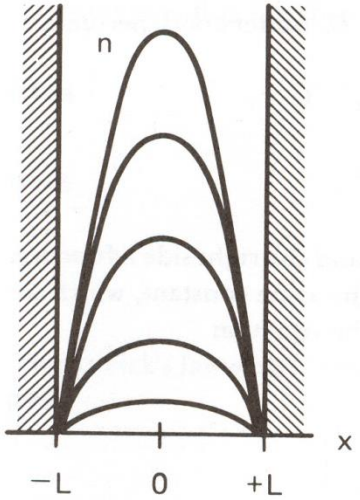

FIGURE 5-3 Density of a plasma at various times as it decays by diffusion to the walls.

- Boundary conditions S=0 at $x = \pm L$

$$\tau = \left(\frac{2L}{\pi}\right)^2 \cancel{D_\alpha}\ \frac{1}{D}$$

$$\tau = \left(\frac{2L}{\pi}\right)^2 \frac{1}{D}$$

$$n = n_0 e^{-t/\tau} \cos\frac{\pi x}{2L}$$

In general,

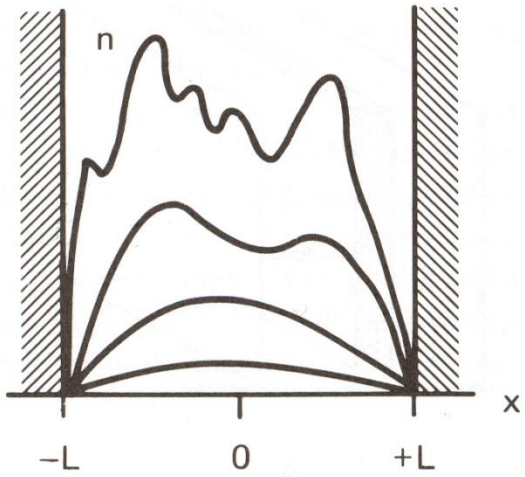

Decay of an initially nonuniform plasma, showing the rapid disappearance of the higher-order diffusion modes.

$$\tau_l = \left(\frac{L}{(l+1/2)\pi} \right)^2 \frac{1}{D_\alpha}$$

$$n = n_0 \left(\sum_l a_l e^{-t/\tau_l} \cos \frac{(l+1/2)\pi x}{L} + \sum_m b_m e^{-t/\tau_m} \sin \frac{m\pi x}{L} \right)$$

Difúze ve válci

- Válec

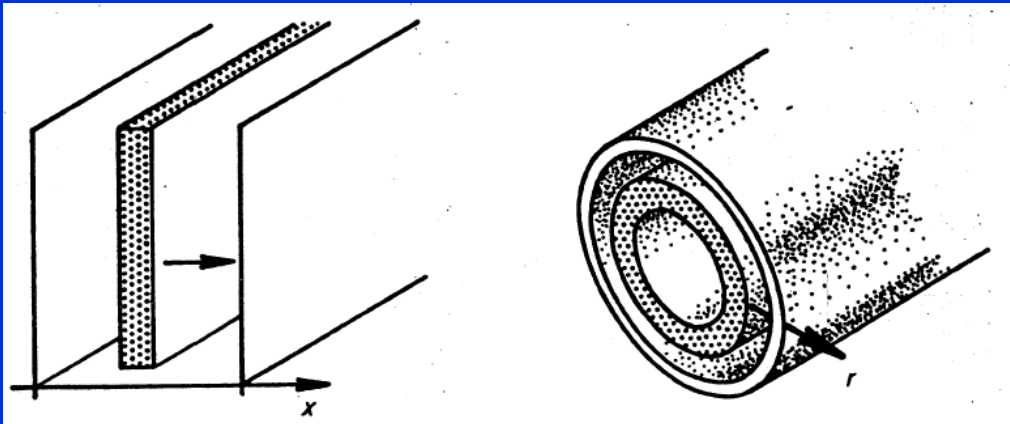

Pohyb plazmatické vrstvy při rovinné a cylindrické konfiguraci. Obrázek slouží k ilustraci rozdílu mezi kosinem a Besselovou funkcí.

$$\frac{1}{T}\frac{\partial T}{\partial t} = \frac{D}{S}\nabla^2 S$$

$$\frac{1}{T}\frac{\partial T}{\partial t} = -\frac{1}{\tau} = \frac{D}{S}\nabla^2 S$$

$$\frac{d^2S}{dr^2} + \frac{1}{r}\frac{dS}{dr} + \frac{1}{D\tau}S = 0$$

$$\frac{\partial N_0}{\partial r^2} + \frac{1}{r}\frac{\partial N_0}{\partial r} + \frac{\partial^2 N_0}{\partial z^2} + \frac{N_0}{D\tau} = 0$$

$$N_0(r,z) = R(r)Z(z)$$

$$\frac{1}{R}\left(\frac{d^2R}{dr^2} + \frac{1}{r}\frac{dR}{r}\right) + \frac{1}{Z}\frac{d^2Z}{dz^2} + \frac{1}{D\tau} = 0$$

$$R(r) = AJ_0(u) = AJ_0(\alpha r)$$

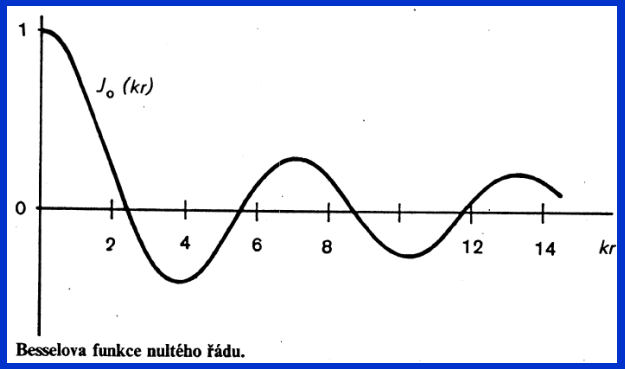

Besselova funkce nultého řádu.

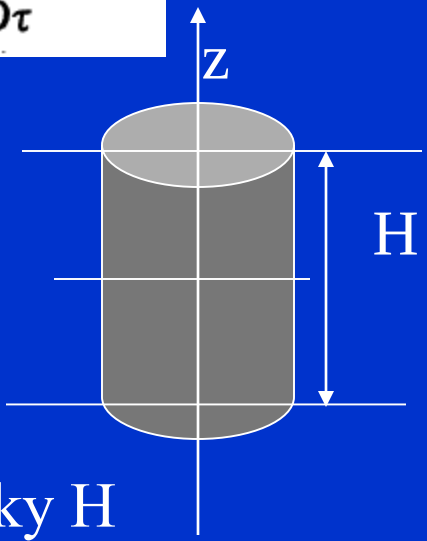

Konečný válec délky H

Okrajové podmínky

$$R(r) = AJ_0\left(\frac{2{,}405r}{r_0}\right)$$

$$\frac{1}{\Lambda_D^{\,2}} = \frac{1}{D\tau_D} = \left(\frac{2.405}{r_0}\right)^2 + \left(\frac{\pi}{H}\right)^2$$

$$N(r,z,t) = G_{11}J_0\left(\frac{2{,}405r}{r_0}\right)\cos\frac{\pi z}{H}e^{-t/\tau_{11}}$$

positive. The solution of the z equation is then

$$Z(z) = C \cos \beta z \tag{10-8-40}$$

The boundary conditions that N_0 must vanish at $z = \pm H/2$ require that $\beta_1 = \pi/H$ for the fundamental mode.

The time-dependent solution for the lowest mode of diffusion can now be written

$$N(r, z, t) = G_{11} J_0\left(\frac{2.405r}{r_0}\right) \cos \frac{\pi z}{H} e^{-t/\tau_{11}} \tag{10-8-41}$$

where

$$\frac{1}{\Lambda_{11}^2} = \frac{1}{\mathscr{D}\tau_{11}} = \left(\frac{2.405}{r_0}\right)^2 + \left(\frac{\pi}{H}\right)^2 \tag{10-8-42}$$

The total solution, containing the radial higher modes as well as the fundamental, is

$$N(r, z, t) = \sum_{i=1}^{\infty} \sum_{j=1}^{\infty} G_{ij} J_0(\alpha_i r) \cos \frac{(2j-1)\pi z}{H} e^{-t/\tau_{ij}} \tag{10-8-43}$$

The diffusion length is given by

$$\frac{1}{\Lambda_{ij}^2} = \frac{1}{\mathscr{D}\tau_{ij}} = \alpha_i^2 + \left[\frac{(2j-1)\pi}{H}\right]^2 \tag{10-8-44}$$

where $\alpha_i r_0$ is the ith root of J_0.

If we assume that $\mathscr{K}^- \gg \mathscr{K}^+$ and $T^- \gg T^+$ and use the relationship

$$\frac{\mathscr{D}}{\mathscr{K}} = \frac{kT}{e} \tag{10-3-2}$$

we find that

$$\mathscr{D}_a \approx \mathscr{D}^- \frac{\mathscr{K}^+}{\mathscr{K}^-} = \frac{kT^-}{e}\mathscr{K}^+ \tag{10-10-5}$$

When $T^+ = T^- = T$, on the other hand,

$$\mathscr{D}_a \approx 2\mathscr{D}^+ = \frac{2kT}{e}\mathscr{K}^+ \tag{10-10-6}$$

B. EXPERIMENTAL RESULTS. The time-dependent diffusion equation for the ambipolar case is

$$\frac{\partial N}{\partial t} = \nabla \cdot (\mathscr{D}_a \nabla N) \tag{10-10-7}$$

If $\mathscr{D}_a$ is taken to be constant and the particle number density is assumed to decay as $e^{-t/\tau}$, the time-independent ambipolar diffusion equation is obtained:

$$\nabla^2 N_0 + \frac{N_0}{\mathscr{D}_a \tau} = 0 \tag{10-10-8}$$

This equation is solved for specific problems by the methods of Section 10-8. $\mathscr{D}_a$ is given in terms of the decay constant τ, and the appropriate diffusion length Λ, by the equation

$$\mathscr{D}_a = \frac{\Lambda^2}{\tau} \tag{10-10-9}$$

Hence $\mathscr{D}_a$ may be evaluated from a determination of the rate of decay of the charged particle density in a cavity after the ionization source has been turned off.

Gas in a cavity may be broken down to form a plasma by the application of microwaves, and the electron density may be determined by measuring the shift in the frequency of resonance[16] (see also Section 12-7). The experimental values of N are then plotted as a function of t on a semilogarithmic scale. If the plot is linear, indicating that the decay is exponential as assumed, the diffusion coefficient may be obtained from the slope. Since the sensitivity of the microwave method is not great enough to allow determination of electron densities below about $10^7/\text{cm}^3$, the diffusion coefficient measured is $\mathscr{D}_a$. Here we assumed that the effects of electron attachment and recombination are negligible, as is frequently the case in practice. The techniques of analyzing diffusion data when attachment and recombination must be considered are discussed by Brown in Chapters 6 and 8 of his book and in Section 12-8 of this book.

Sometimes the plots are not linear on a semilogarithmic scale even though diffusion is the controlling mechanism. Nonlinearity, in this case, indicates the simultaneous presence of more than one mode of diffusion. (The higher modes may be excited by breaking down the gas in an asymmetric discharge.) The discussion in Section 10-8 shows that the higher modes decay faster than the fundamental mode, and regardless of its initial complexity

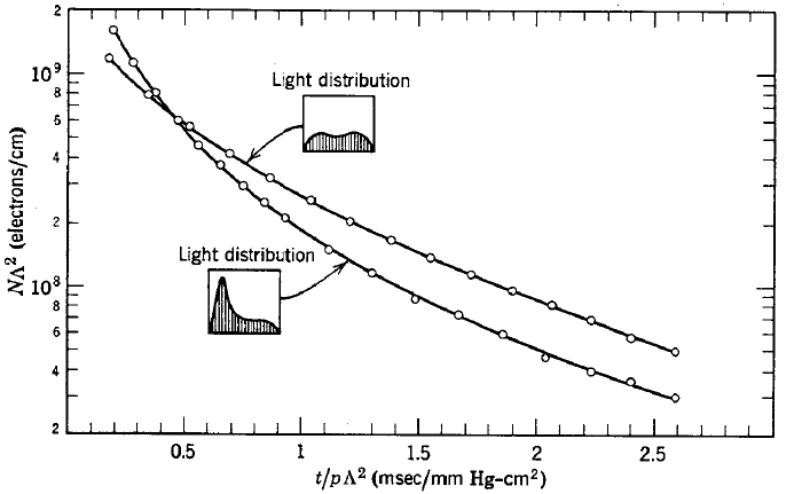

FIG. 10-10-1. The influence of the initial spatial distribution on the decay of electron density. K. B. Persson and S. C. Brown, *Phys. Rev.* **100,** 729 (1955).

the plot will approach linearity for large values of t. Two plots corresponding to different discharge conditions and different combinations of modes are shown in Fig. 10-10-1.[17] Note that the curves become straight and parallel to one another at large t, each having the slope corresponding to the lowest mode of diffusion. The "light distributions" shown in the figure are qualitative measures of the initial spatial electron density at the start of the decay period. They were obtained by scanning the discharge with a photomultiplier and slit system and displaying the signal on an oscilloscope.

Theory predicts that $\mathscr{D}_a$ will vary inversely with the pressure if the electrons and ions are in thermal equilibrium with the gas at a temperature that is held constant as the gas pressure is varied. A verification of this prediction taken from a paper on ambipolar diffusion in helium by Biondi and Brown,[18] is presented in Fig. 10-10-2. (The identity of the ions to which these data refer is uncertain. The $\mathscr{D}_a p$ products for He^+ and He_2^+ ions in helium are given in Table 10-10-1.) Figure 10-10-3, taken from the same

5.3 Steady state solutions

$$\frac{\partial n}{\partial t} - D_\alpha \nabla^2 n = Q(\vec{r})$$

In steady state, we have $\frac{\partial n}{\partial t} = 0$

$$\nabla^2 n = -\frac{1}{D} Q(\vec{r})$$

- For constant Ionization function , Q=Zn

$$\nabla^2 n = -\frac{Z}{D} n$$

The solution is Cosine or Bessel function.

- Plane source

$$Q(\vec{r}) = Q_0 \delta(0)$$

$$\frac{d^2 n}{dx^2} = -\frac{Q_0}{D}\delta(0)$$

$$n = n_0 (1 - \frac{|x|}{L})$$

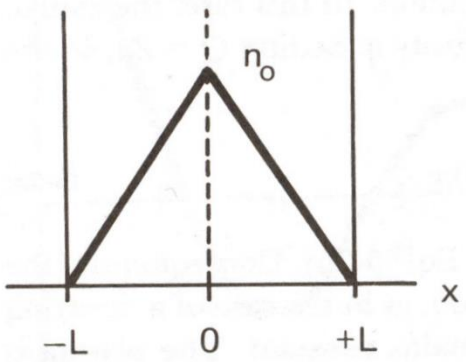

The triangular density profile resulting from a plane source under diffusion.

- Line source

$$\frac{1}{r}\frac{\partial}{\partial r}(r\frac{\partial n}{\partial r}) = 0$$

$$n = n_0 \ln(a/r)$$

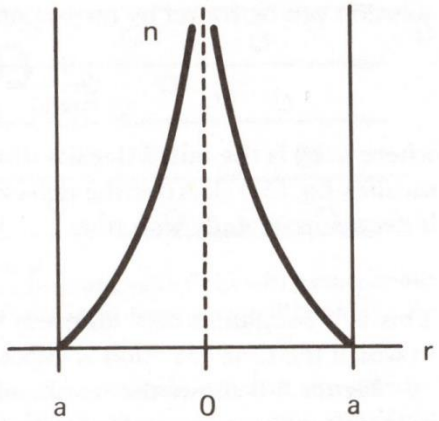

The logarithmic density profile resulting from a line source under diffusion.

- A

Vývoj plazmatu řízený difúzi

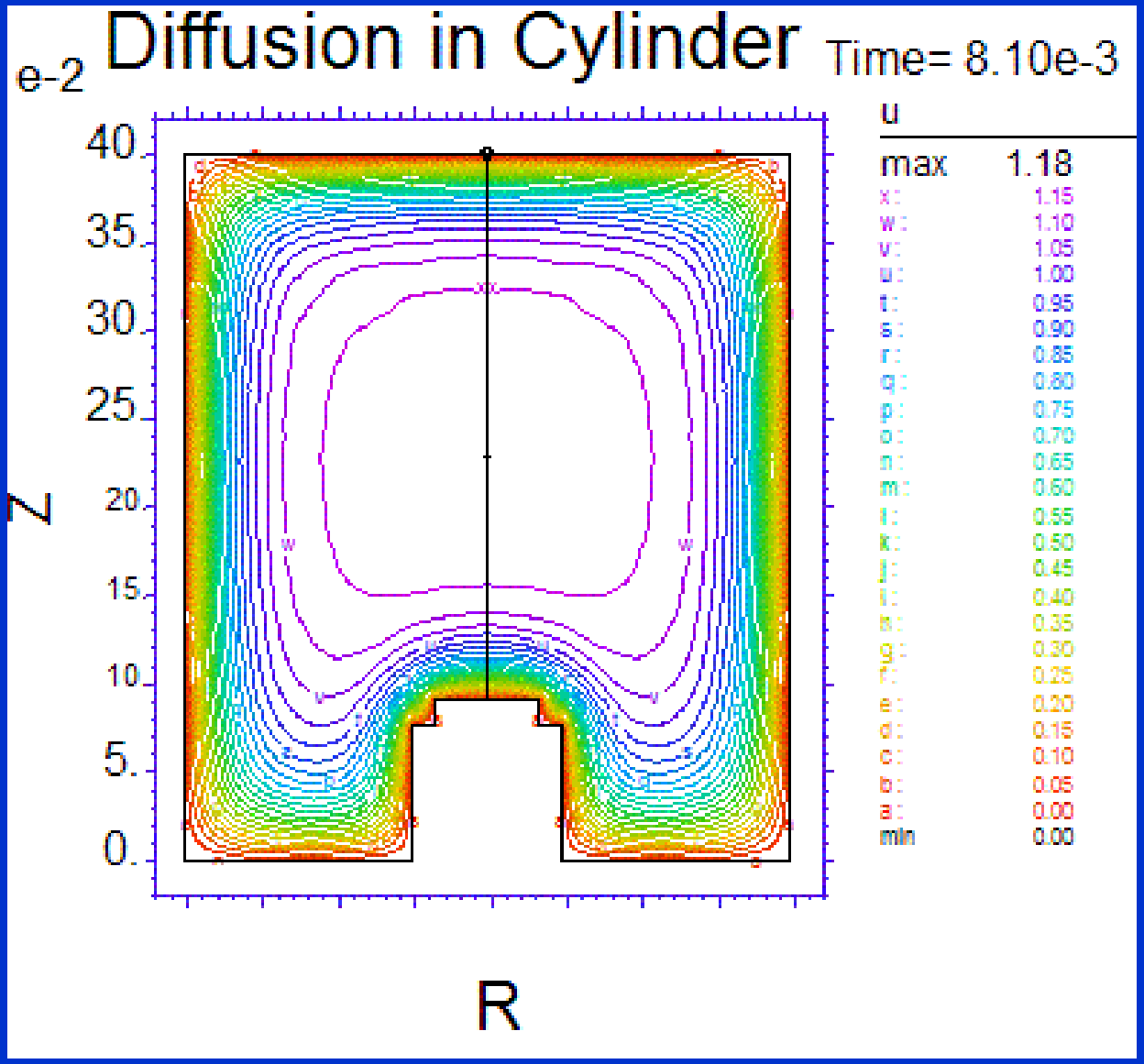

Radiální a axiální rozložení elektronů a iontů

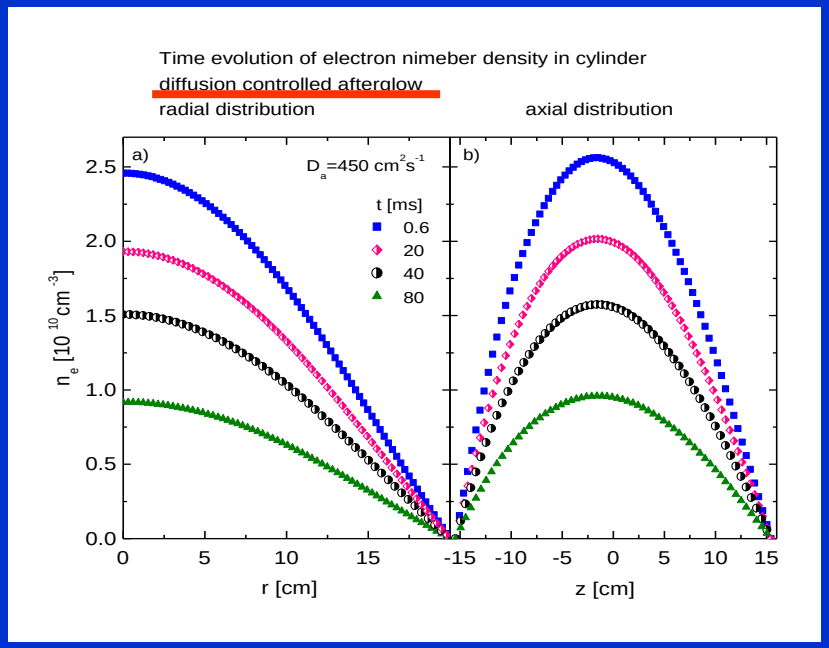

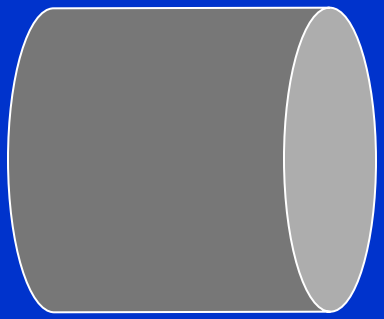

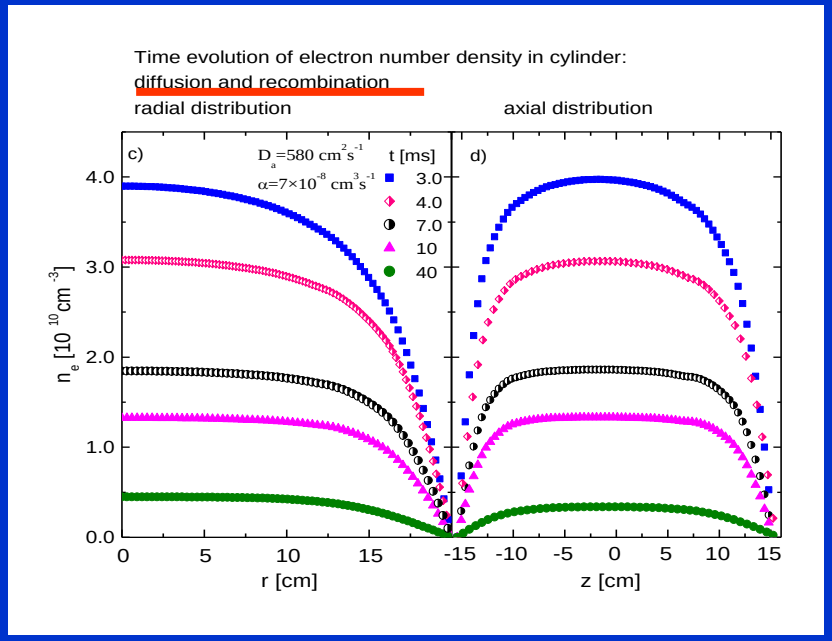

CALCULATION OF PLASMA DECAY IN CYLINDER

DIFFUSION AND RECOMBINATION

τ_D=60 ms, α=1x10^{-7}cm^{3}s^{-1} and α=5x10^{-9}cm^{3}s^{-1}

$$\tau = \left(\frac{2L}{\pi}\right)^2 \frac{1}{D}$$

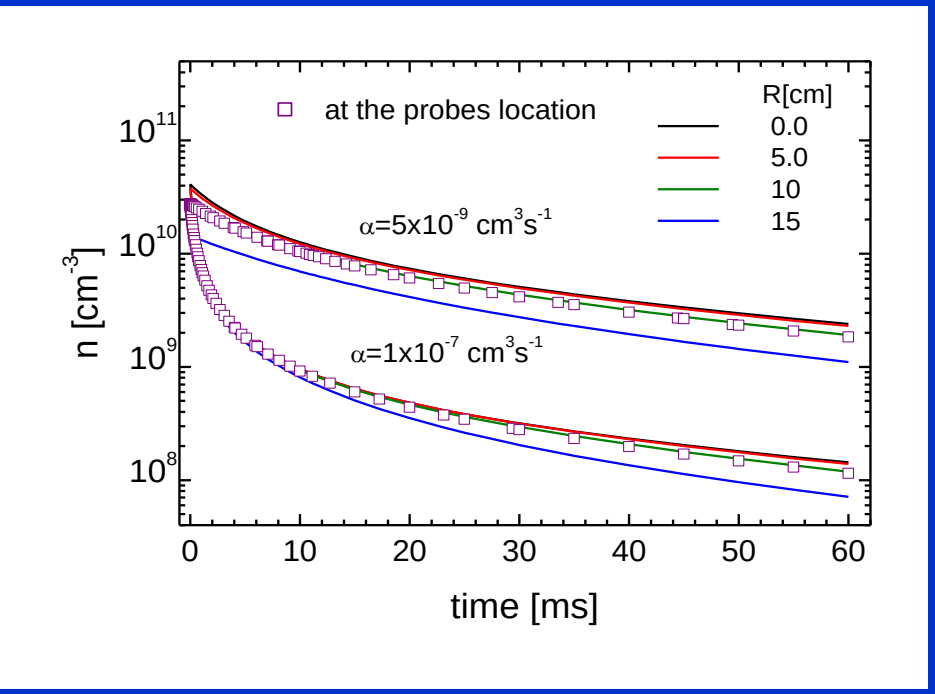

Time evolution

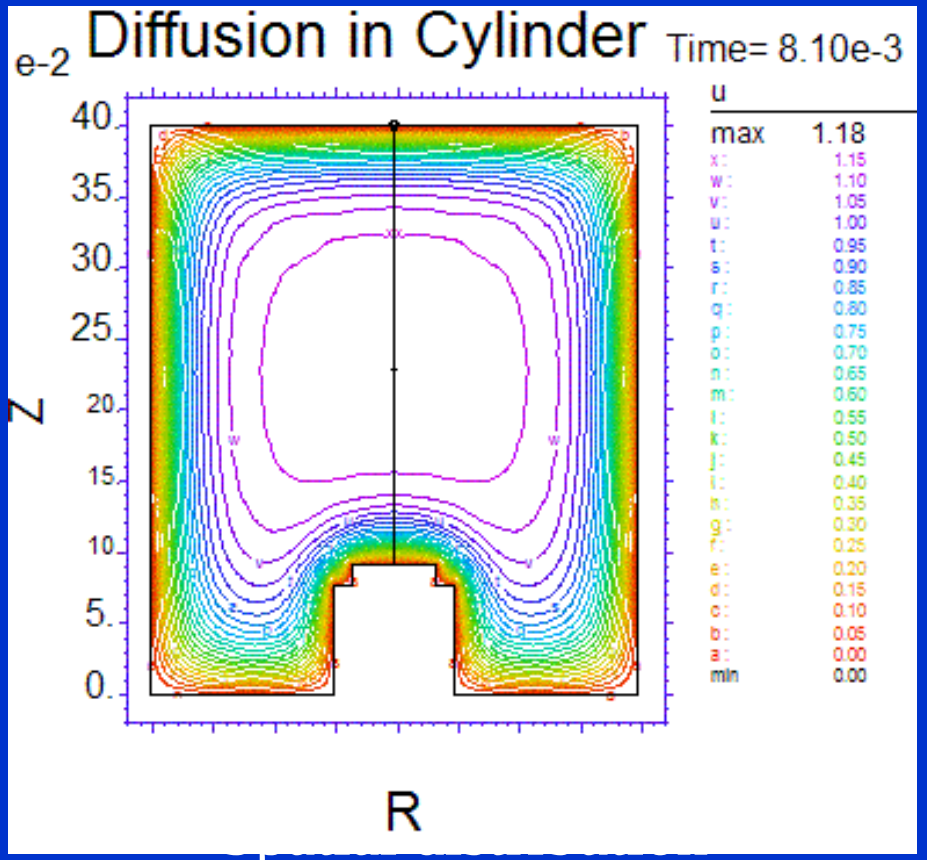

after 8 ms

Decay in diffusion and recombination governed plasma

$$\frac{dn_e}{dt} = -\alpha\, n_e^2 + D_a \nabla^2 n_e$$

$$\frac{dn_e}{dt} = -\alpha\, n_e^2 - \frac{D_a}{\Lambda^2} n_e$$

n_0

$$\frac{1}{n_e} - \frac{1}{n_0} = \alpha (t_e - t_0)$$

$$n_e = n_0 \exp(-\nu t)\ ; \nu = D_a / \Lambda^2$$

$$\frac{1}{n_e} = \alpha\ \frac{\exp(\nu t) - 1}{\nu} + \frac{1}{n_0} \exp(\nu t)$$

Diffusion and recombination

$$\frac{dn_e}{dt} = -\alpha\, n_e^2 - \frac{D_a}{\Lambda^2} n_e$$

$$\frac{1}{n_e} = \alpha\, \frac{\exp(\nu t) - 1}{\nu} + \frac{1}{n_0} \exp(\nu t)$$

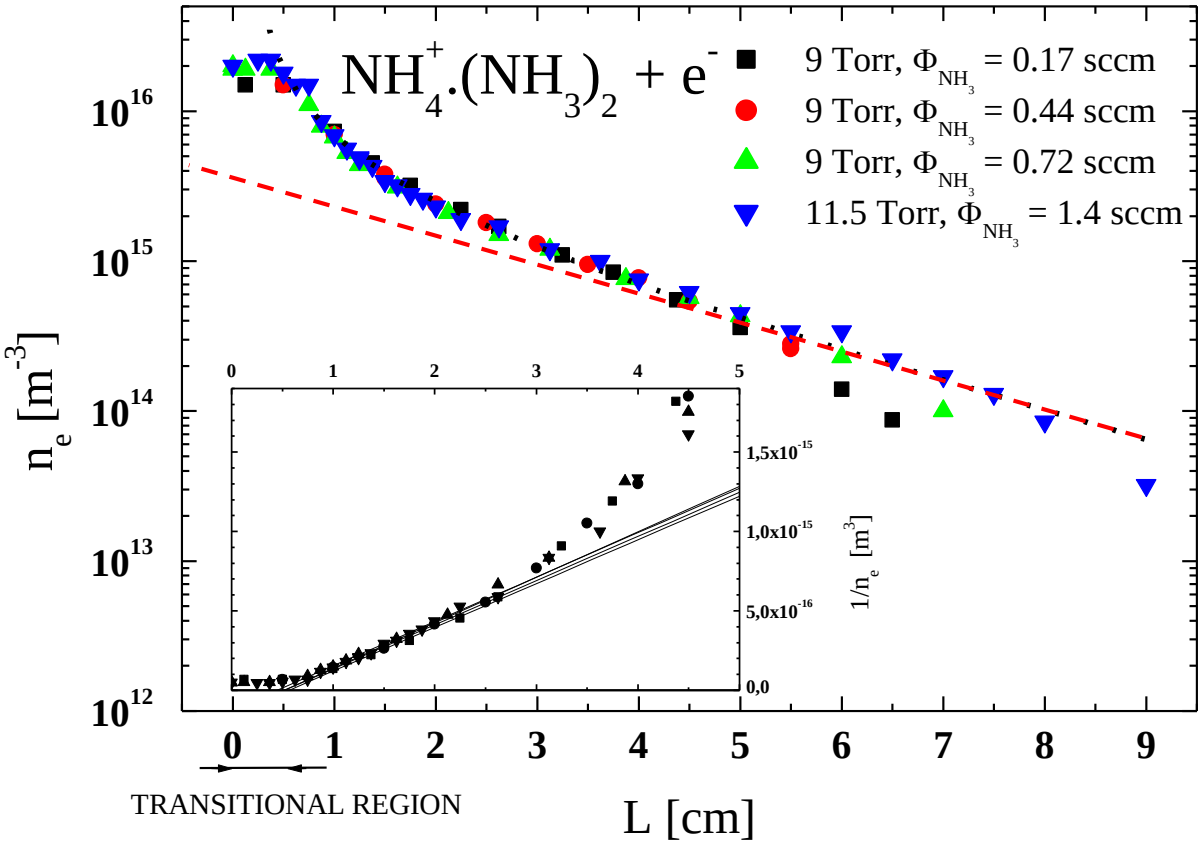

AISA vypočtené difúzní ztráty

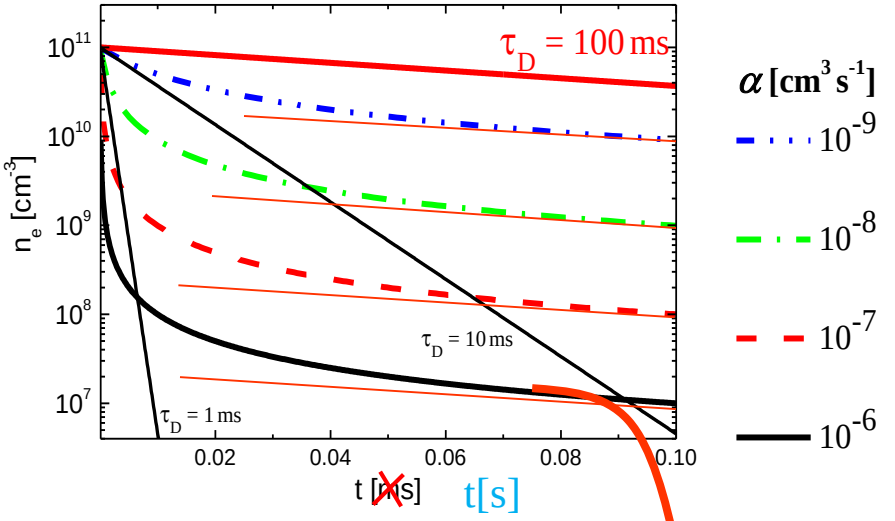

Free diffusion

Experimentální data

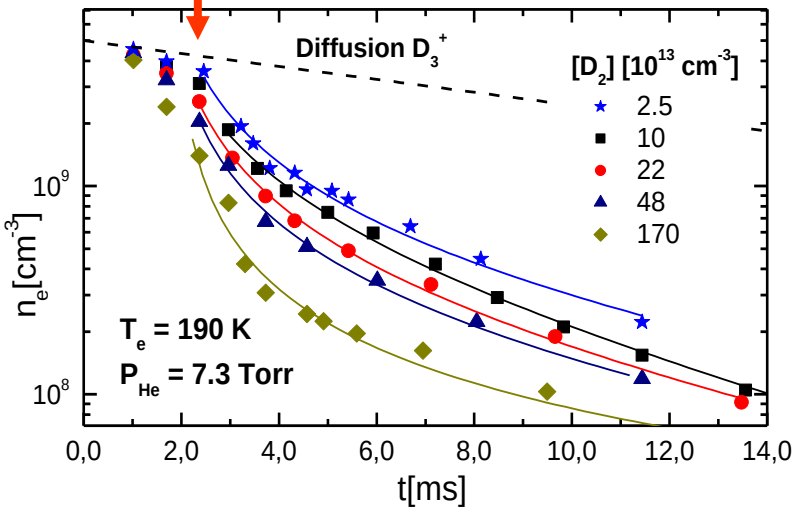

Difúze v plazmatu

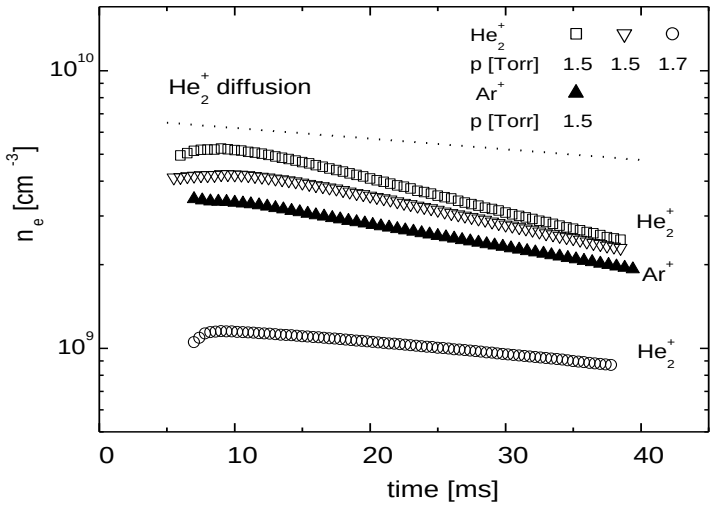

$$T = T_0 e^{-t/\tau} = T_0 e^{-\left(\frac{2L}{\pi}\right)^2 Dt}$$

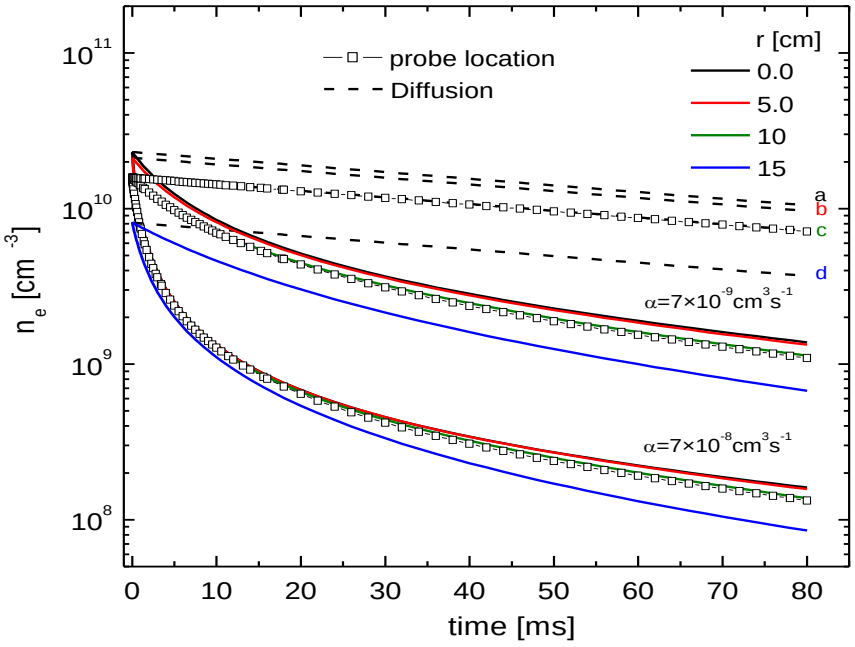

Recombination of $H_3^+(v=0)$ in He/Ar/H_2 Stationary afterglow

PULSE REGIME

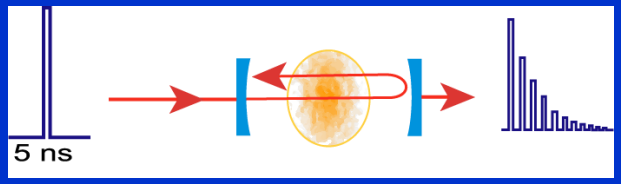

TEST TUBE

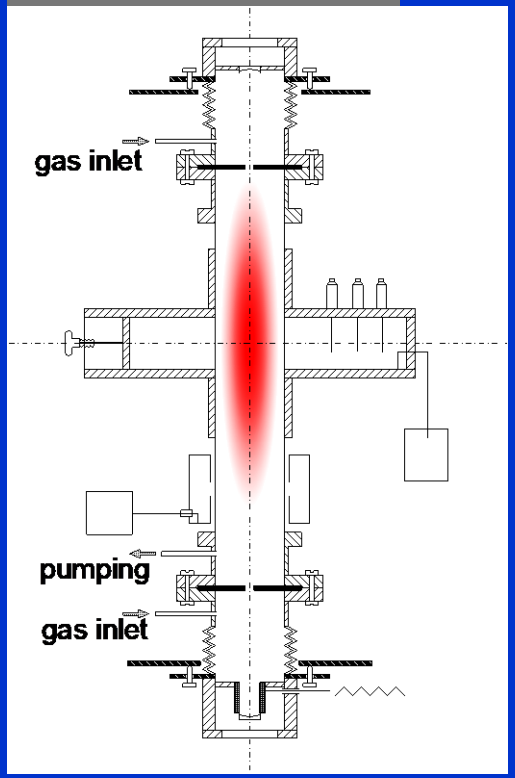

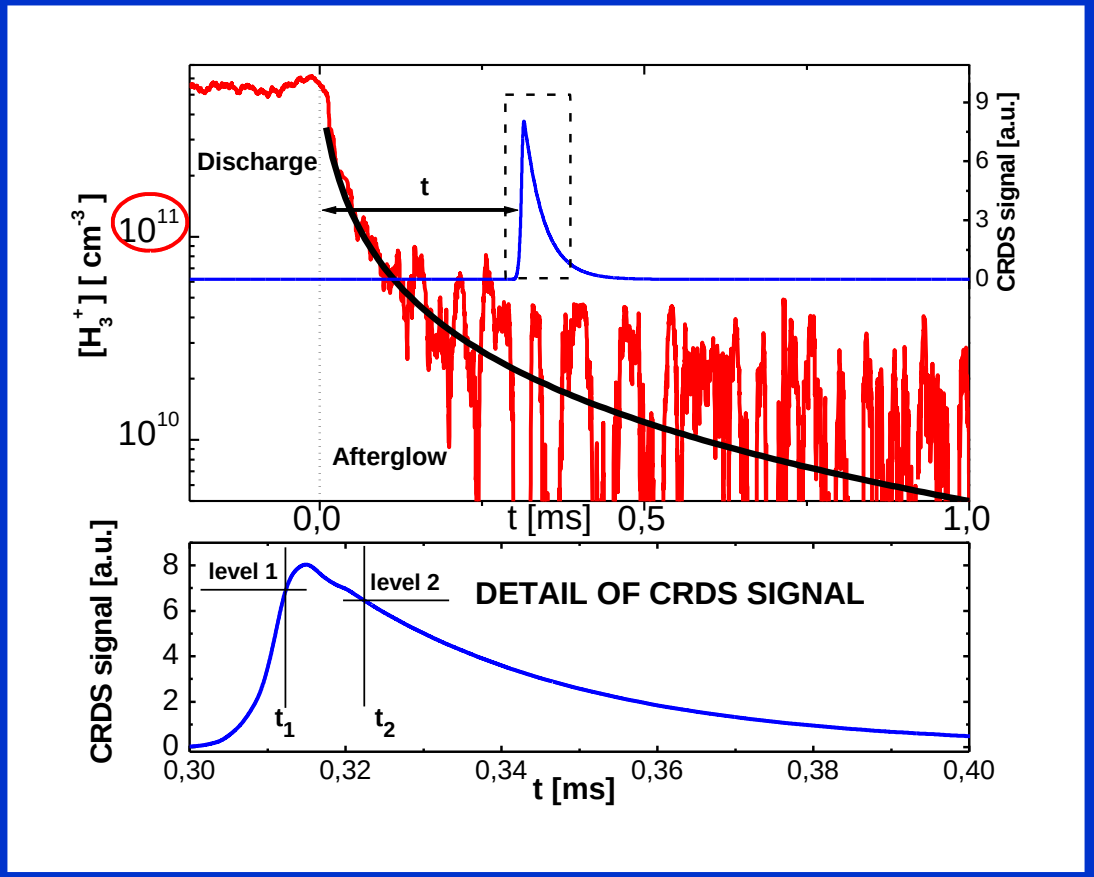

Rate Law

- **rate = $k[A]^x[B]^y$**
- **rate order = x + y**
- **knowledge of order can help control reaction**
- **rate must be experimentally determined**

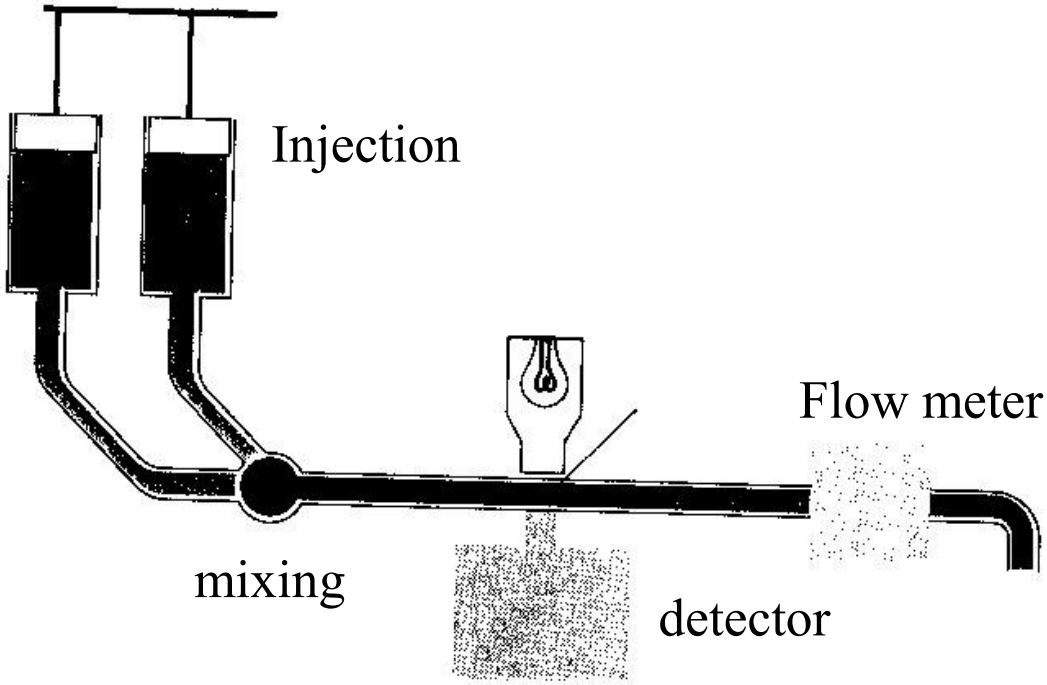

FA– Flowing Afterglow principle

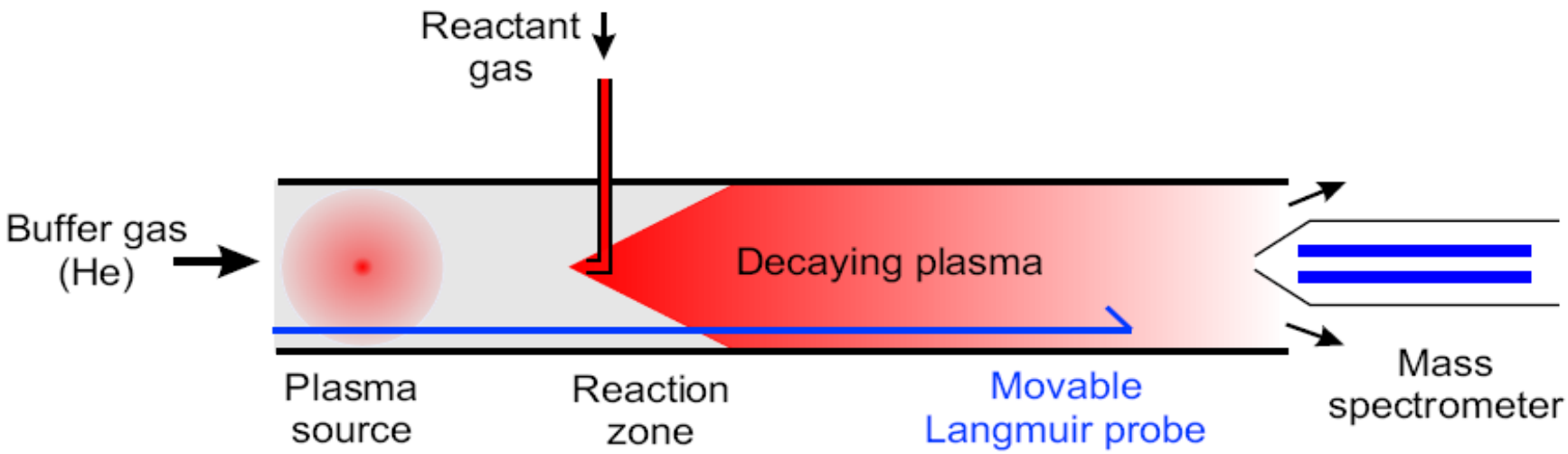

Figure 1.1: The basic principle of FA and FALP techniques.

Flowing afterglow

FA

FALP

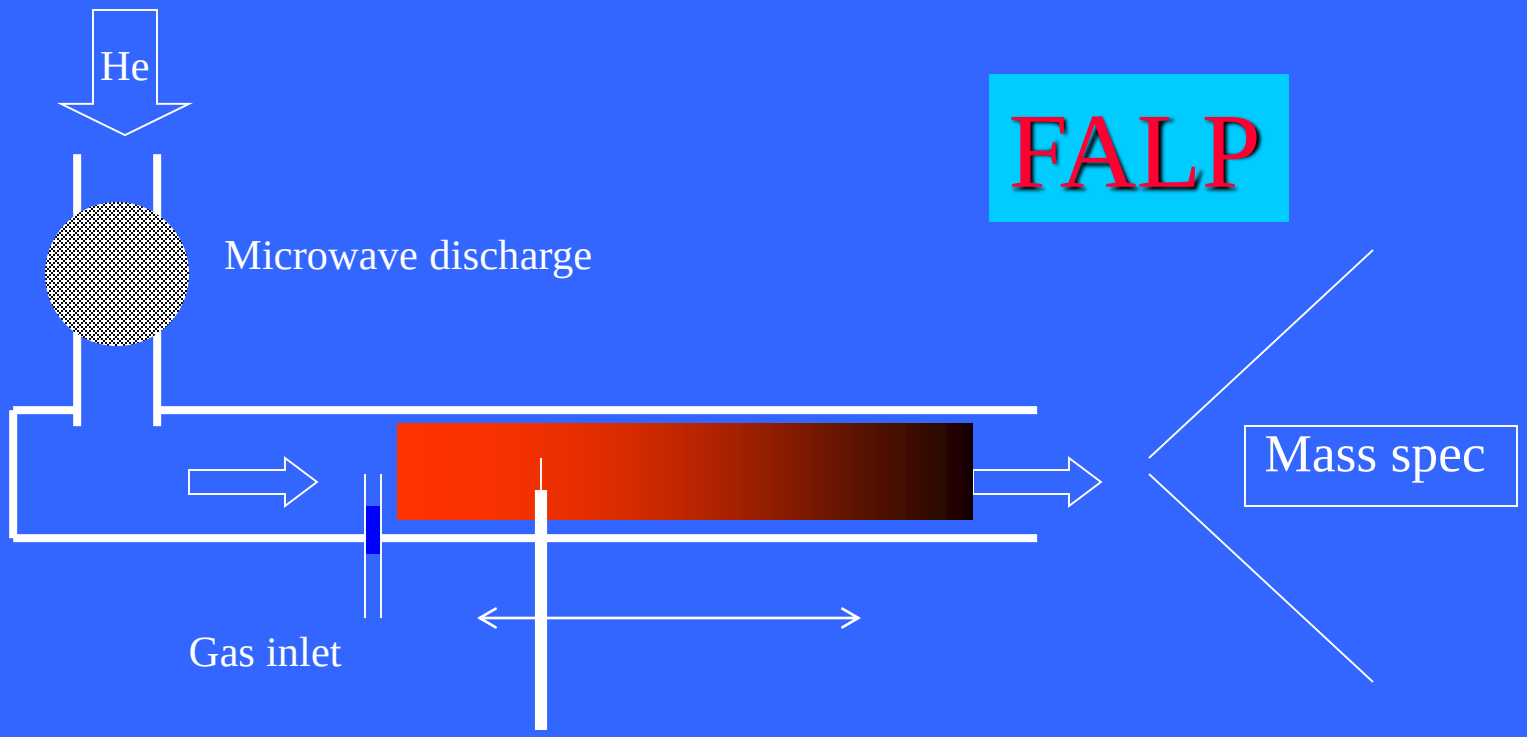

Langmuir probe measures $n_e(z)$

$z \sim v_{flow} t$

Techniques for study of IMR – FALP 1965

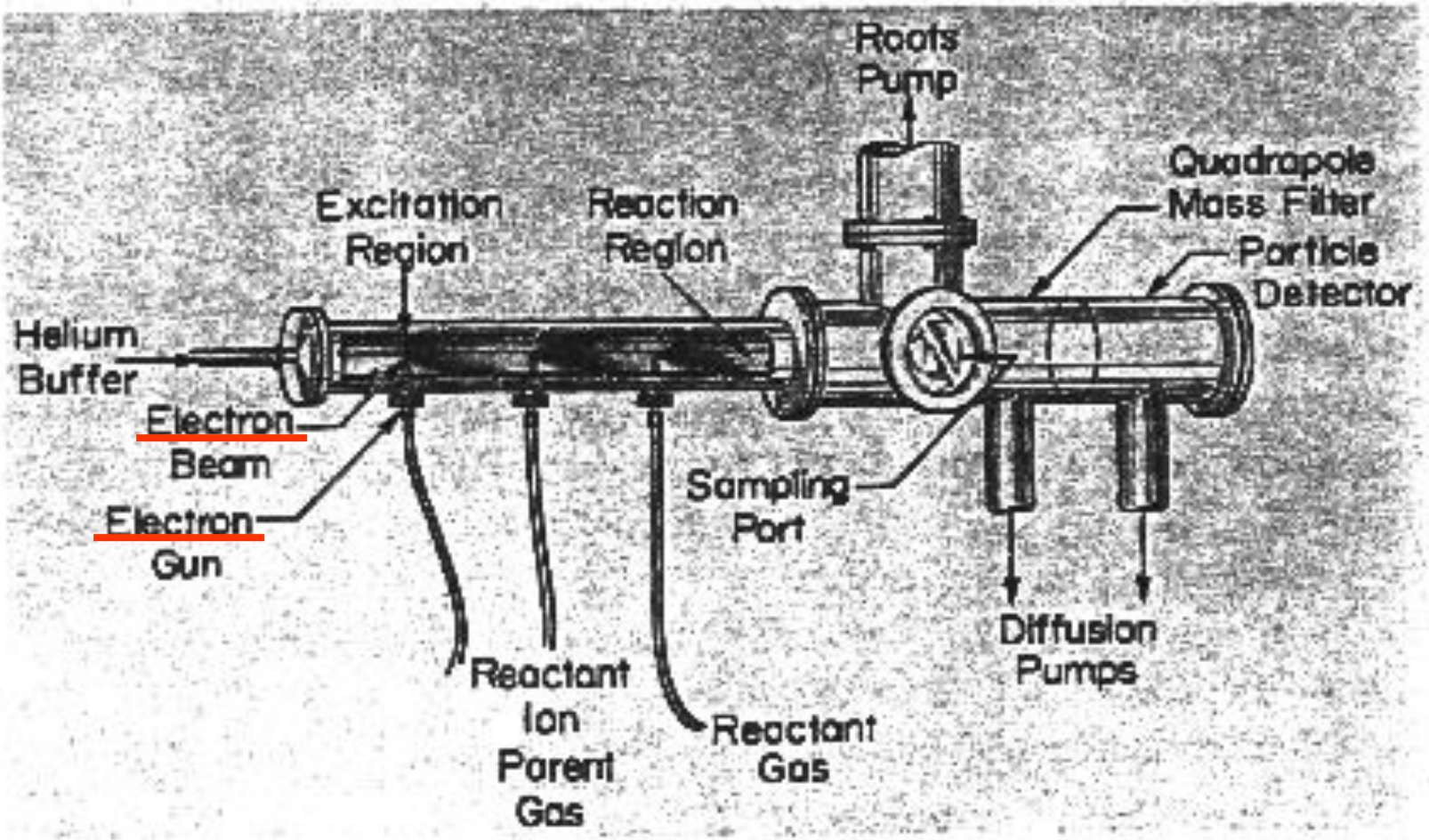

FIG. 1. Pictorial representation of the flowing afterglow tube.

Experimental studies of IMR ➔FA

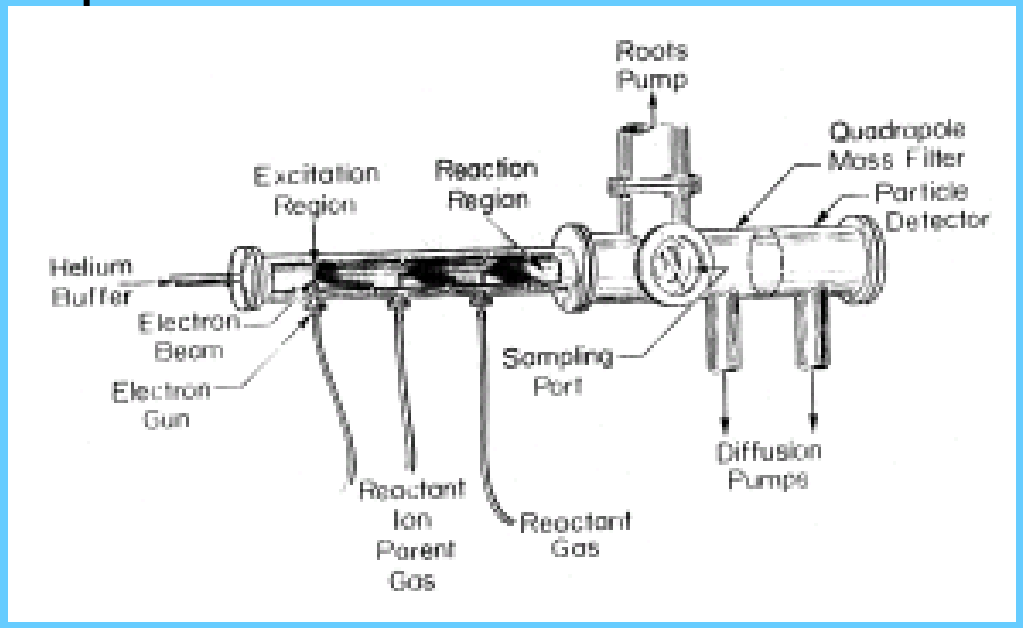

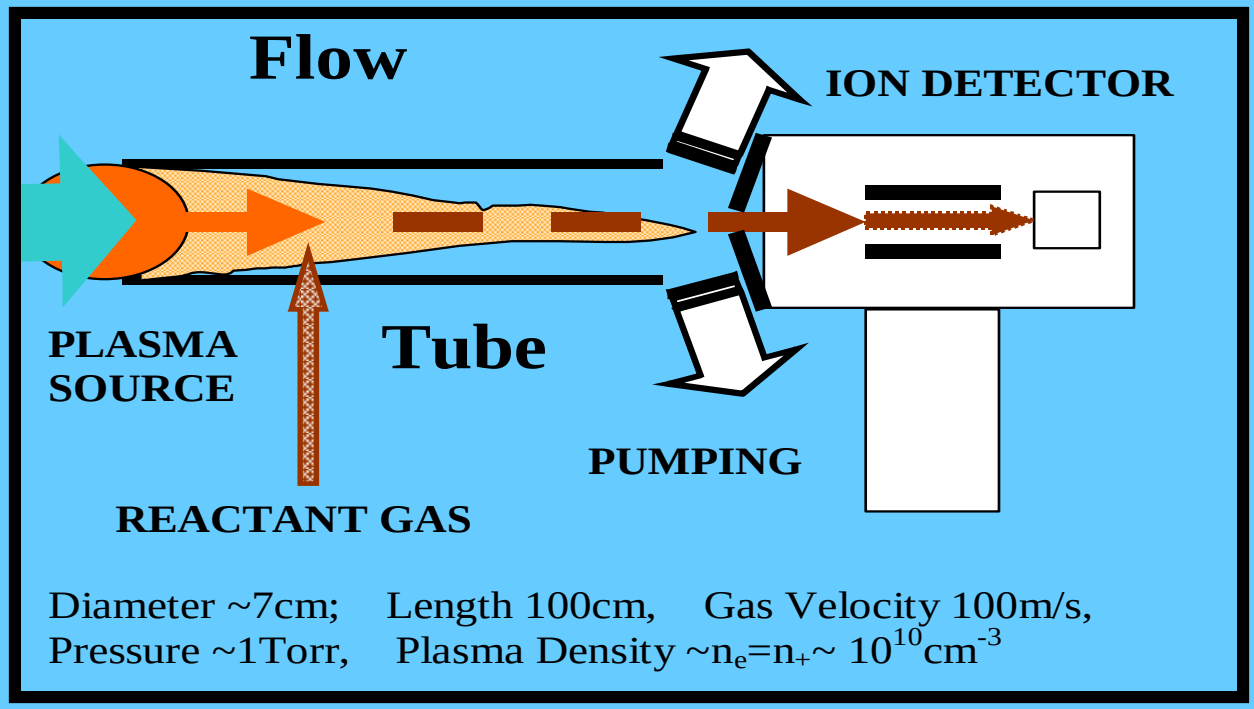

VT-HPFA

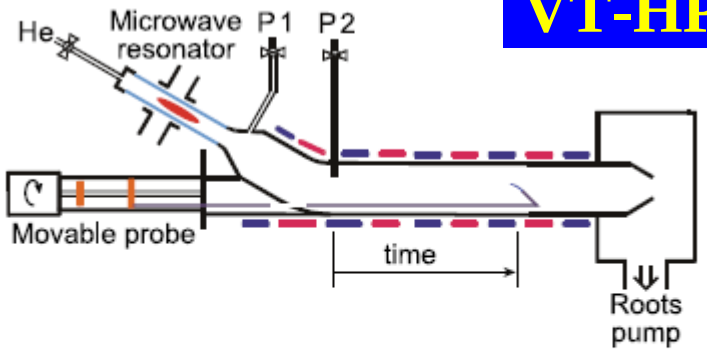

Fig. 1. (Color online) Schematic of FALP apparatus. Buffer gas flows from discharge region (upper left corner) towards the Roots pump (right). The plasma formed in the discharge is driven along the flow tube. The plasma parameters on the axis of the flow tube are measured by an axially movable Langmuir probe (from the port P2 up to the end of the flow tube).

Eur. Phys. J. D **54**, 391–398 (2009)
DOI: 10.1140/epjd/e2009-00144-3

THE EUROPEAN PHYSICAL JOURNAL D

Regular Article

Non-Maxwellian electron energy distribution function in He, He/Ar, He/Xe/H_2 and He/Xe/D_2 low temperature afterglow plasma

R. Plasil[1,a], I. Korolov[1,2], T. Kotrik[1], P. Dohnal[1], G. Bano[2], Z. Donko[2], and J. Glosik[1]

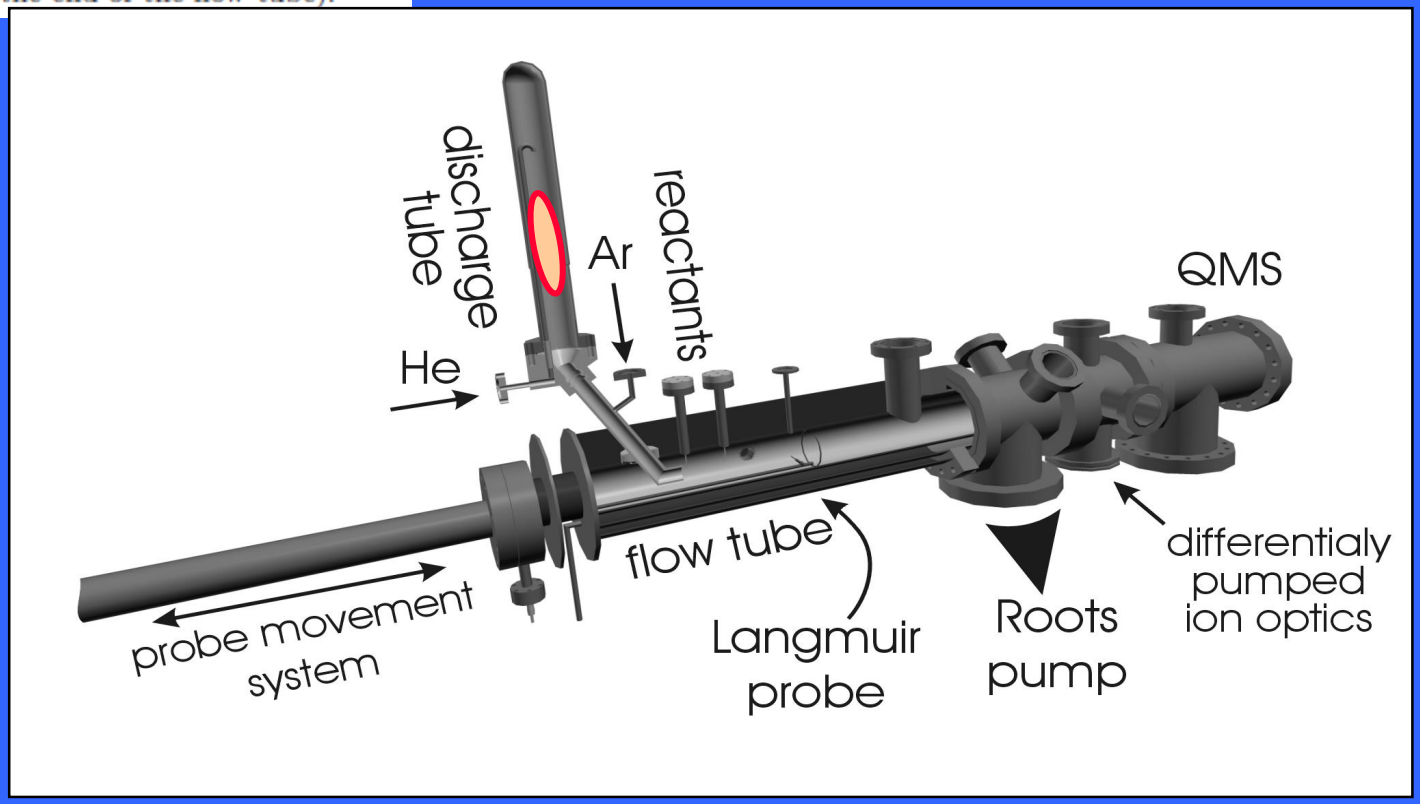

FA– Flowing Afterglow

100-700 K

$$H_3^+ + CO \Rightarrow HCO^+ + H$$

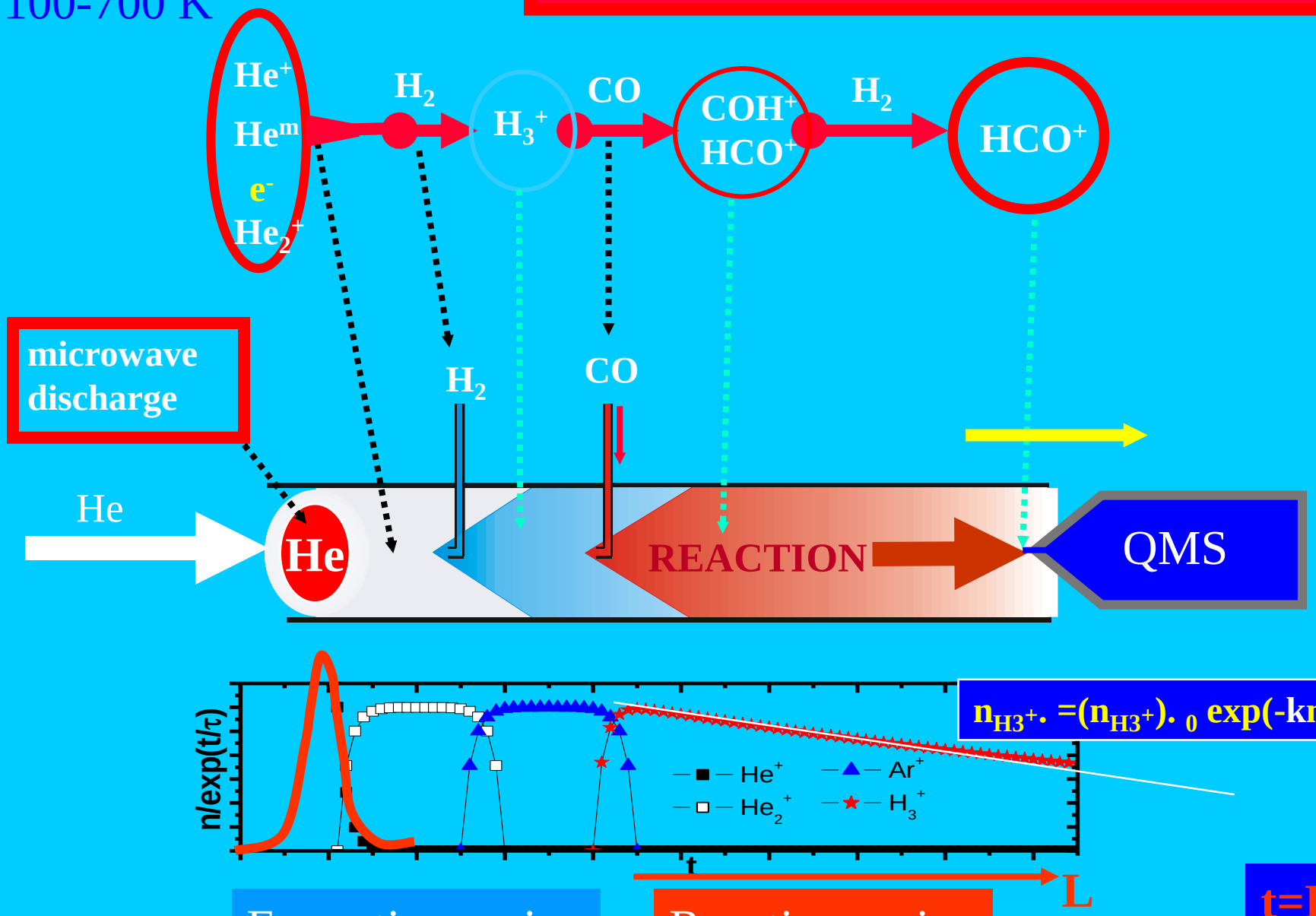

Principle of Flowing Afterglow Langmuir Probe - FALP

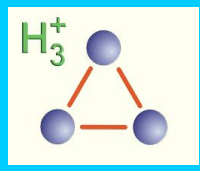

microwave discharge

T_e~ 2eV

Formation of H_3^+ in He/Ar/H_2 mixture (10 Torr)

He^+
He^m
e^-
He_2^+

Ar

Ar^+

H_2

ArH^+, H_2^+

H_2

$H_3^+ + e^-$

H_2

$H_5^+ + e^-$

μw

Ar

H_2

He

He

RECOMBINATION

2eV

T_e

$T_e = T_i = T_G$ = 170 - 260K

Table 1. Table of reactions taking place in He/Ar plasma. The values in the middle column are calculated for 80 K if temperature dependence was known.

N	Reaction	Rate coef. [cm^3s^{-1}], [cm^6s^{-1}]	Ref.
1	$He^+ + He + He \rightarrow He_2^+ + He$	1×10^{-31}	[*Ikezoe et al.*, 1987]
2	$He^m + He^m \rightarrow He^+ + He + e^-$	5×10^{-9}	[*Deloche et al.*, 1976]
3	$\rightarrow He_2^+ + e^-$	5×10^{-9}	[*Urbain et al.*, 1999]
4	$He_2^+ + e^- \rightarrow 2He$	$<5\times10^{-10}$	[*Deloche et al.*,1976]
Ar+ formation and destruction			
5	$He^+ + Ar \rightarrow Ar^+ + He$	$<1\times10^{-13}$	[*Johnsen et al.,* 1973]
6	$He^m + Ar \rightarrow Ar^+ + He + e^-$	7×10^{-11}	[*Glosík et al.*, 1999]
7	$He_2^+ + Ar \rightarrow Ar^+ + 2He$	2×10^{-10}	[*Ikezoe et al.*, 1987]
8	$Ar^+ + e^- + e^- \rightarrow Ar + e^-$	1.1×10^{-17}	[*Kotrík et al.*, 2011]
9	$Ar^+ + e^- + He \rightarrow Ar + He$	2.7×10^{-26}	[*Bates et al.*, 1965]
Ar_n^+ formation and destruction			
10	$Ar^+ + Ar + He \rightarrow Ar_2^+ + He$	1.3×10^{-31}	[*Smirnov*, 1977]
11	$Ar_2^+ + e^- \rightarrow 2Ar$	8×10^{-7}	[*Okada et al.*, 1993]
12	$Ar_2^+ + Ar + Ar \rightarrow Ar_3^+ + Ar$	3.2×10^{-30}	[*Hiraoka et al.*, 1989]
13	$Ar_2^+ + Ar + He \rightarrow Ar_3^+ + He$	5.5×10^{-31}	[*Smirnov*, 1977]
14	$Ar_3^+ + e^- \rightarrow 3Ar$	3.6×10^{-5}	Estimate
15	$Ar_3^+ + Ar + He \rightarrow Ar_4^+ + He$	5.5×10^{-31}	Estimate
16	$Ar_4^+ + e^- \rightarrow 4Ar$	3.6×10^{-5}	Estimate

Techniques for study of IMR

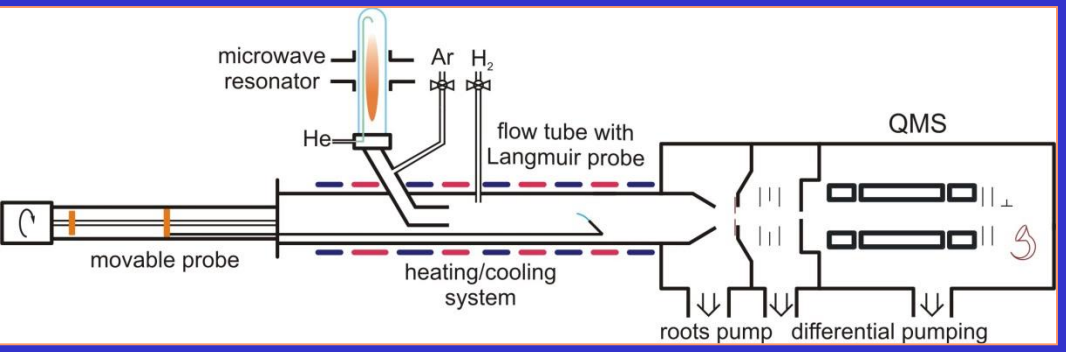

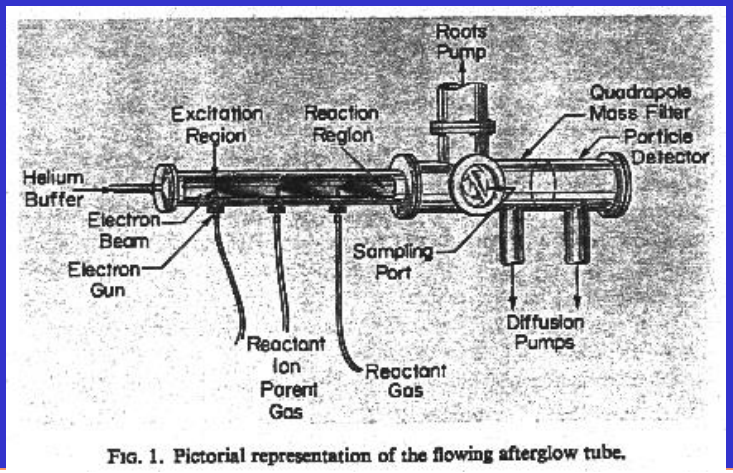

FIG. 1. Pictorial representation of the flowing afterglow tube.

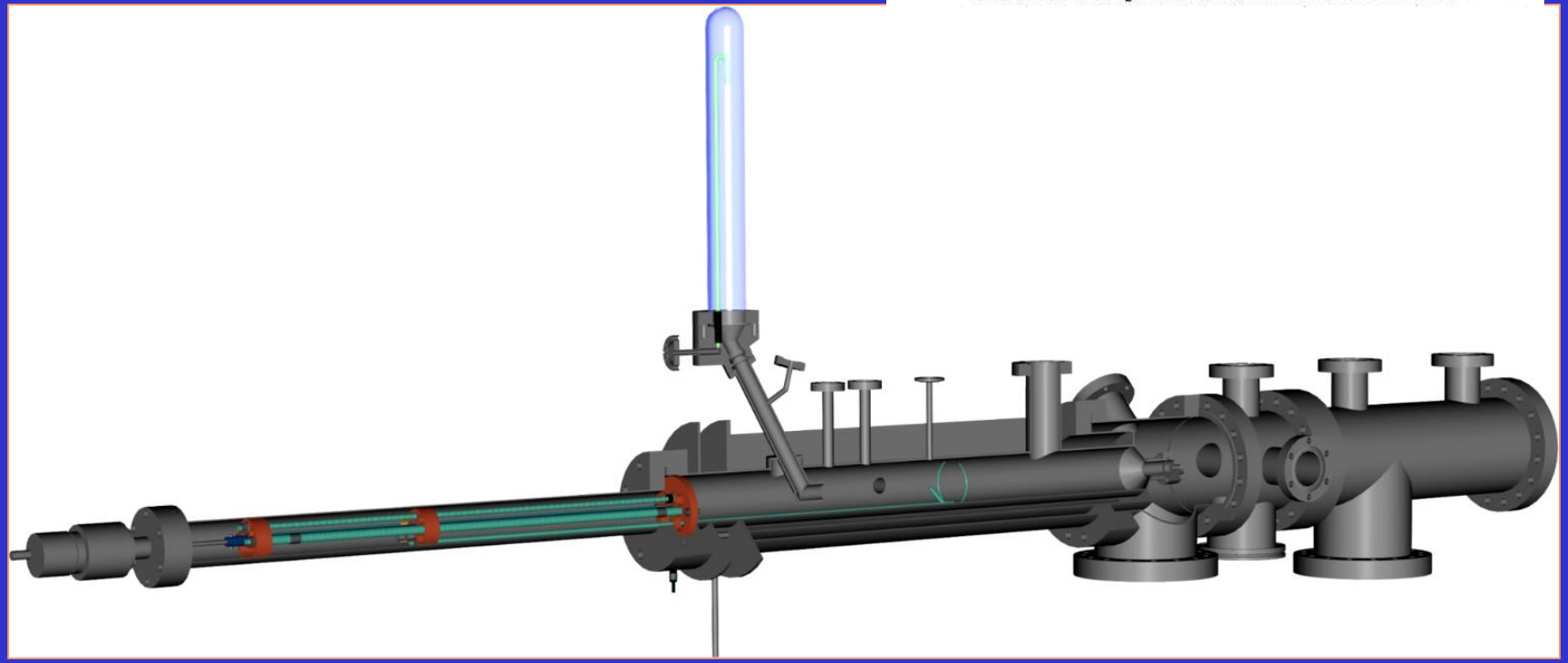

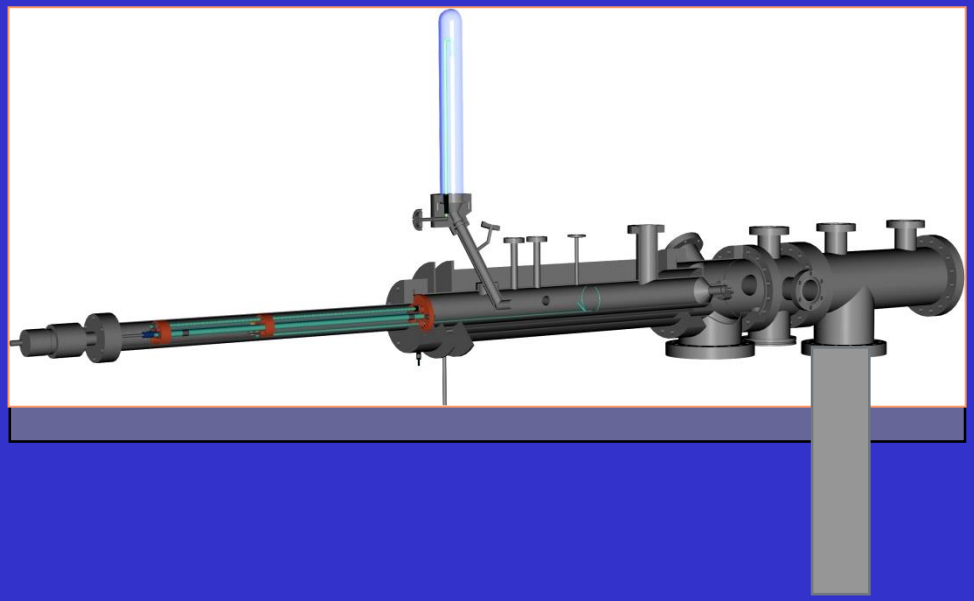

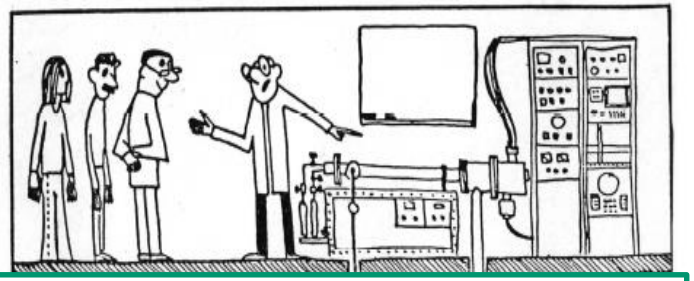

Two faces of a flowing afterglow.

(Opening picture to a seminar in Boulder, 1980)

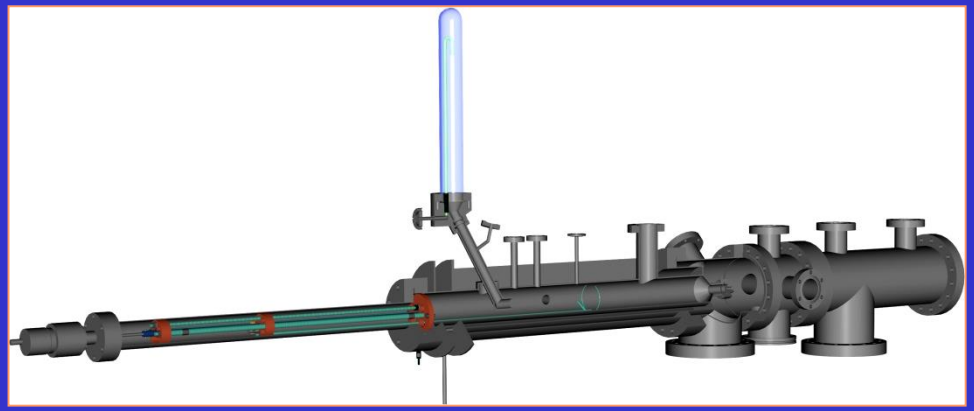

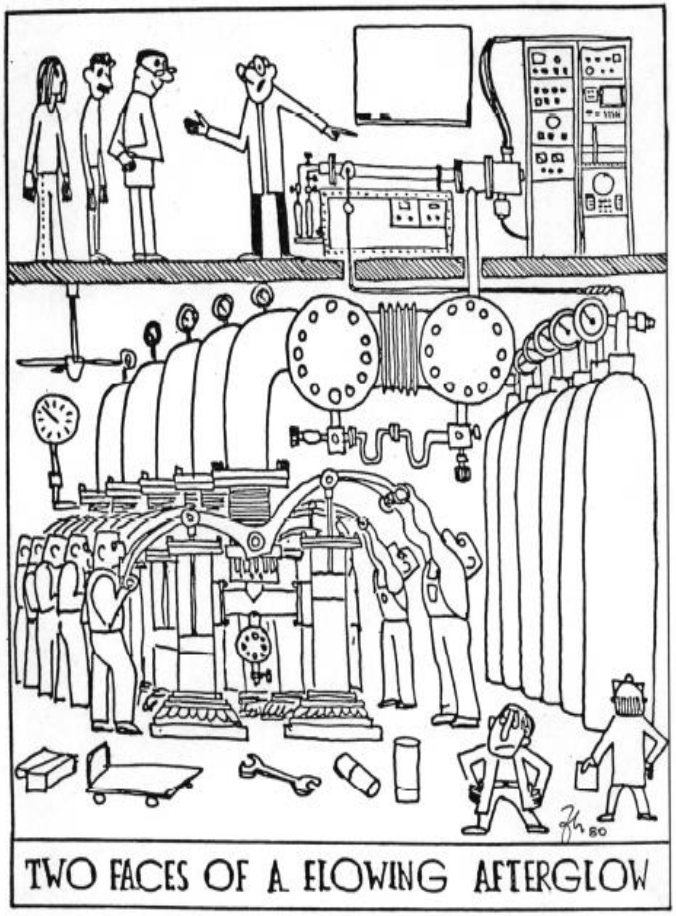

Two faces of a flowing afterglow.

(Opening picture to a seminar in Boulder, 1980)

Techniques for study of IMR – reality

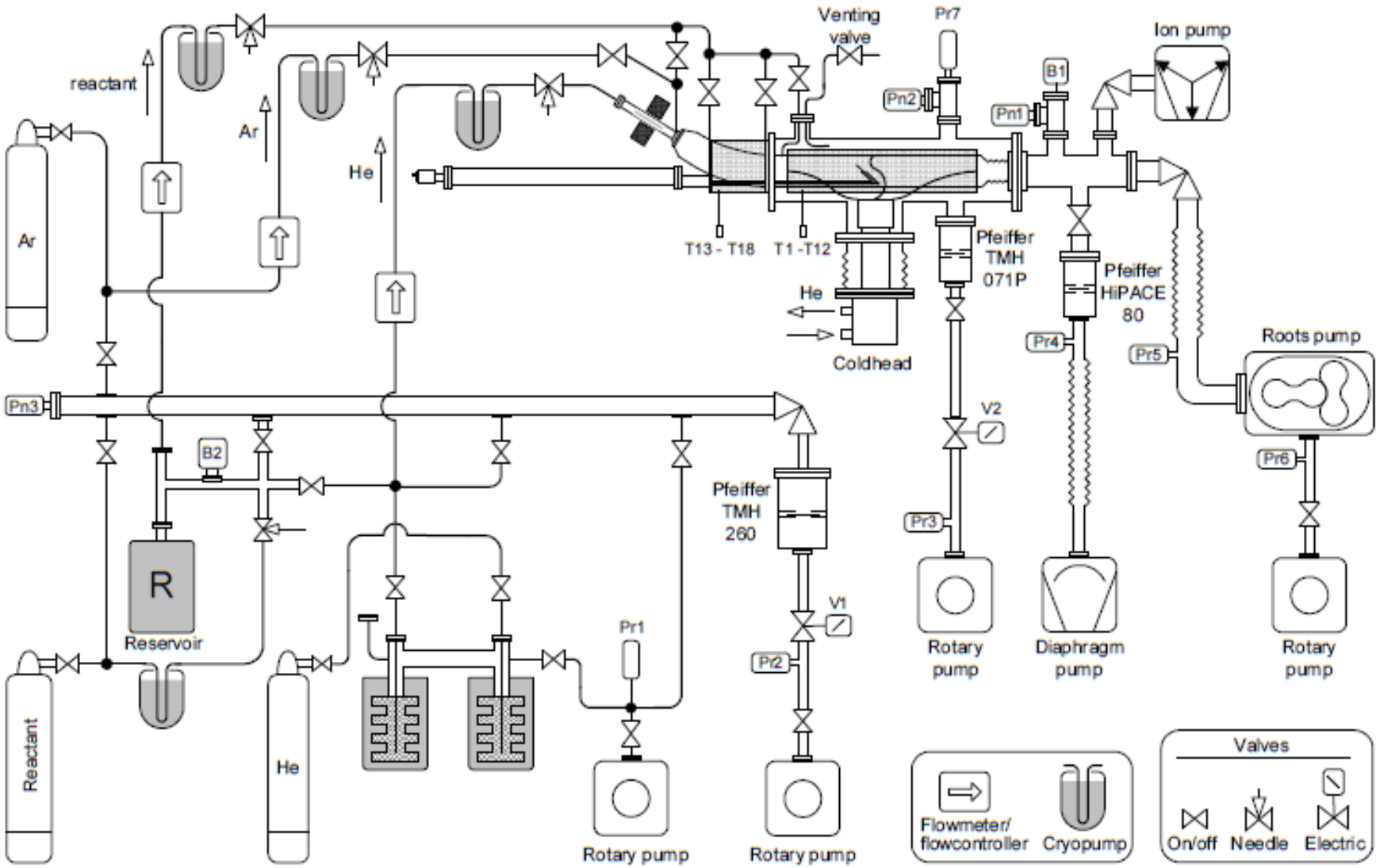

Figure 2.4 Vacuum scheme of the Cryo-FALP II apparatus.

FLOWING AFTERGLOW

Ion-molecule reactions

FA

FA	**E.E.Ferguson, Fehsenfeld, ~1965**
FALP	**J. Hasted, D. Smith, N. Adams, ….**

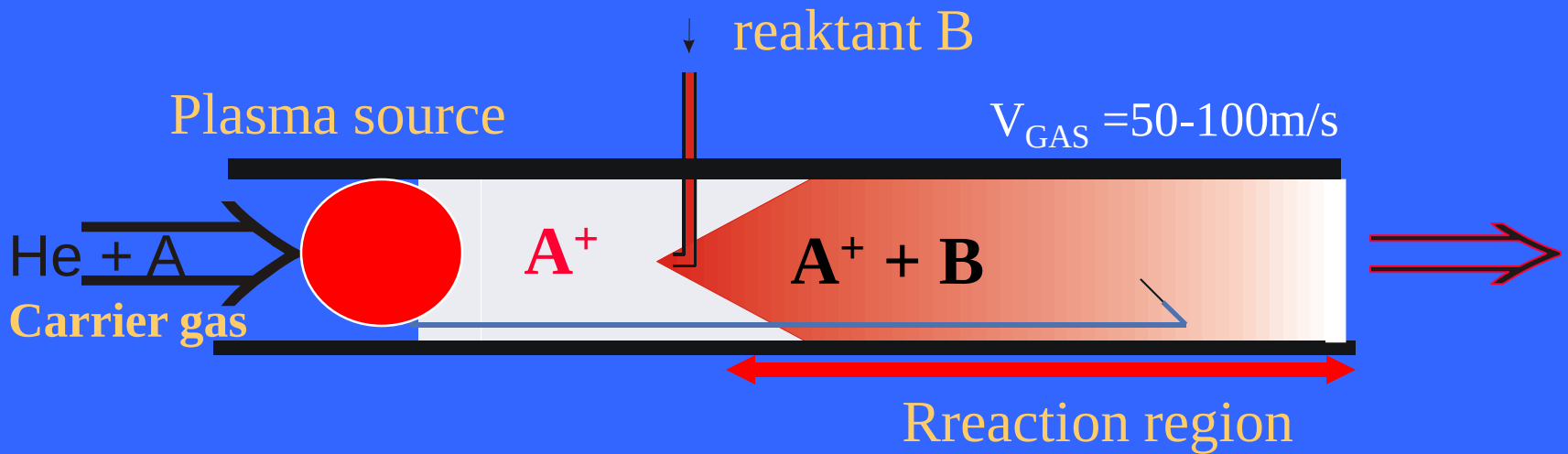

$$A^+ + B \xrightarrow{k} products,$$

$$d[A^+]/dt = -k[B][A^+], \qquad at\ [A^+] << [B]$$

$$[A^+] = [A^+]_0 \exp(-k[B]t) = [A^+]_0 \exp(-k[B]L_0/v)$$

SIFT

D. Smith, N. Adams, ….

SIFT

100-700 K

$$H_3^+ + CO \Rightarrow HCO^+ + H$$

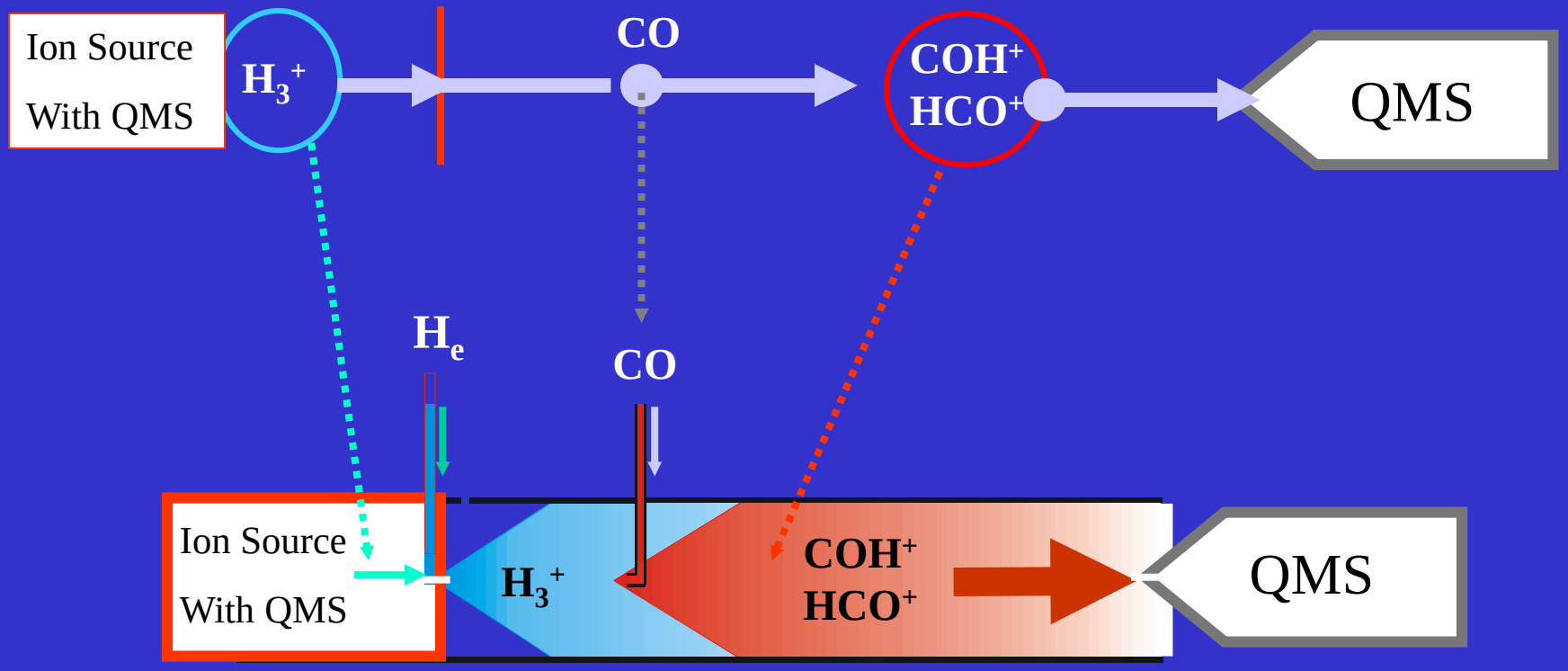

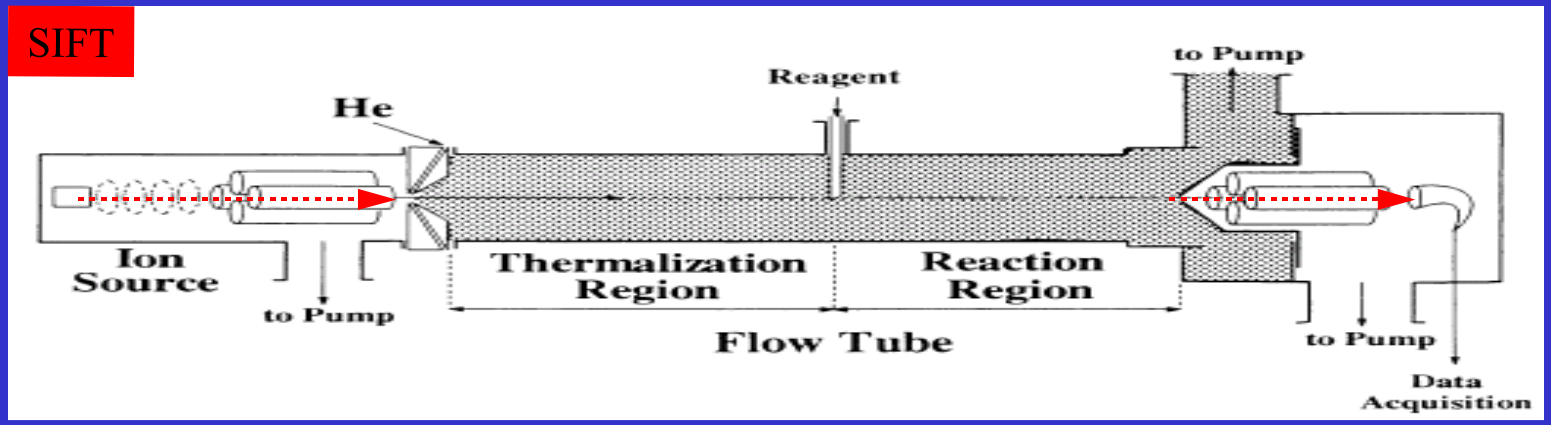

Flowing Afterglow Langmuir Probe - FALP

Recombination
Attachment

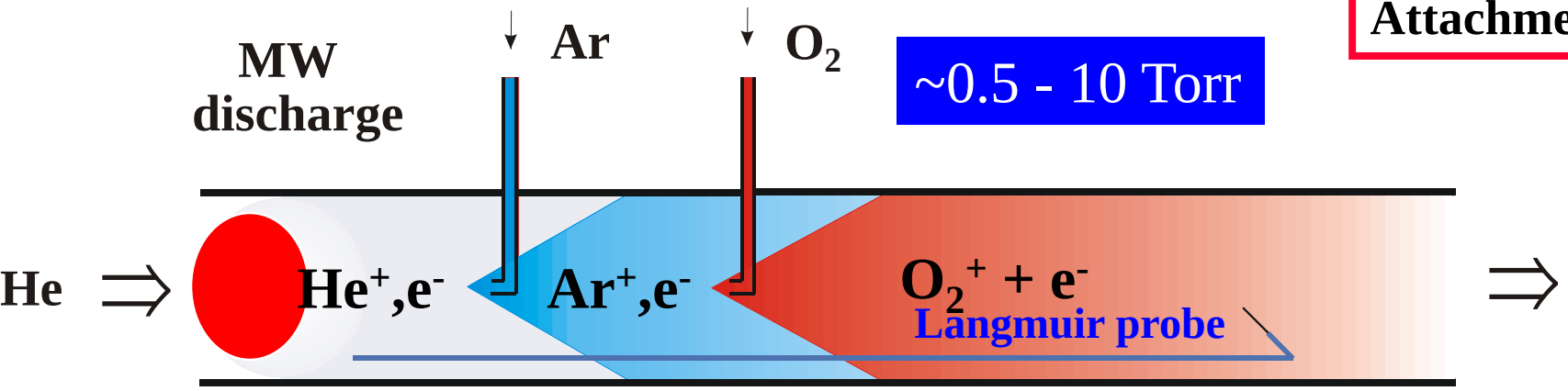

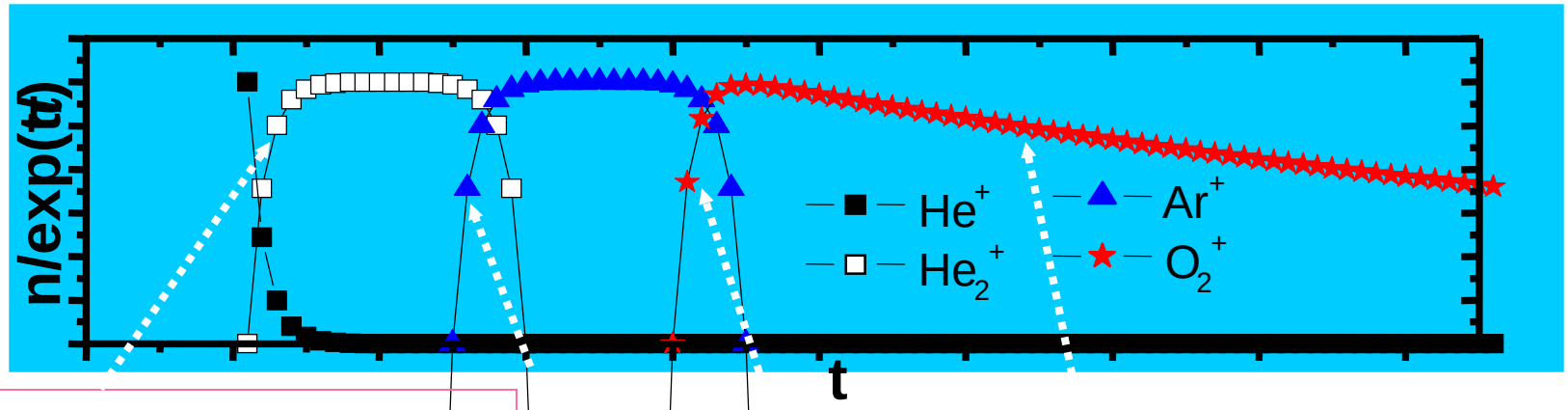

$He^+ + 2He \rightarrow He_2^+ + He$

$He_2^+ + Ar \rightarrow Ar^+ + 2He$

$He^m + Ar \rightarrow Ar^+ + He$

$Ar^+ + O_2 \rightarrow O_2^+ + Ar$

Diffusion, IMR
Recombination

Diffusion in FA

Diffusion losses
Ambipolar diffusion

$$[A^+] = [A^+]_0 \exp(-Dt/\Lambda^2) = [A^+]_0 \exp(-Dpt/p\Lambda^2) = [A^+]_0 \exp(-D_0 p_0 L/vp\Lambda^2)$$
$$\sim [A^+]_0 \exp(-D_0 p_0 L/vp\Lambda^2) \sim [A^+]_0 \exp(-const.L/Q)$$

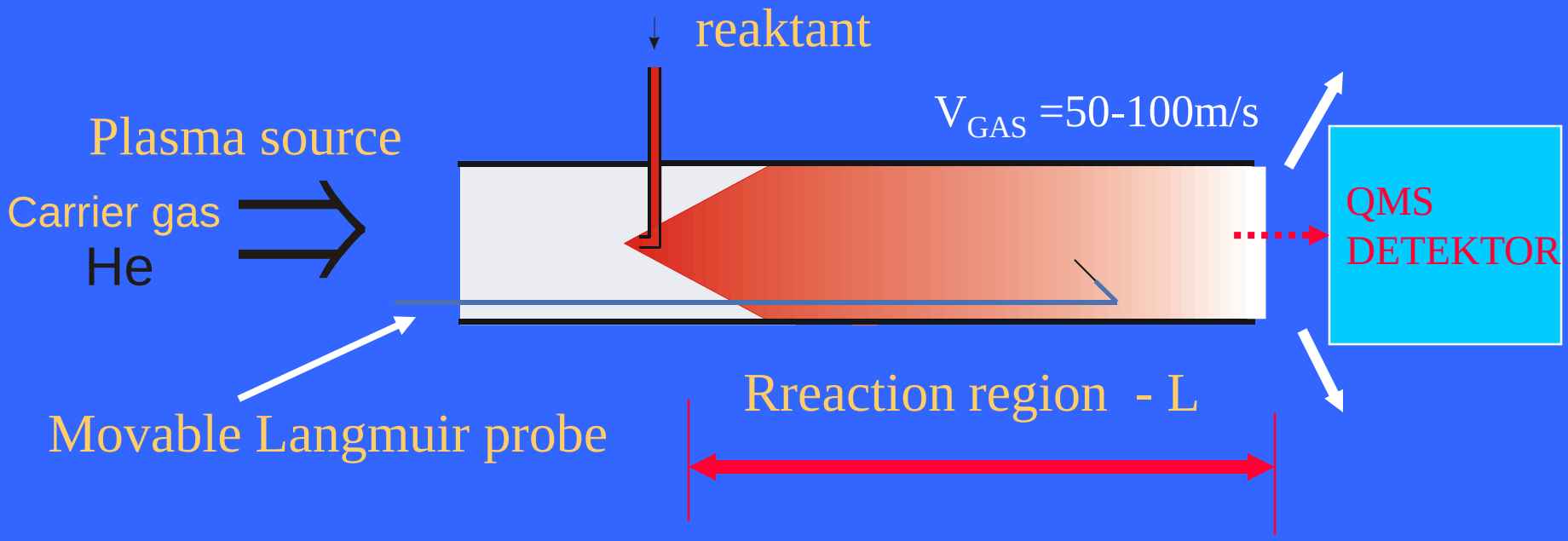

$$[A^+] \sim [A^+]_0 \exp(-const.L/Q)$$

VT-HPFA

P: ~10 Torr

T: 100-300 K

Flow-tube diameter: 50mm

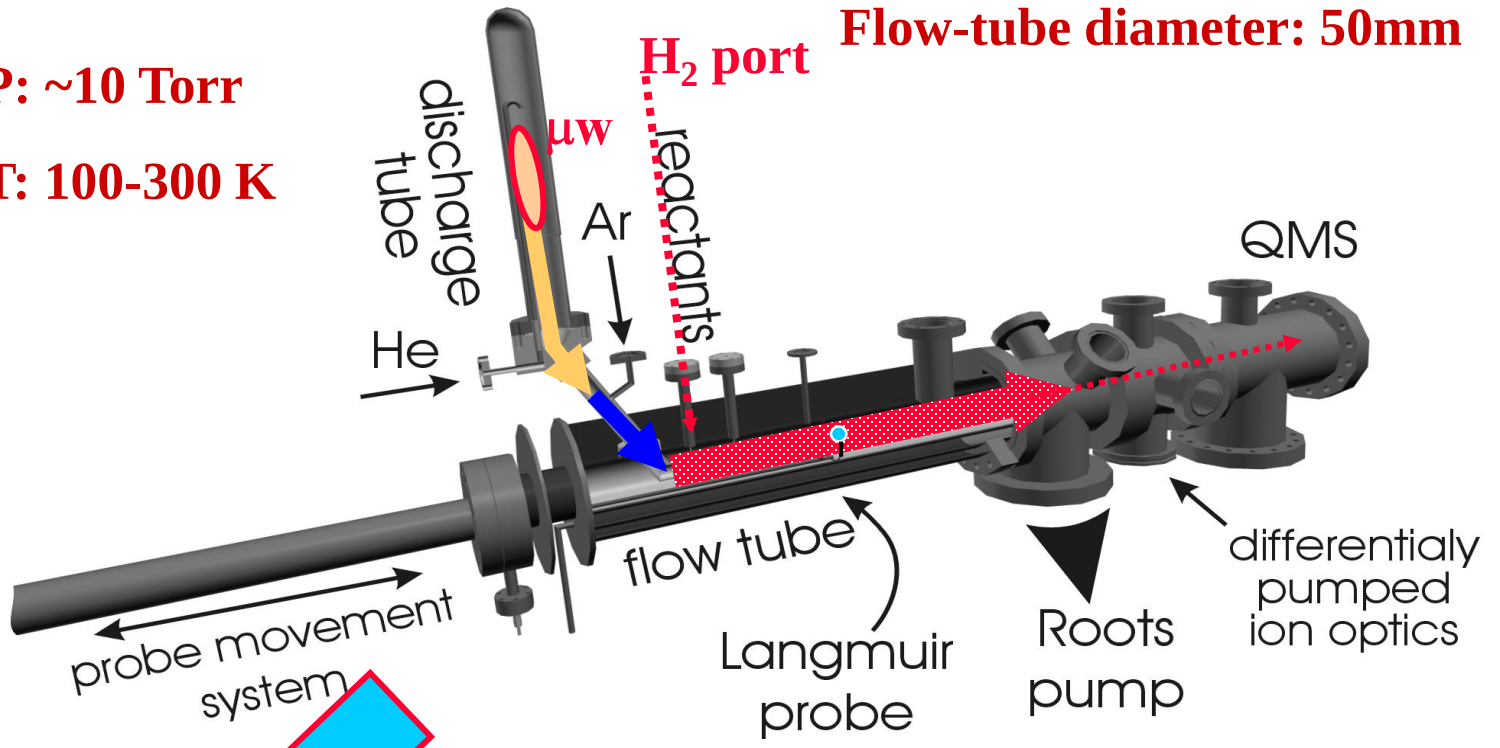

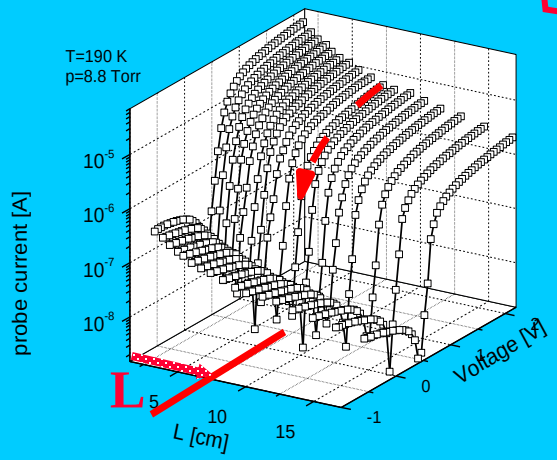

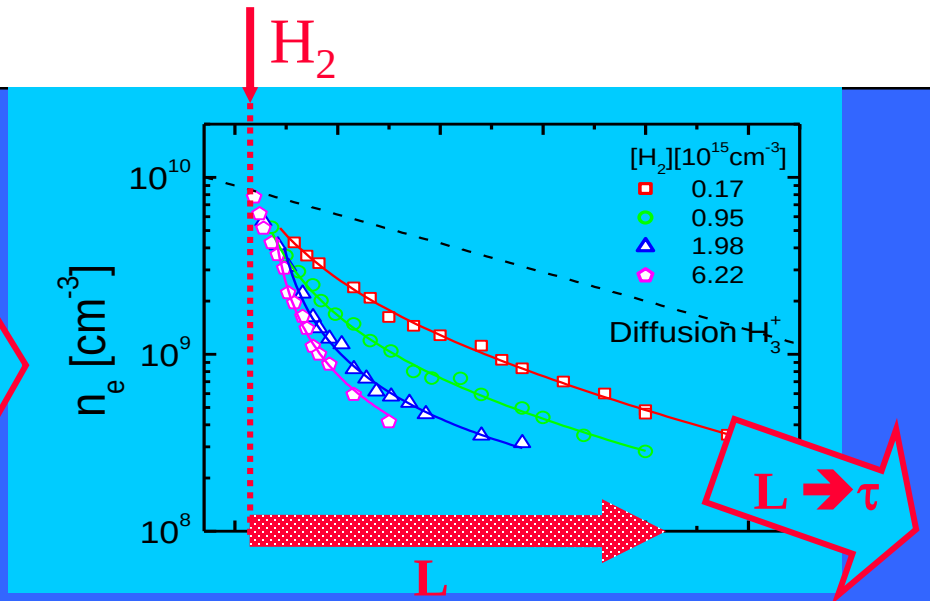

α_{eff}

Positive ion/electron dissociative recombination

- e.g. $NO^+ + e \rightarrow N + O$

$$\frac{dn_e}{dt} = -\alpha\, n_e^2 + D_a \nabla^2 n_e$$

diffusion

recombination

$$\frac{dn_e}{dt} = -\alpha\, n_e^2 - \frac{D_a}{\Lambda^2} n_e$$

$$\frac{1}{n_e} - \frac{1}{n_0} = \alpha (t_e - t_0)$$

recombination

diffusion and recombination

$$\frac{1}{n_e} = \alpha\, \frac{\exp(\nu t) - 1}{\nu} + \frac{1}{n_0} \exp(\nu t) \;;\nu = D_a/\Lambda^2$$

Example: PLASMA DECAY
H_3^+ and H_5^+ in thermodynamic equilibrium

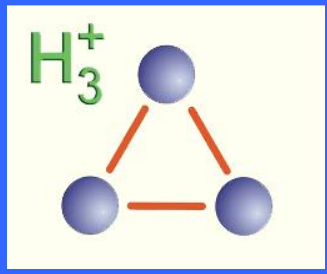

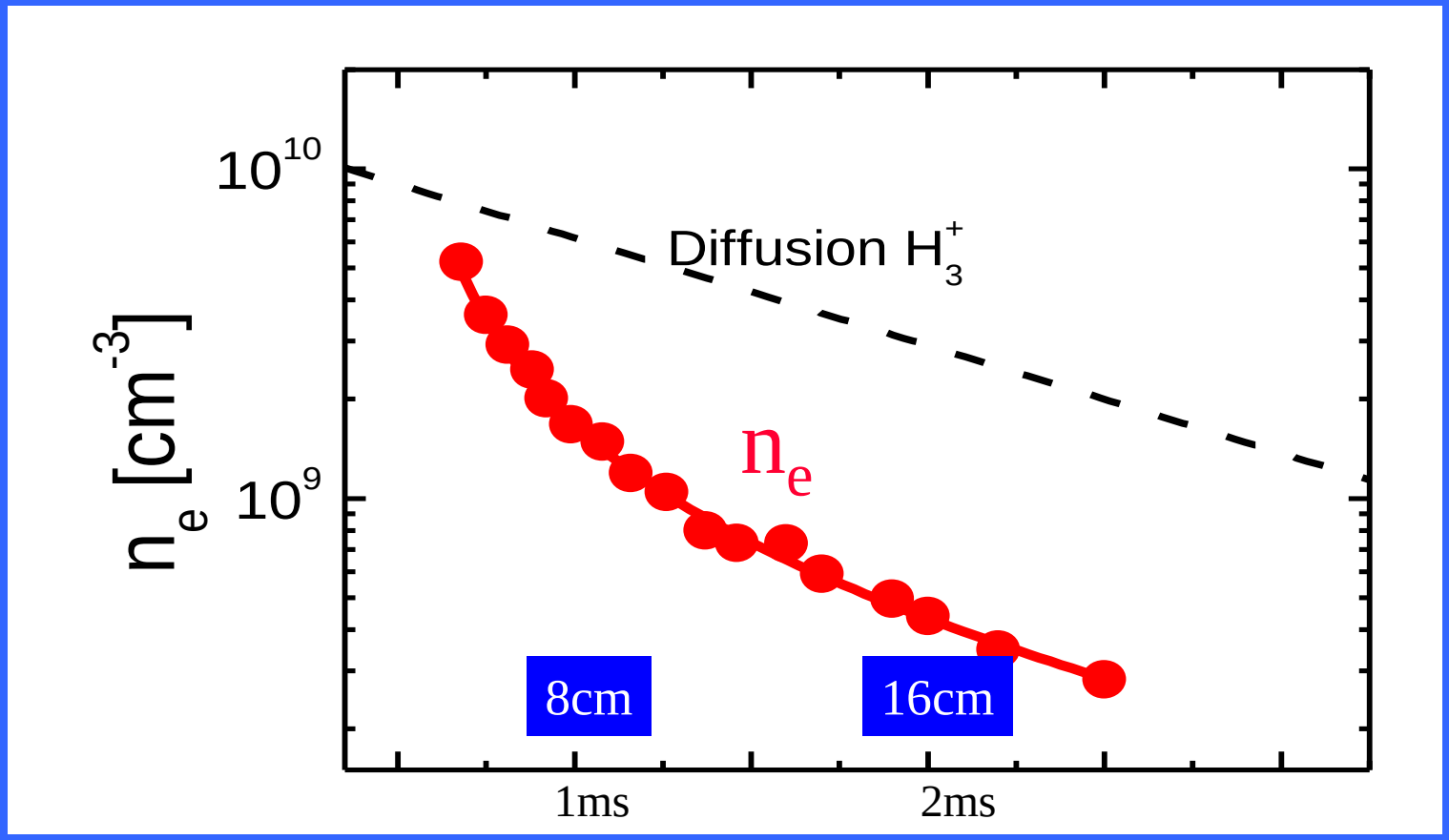

190 K, 9 Torr

Note very different time scale!!!

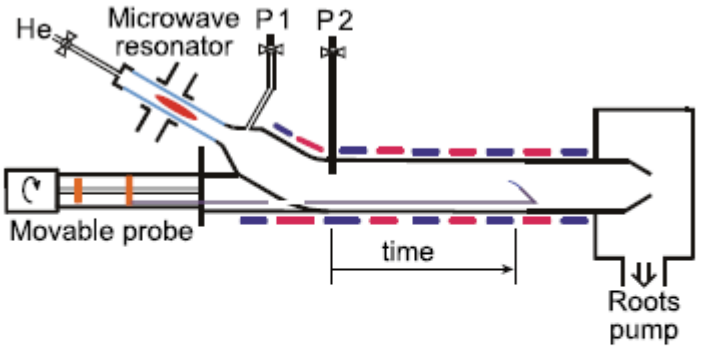

Fig. 1. (Color online) Schematic of FALP apparatus. Buffer gas flows from discharge region (upper left corner) towards the Roots pump (right). The plasma formed in the discharge is driven along the flow tube. The plasma parameters on the axis of the flow tube are measured by an axially movable Langmuir probe (from the port P2 up to the end of the flow tube).

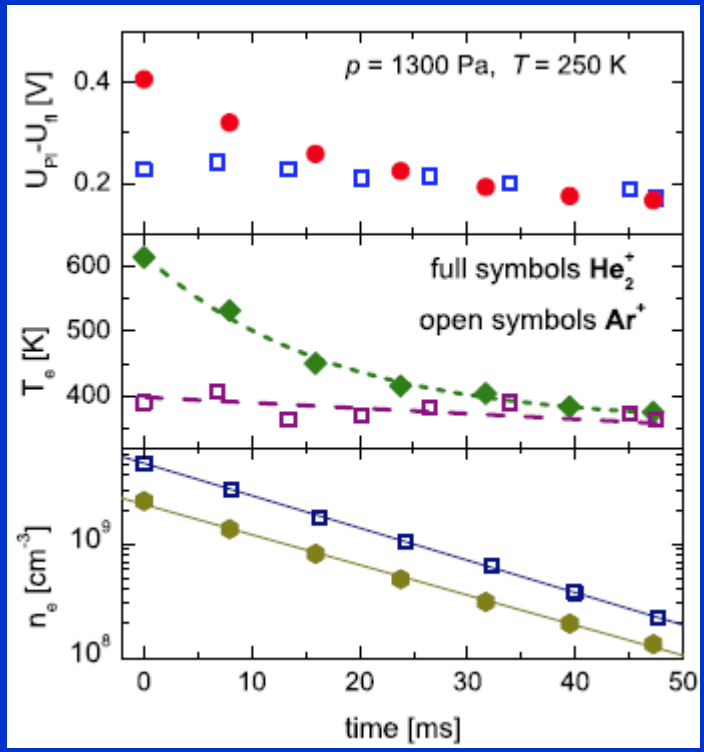

Fig. 2. (Color online) The evolution of afterglow plasma along the flow tube in He_2^+ (full symbols) and Ar^+ (open symbols) dominated plasmas. Upper panel: the difference between plasma and floating potential $\Delta = (U_{Pl} - U_{fl})$. Middle panel: the measured electron temperature evolutions in He_2^+ and Ar^+ dominated plasmas. Lower panel: the decays of electron densities along the flow tube.

Eur. Phys. J. D **54**, 391–398 (2009)
DOI: 10.1140/epjd/e2009-00144-3

THE EUROPEAN PHYSICAL JOURNAL D

Regular Article

Non-Maxwellian electron energy distribution function in He, He/Ar, He/Xe/H_2 and He/Xe/D_2 low temperature afterglow plasma

R. Plasil[1,a], I. Korolov[1,2], T. Kotrik[1], P. Dohnal[1], G. Bano[2], Z. Donko[2], and J. Glosik[1]

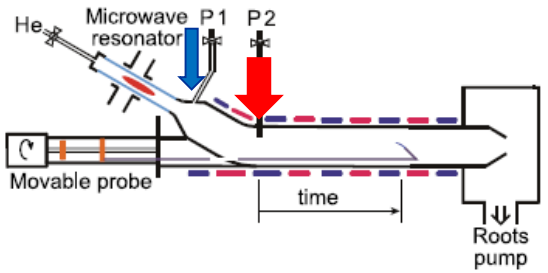

Fig. 1. (Color online) Schematic of FALP apparatus. Buffer gas flows from discharge region (upper left corner) towards the Roots pump (right). The plasma formed in the discharge is driven along the flow tube. The plasma parameters on the axis of the flow tube are measured by an axially movable Langmuir probe (from the port P2 up to the end of the flow tube).

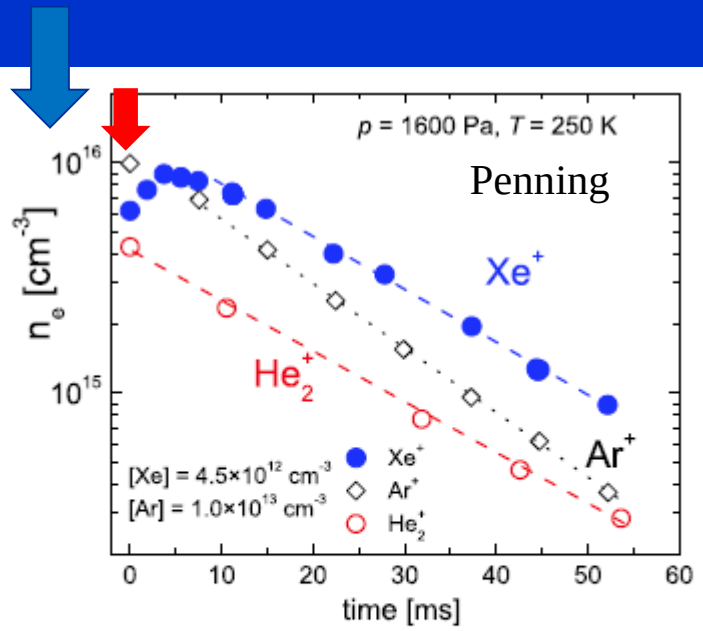

Fig. 3. (Color online) The measured decay of electron density in He_2^+ dominated plasma in pure He and the increase of the electron density in the afterglow plasma after injection of Xe via port P2. Indicated are the dominant ions. For comparison the electron density decay of argon plasma is plotted. In this case Ar is added to the afterglow via port P1.

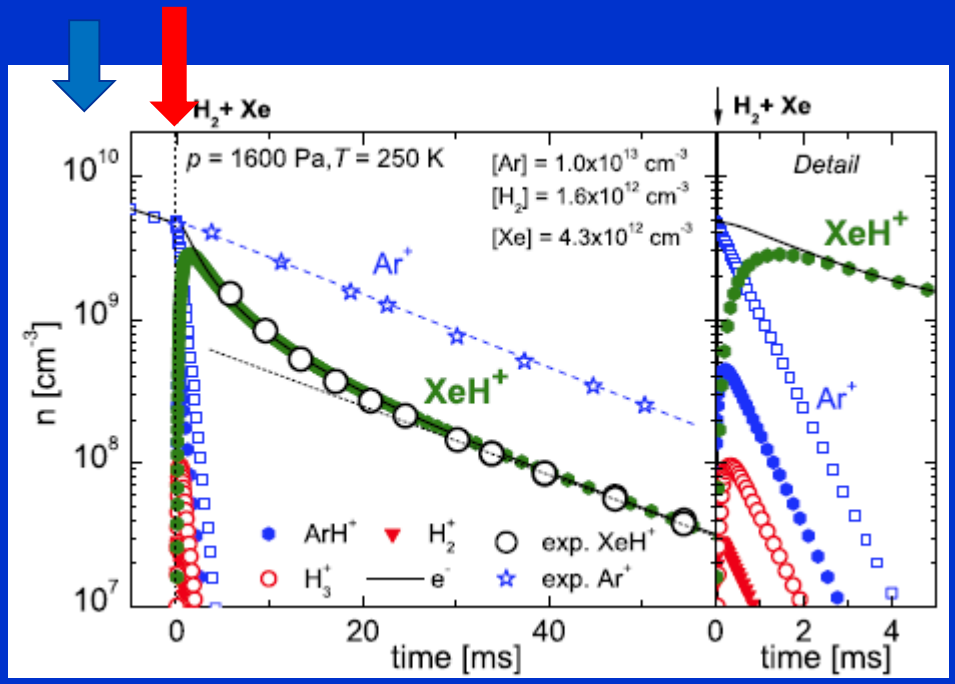

Fig. 7. (Color online) The calculated plasma formation and decay along the flow tube in He/Ar/Xe/H_2 mixture. We do not plot whole evolution between discharge and port P2, plotted is only the section shortly before port P2. Data were obtained by solving the set of partial differential equations corresponding to considered processes. The diffusion and the recombination losses are also included in the model. Plotted is also the electron density decay measured at corresponding conditions (large circles). For comparison the decay measured in He/Ar mixture dominated by Ar^+ ion is also plotted; this decay is governed by diffusion losses only.

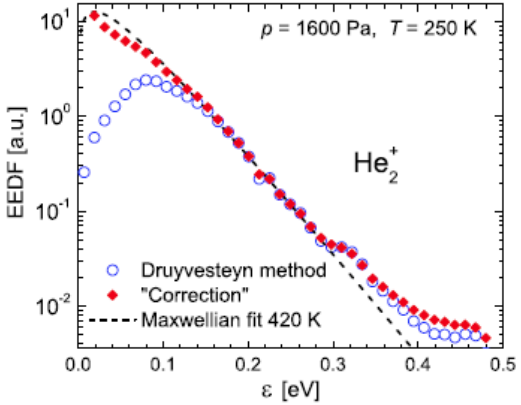

Fig. 5. (Color online) The electron energy distribution function "EEDF" measured in the very late afterglow in the helium buffered plasma dominated by ions He_2^+. In first approximation the EEDF is obtained from the probe characteristic using Druyvesteyn method (open symbols). Better approximation is obtained with correction to influence of collisions in vicinity of the probe (closed symbols) [7]. The dashed curve indicates Maxwellian EEDF fitted to measured data for $\varepsilon > 3k_BT_e$.

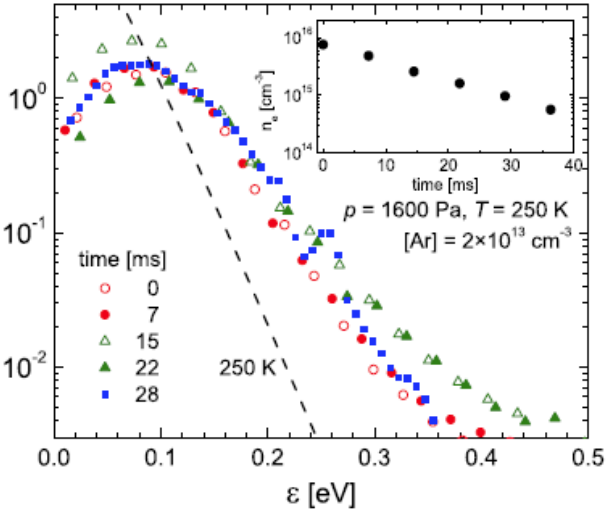

Fig. 6. (Color online) The evolution of electron energy distribution function along the flow tube in Ar^+ dominated plasma in He with admixture of Ar. The plotted EEDFs are normalised to 1. In the inset the corresponding electron density n_e decay is plotted.

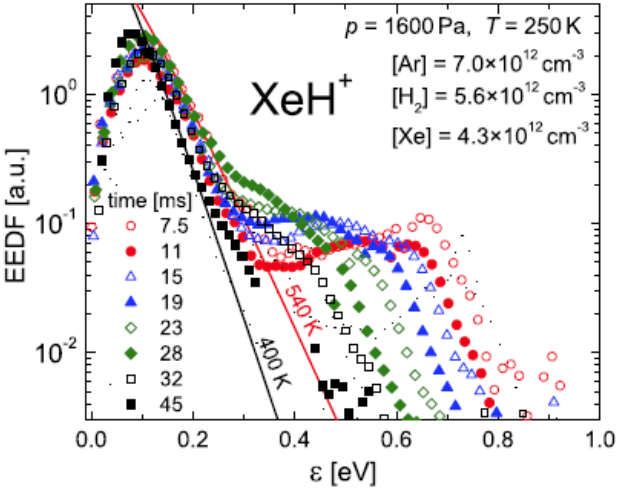

Fig. 8. (Color online) Evolution of EEDF in He/Ar/Xe/H_2 plasma obtained from measured characteristics of Langmuir probe. In low energy region (<0.15 eV), the EEDFs are expected to be Maxwellian [7]. The solid curves correspond to Maxwellian electron energy distributions fitted to the measured data for the decay time 7.5 ms and 45 ms. The plotted EEDFs are normalised to 1. Experimental conditions are indicated.

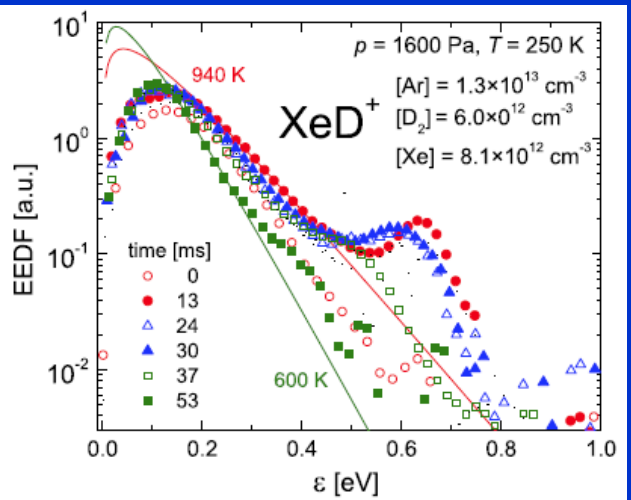

Fig. 9. (Color online) The measured evolution of EEDF in He/Ar/Xe/D_2 plasma. The solid curves correspond to Maxwellian electron energy distribution fitted to the measured data for the decay times 13 ms and 53 ms. The plotted EEDFs are normalised to 1. Experimental conditions are indicated.

EEDF Argon plasma

- Ricard

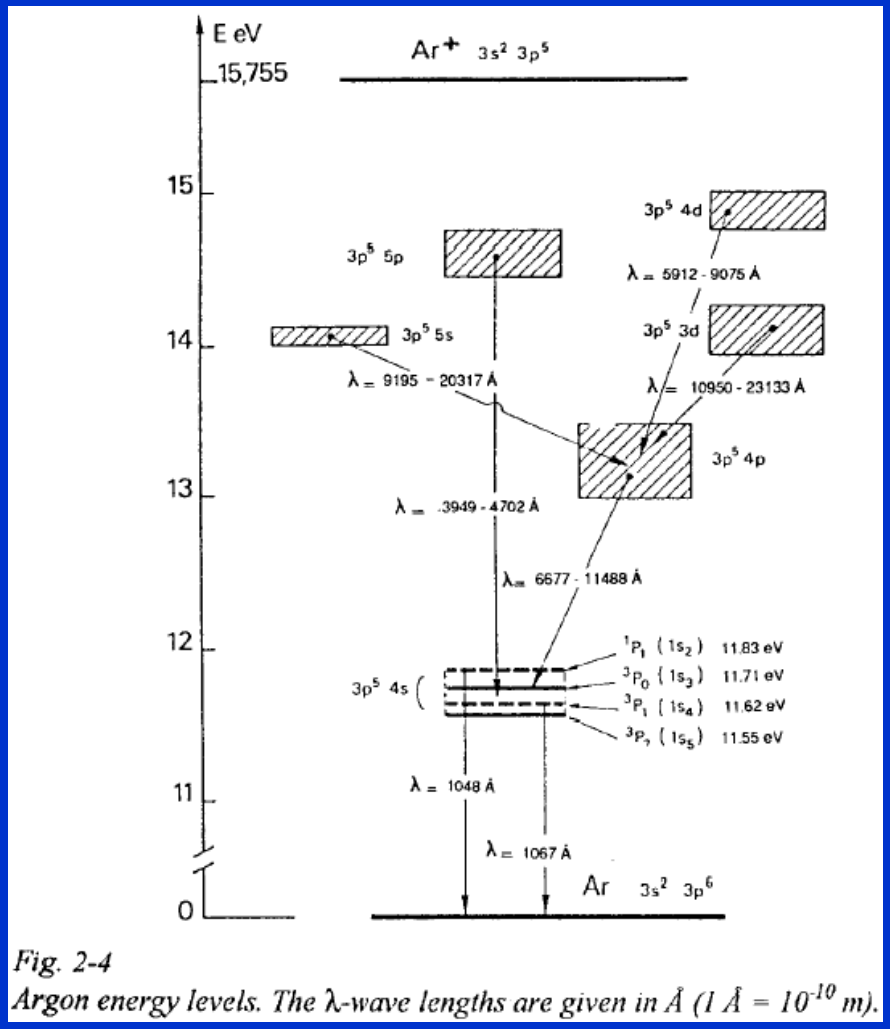

Fig. 2-4
Argon energy levels. The λ-wave lengths are given in Å (1 Å = 10^{-10} m).

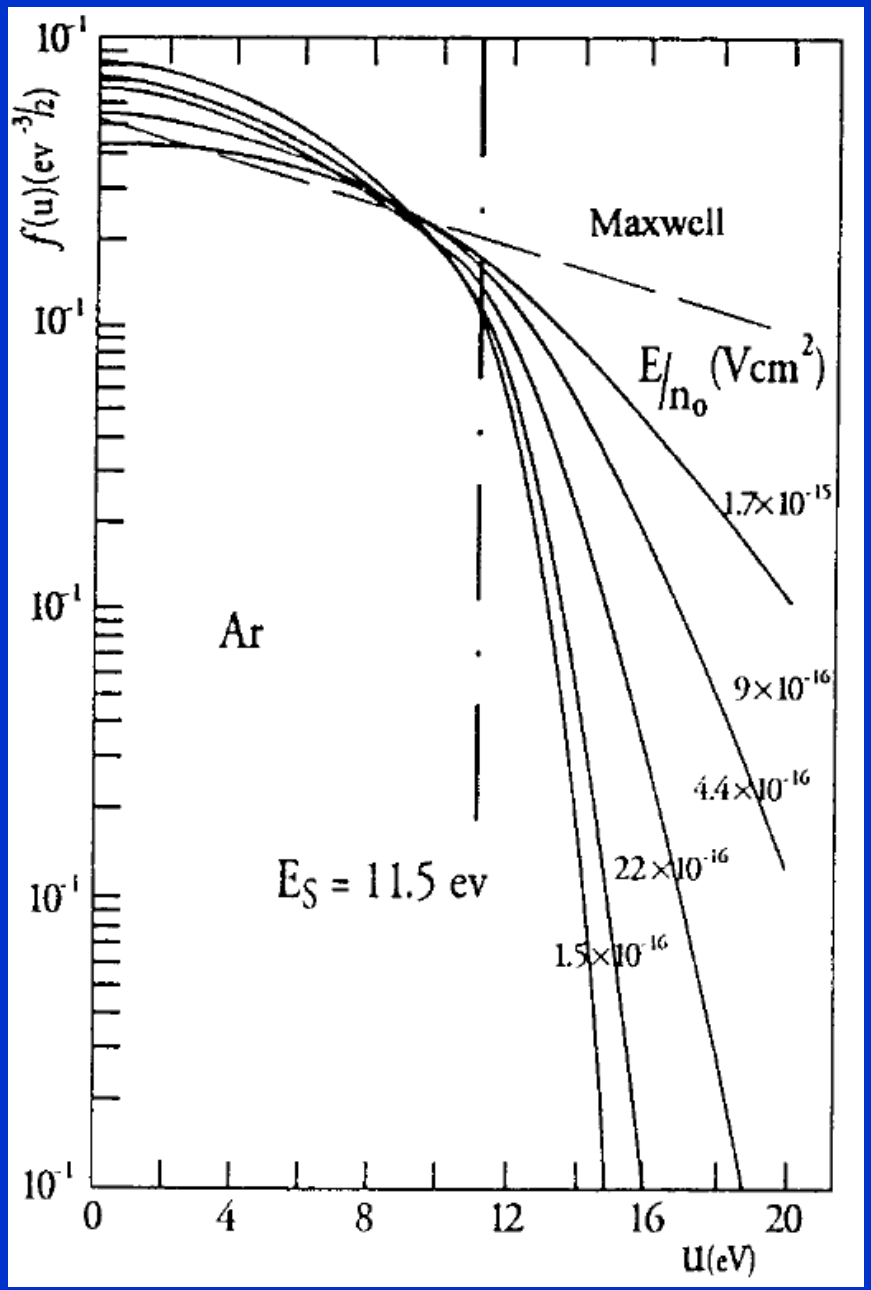

FALP – MFF.CUNI.CZ

Plasma, IMR, Recombination Diagnostics

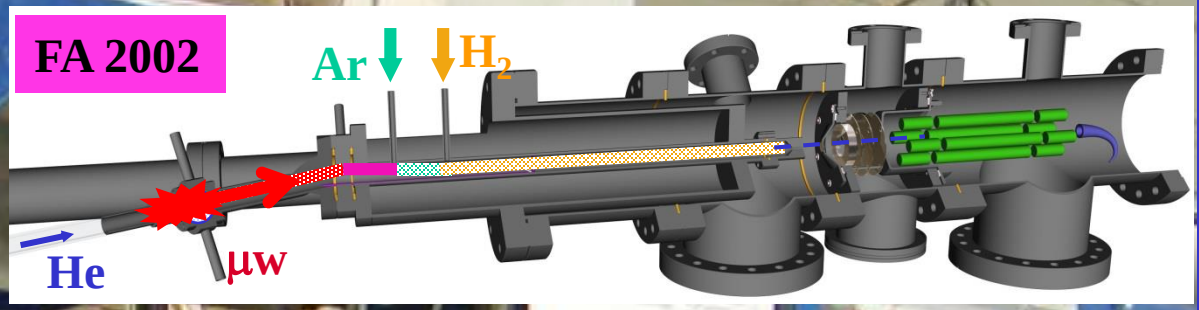

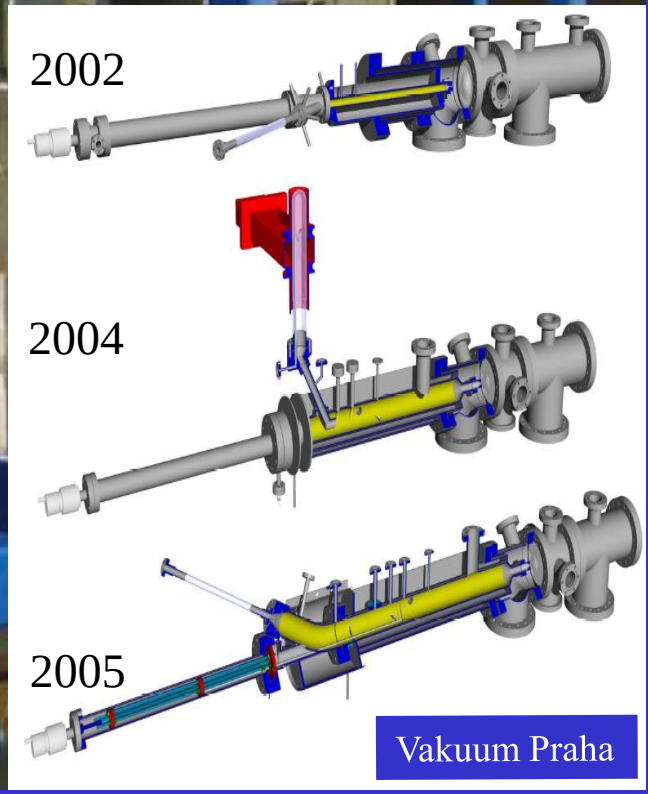

Vakuum Praha

O.Novotný

FA– Flowing Afterglow 2005

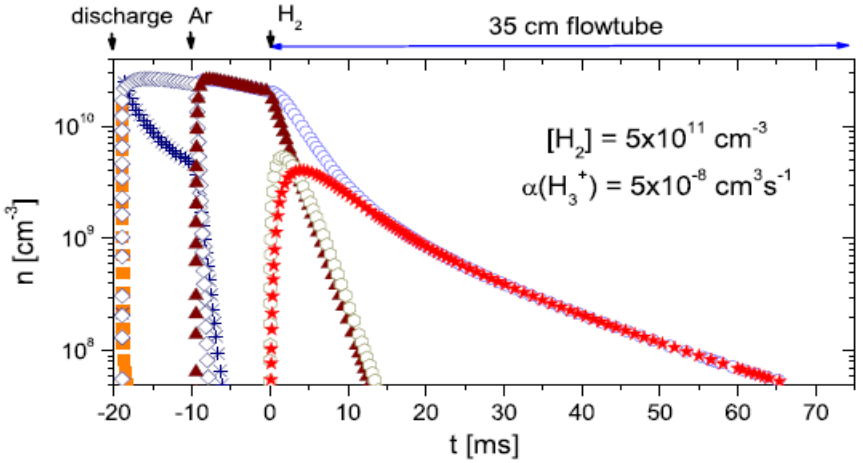

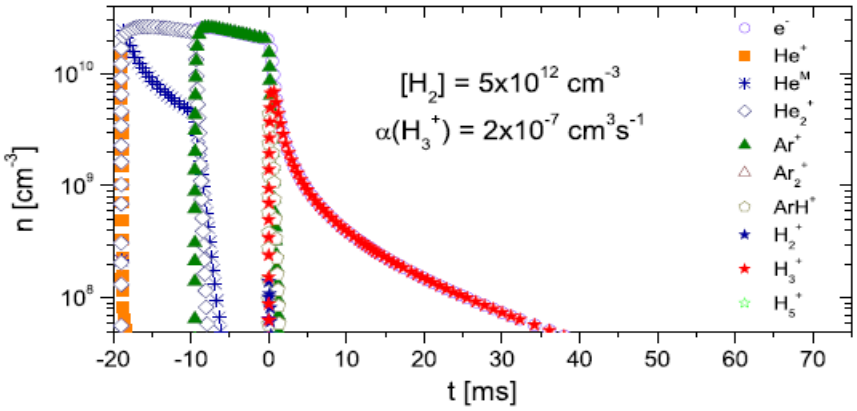

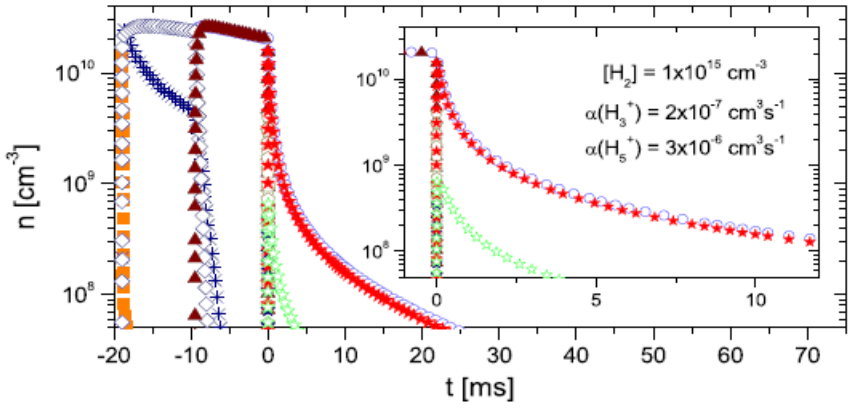

MFF.CUNI.CZ

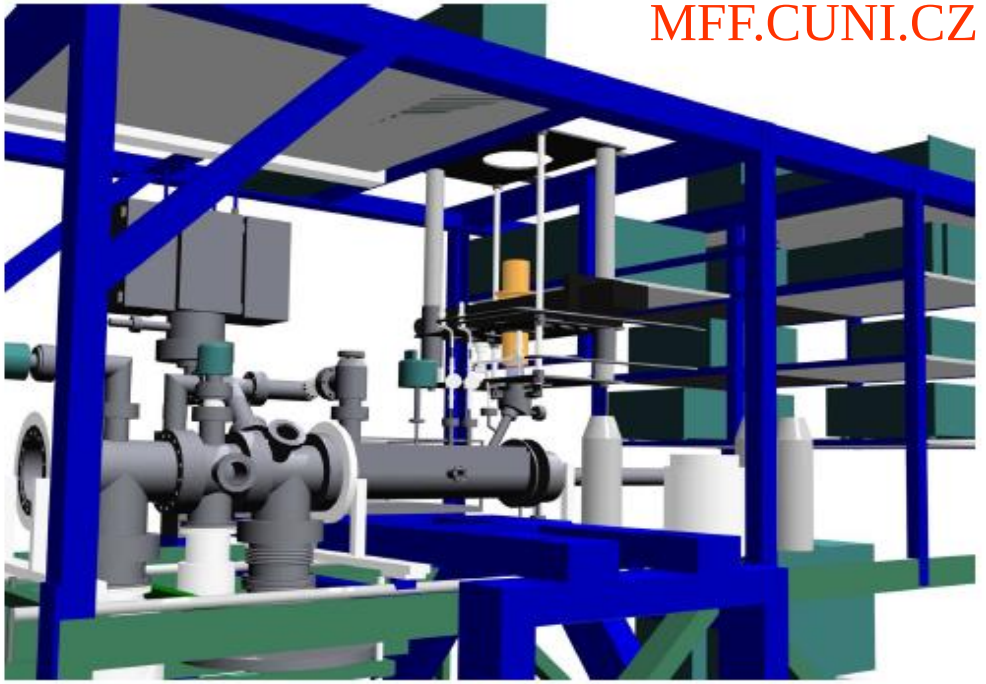

SIFDT

100 K – 3eV

$$N_4^+ + He \rightarrow N_2^+ + N_2 + He$$

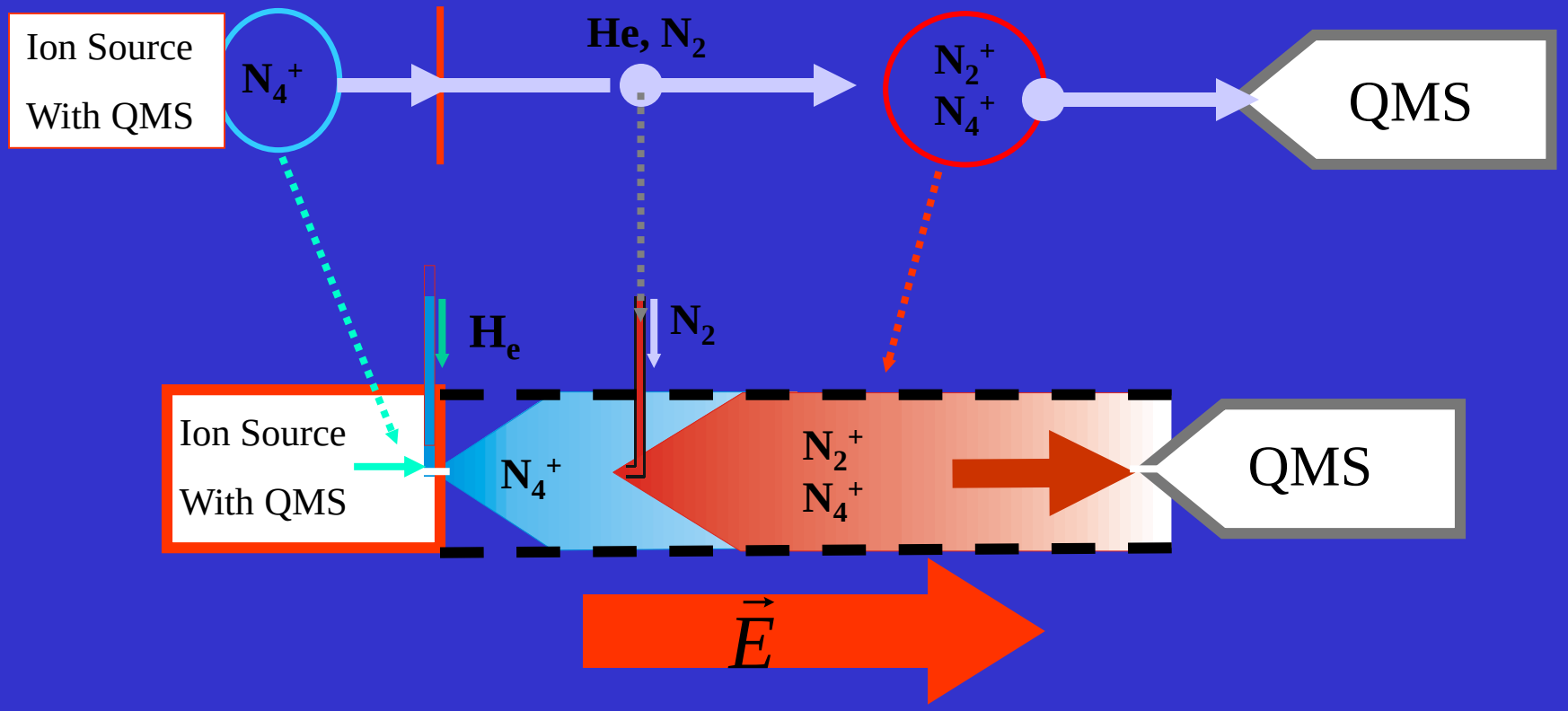

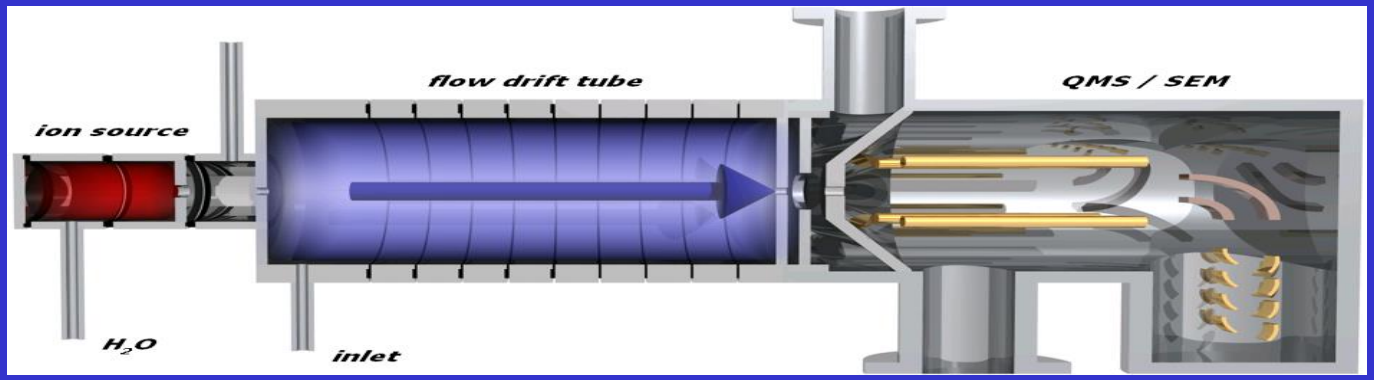

FA– Flowing Afterglow

100-700 K

$$H_3^+ + CO \Rightarrow HCO^+ + H$$

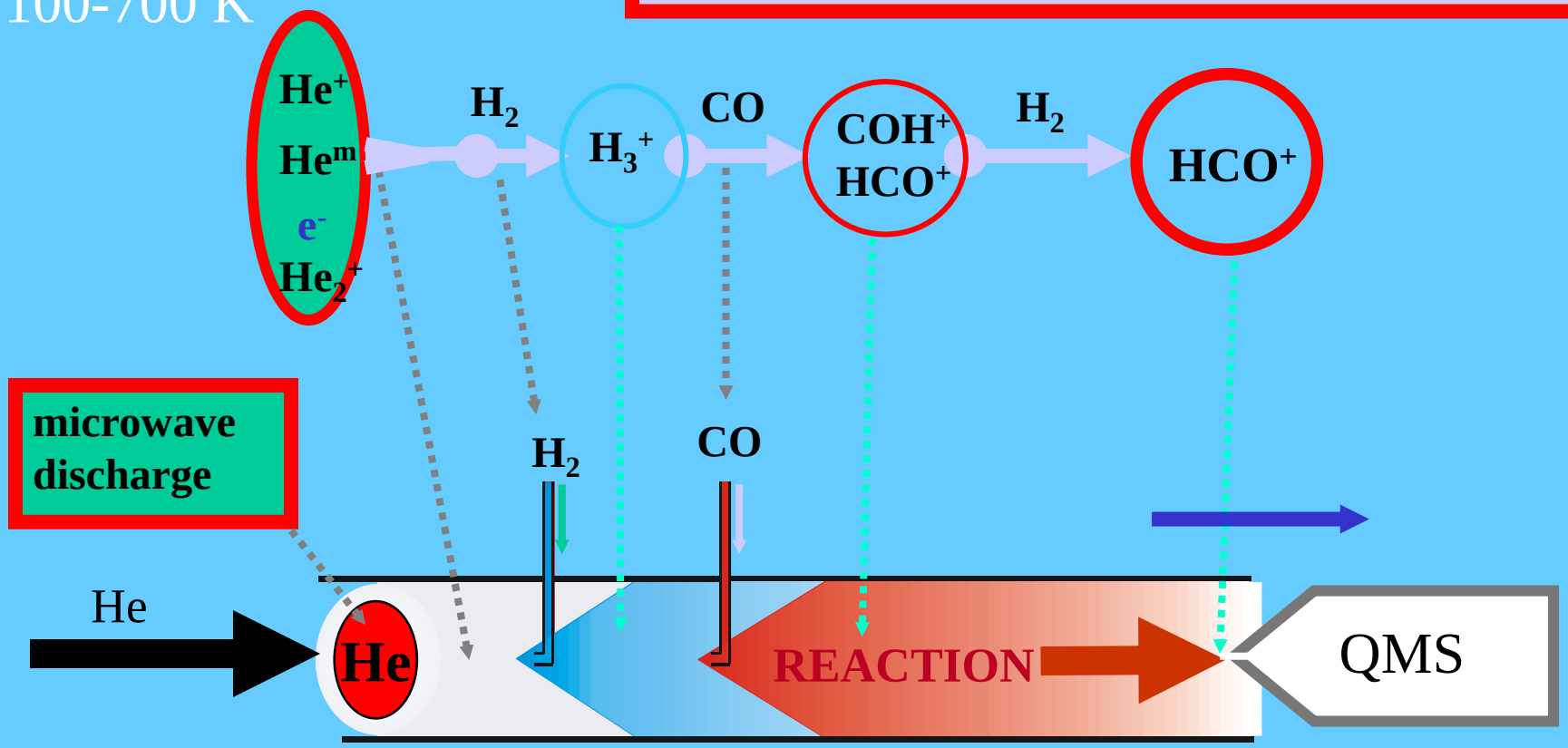

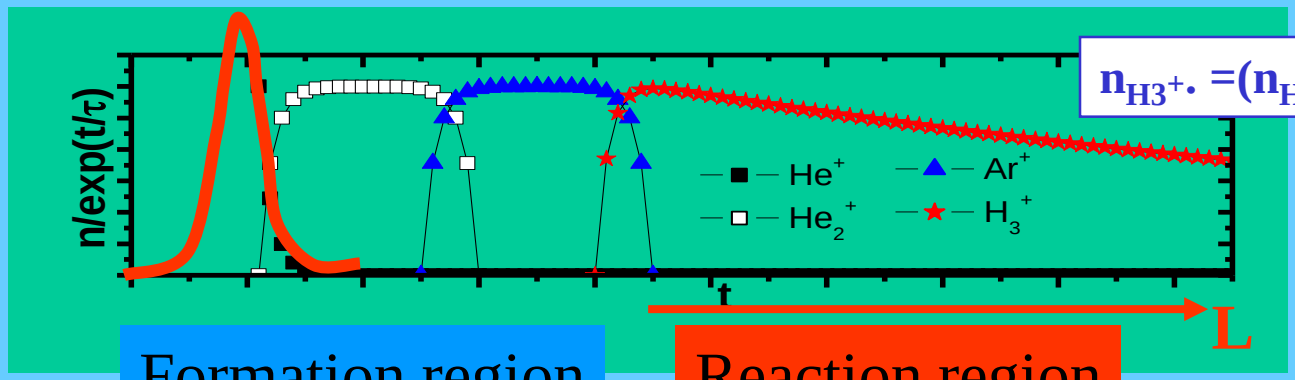

$n_{H3^+}. = (n_{H3^+})._0 \exp(-k n_{Ar} t)$

$t = L/v$

Formation region

Reaction region

FA – Flowing Afterglow

100-700 K

$$H_3^+ + CO \Rightarrow HCO^+ + H$$

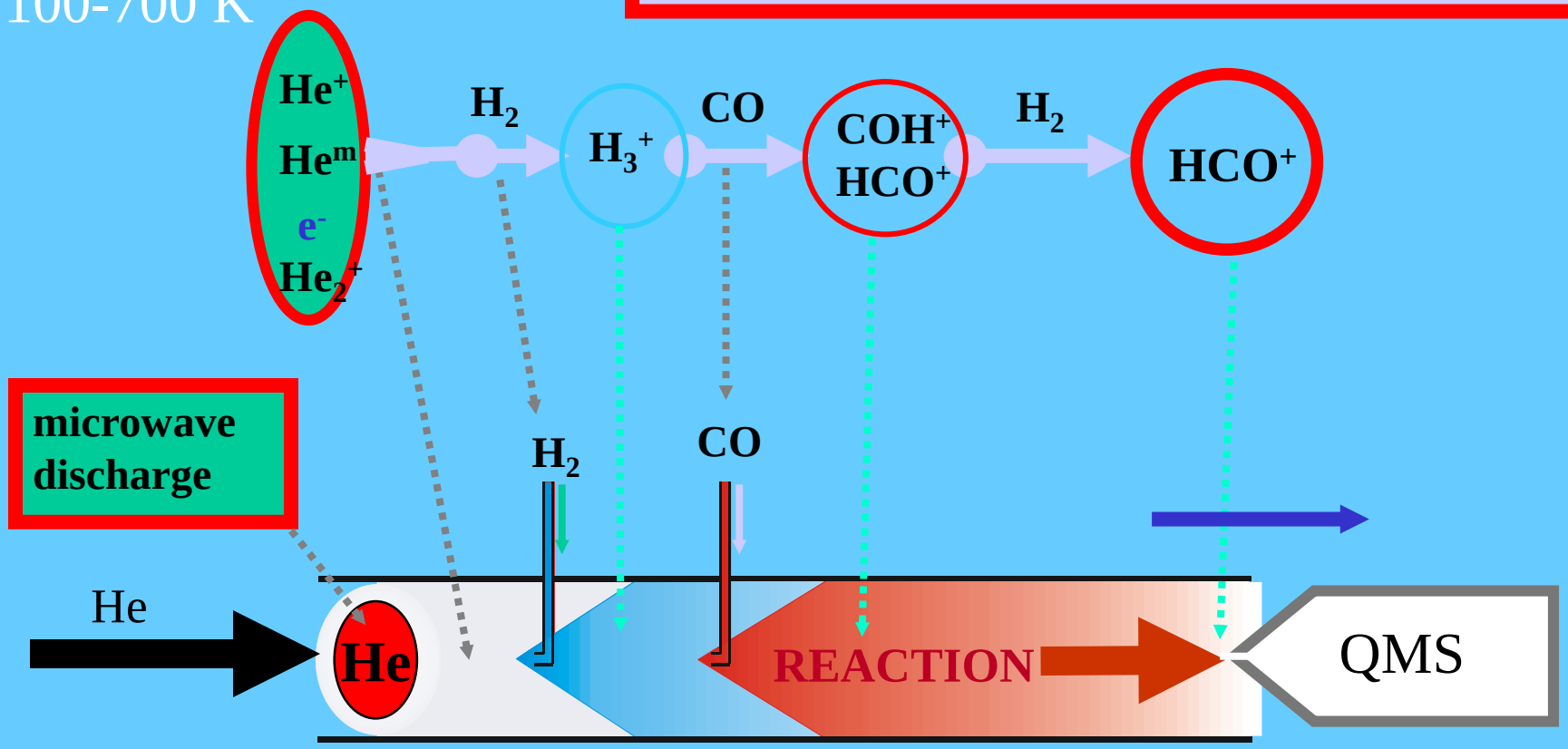

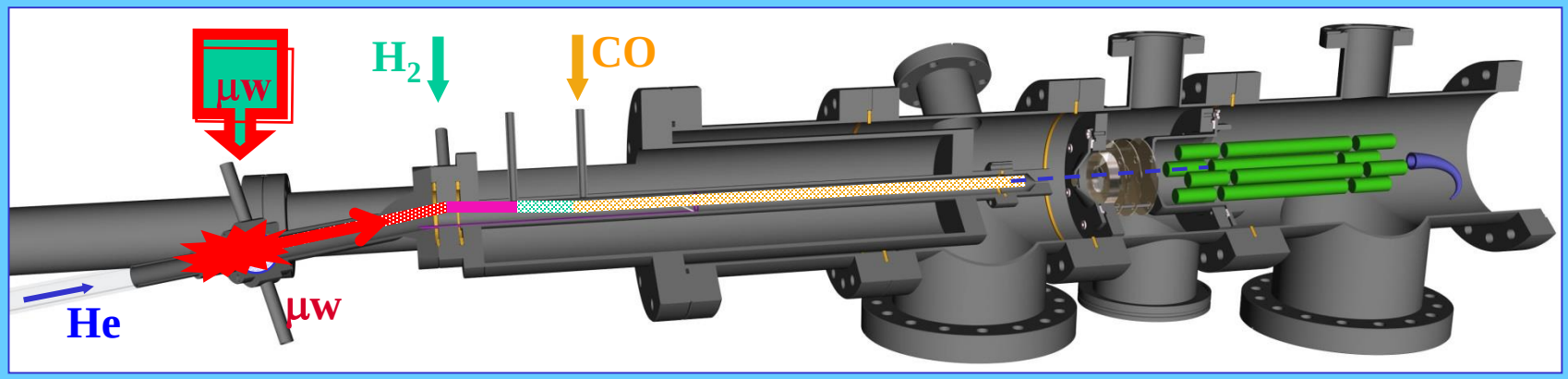

Evolution along the flow tube

$$[A^+]_L = [A^+]_{L=0} \cdot e^{-DL/\lambda^2 v}$$

$$[A^+]_L = [A^+]_{L=0} \cdot e^{-const_1 . D_0 p_0 L/Q} = [A^+]_{L=0} \cdot e^{-const_2 . L/Q}$$

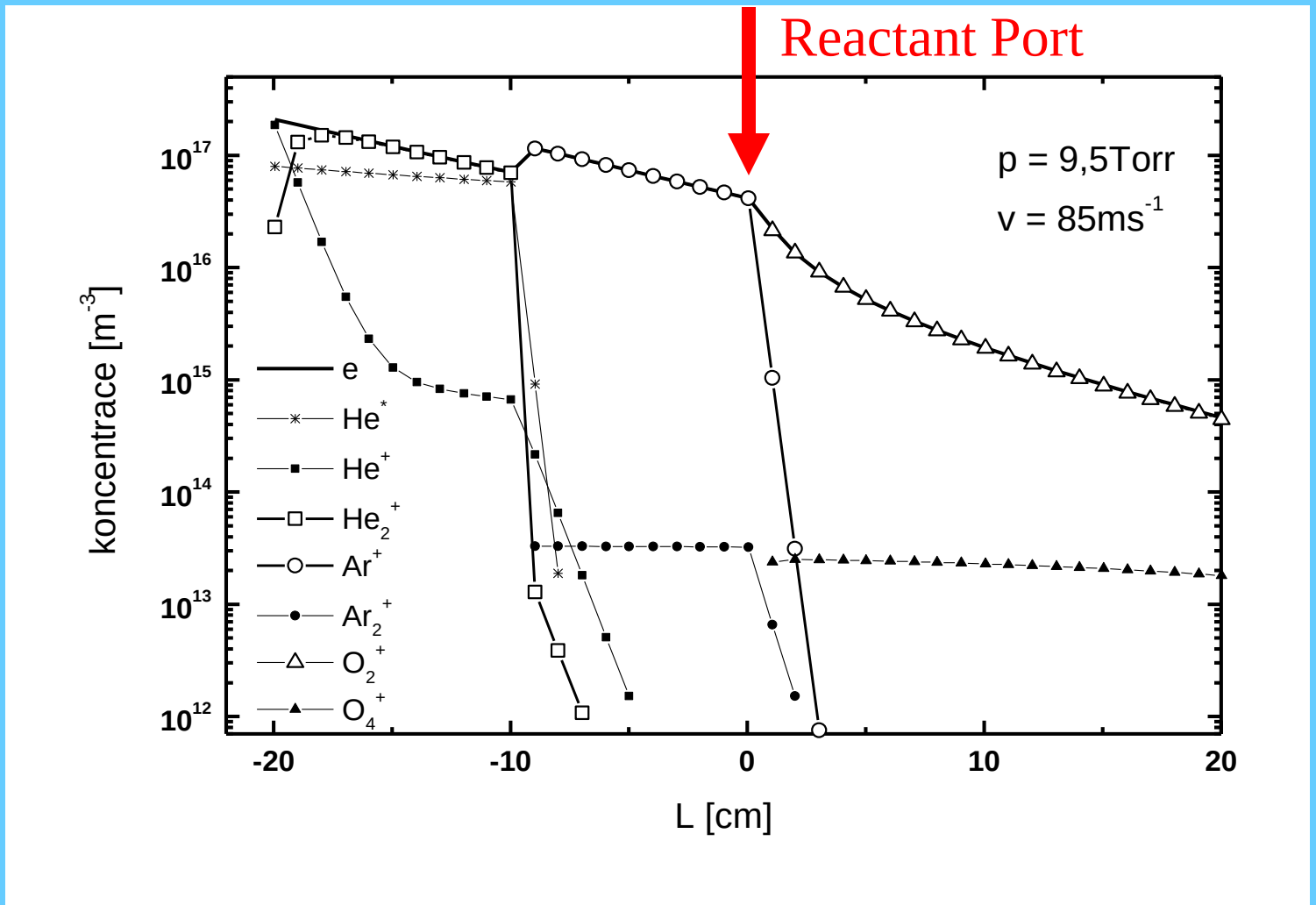

High temperature study

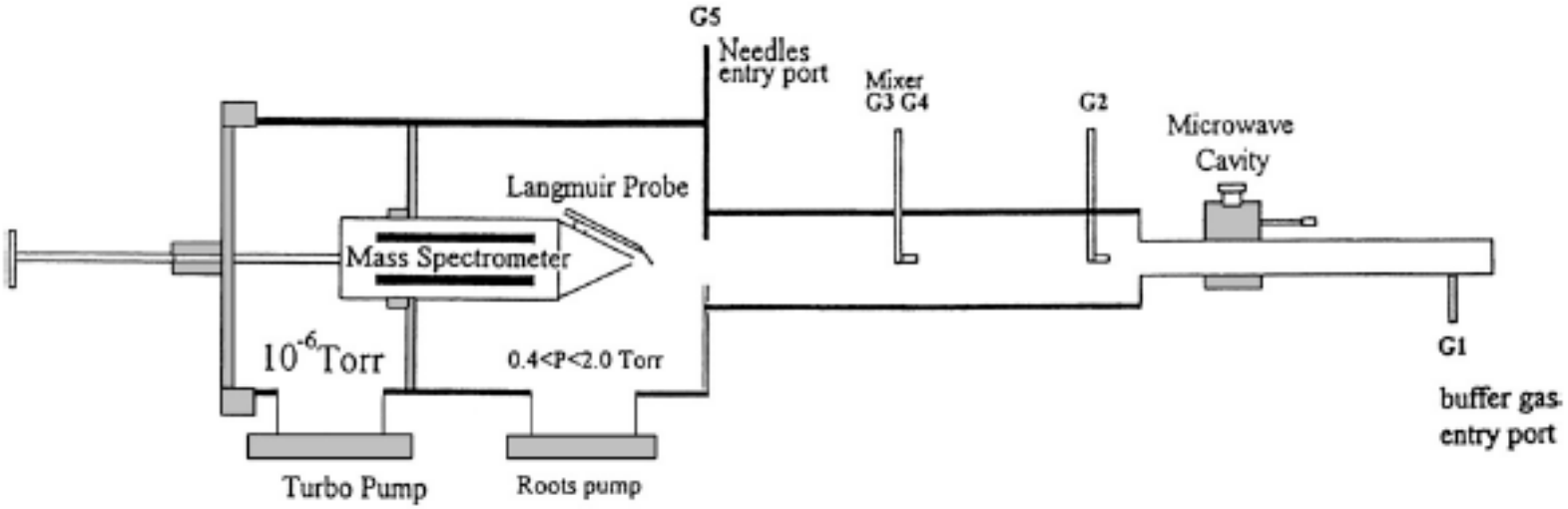

Fig. 12. Schematic view of the Rennes FALP-MS [164]

RENNES MS - FALP

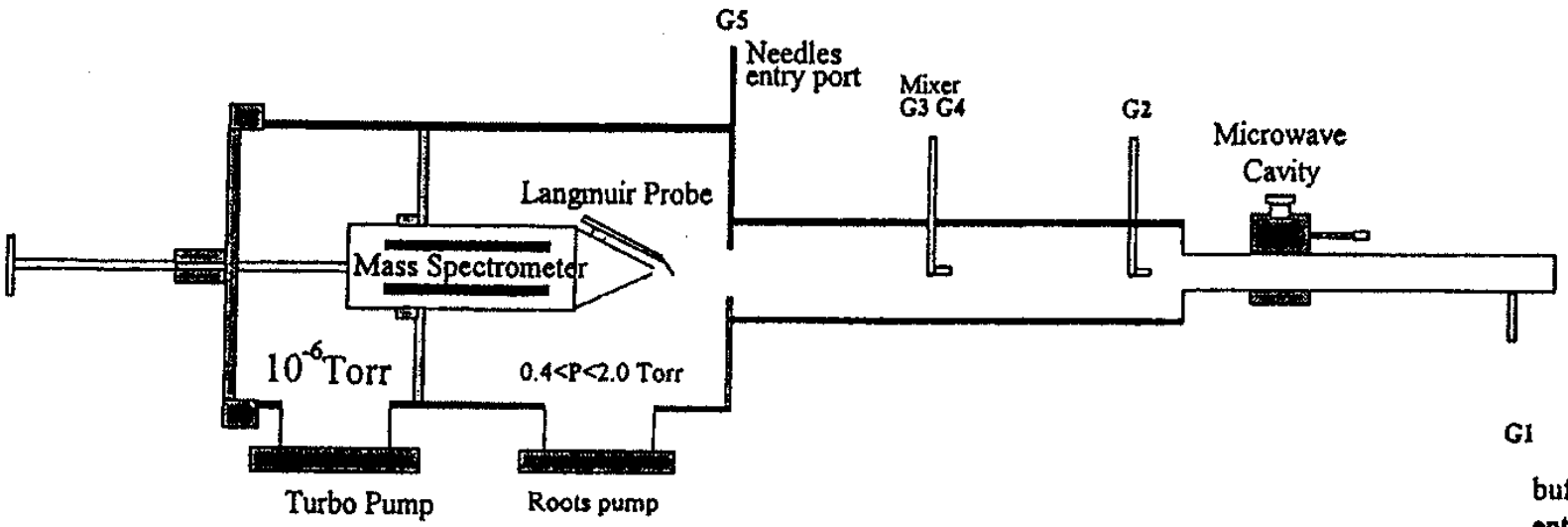

Figure 1. Sketch of the FALP apparatus.

RENNES absorption studies

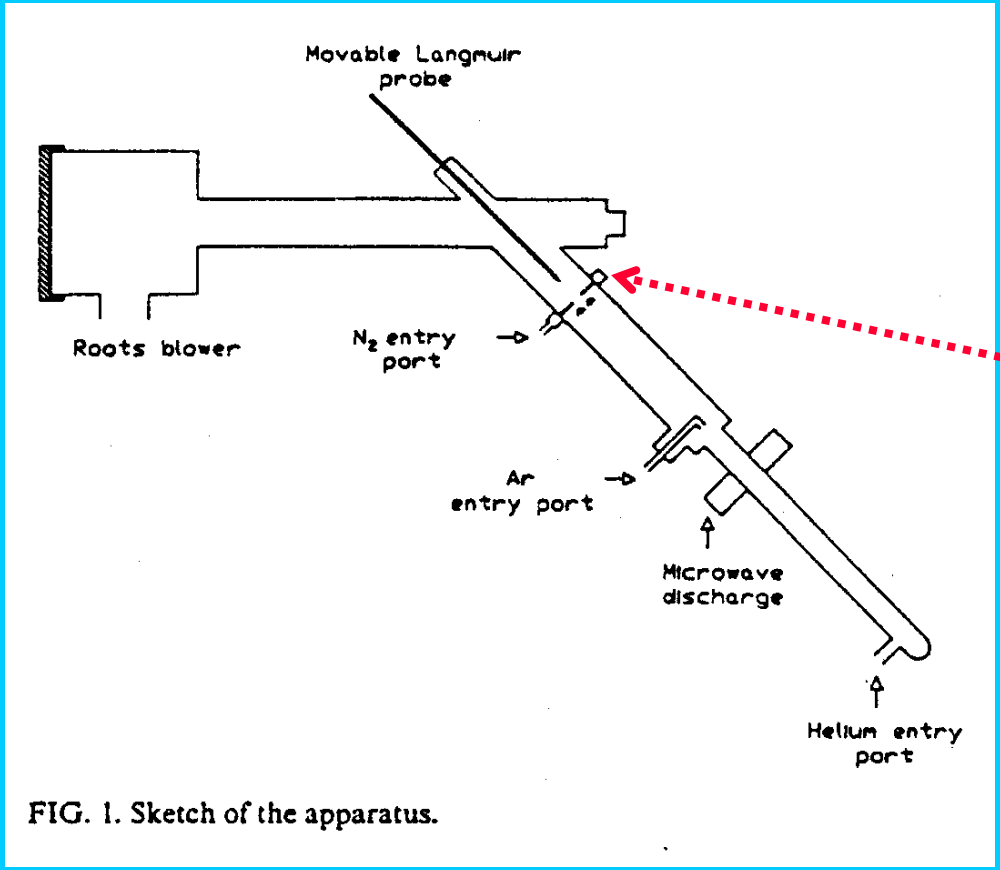

FIG. 1. Sketch of the apparatus.

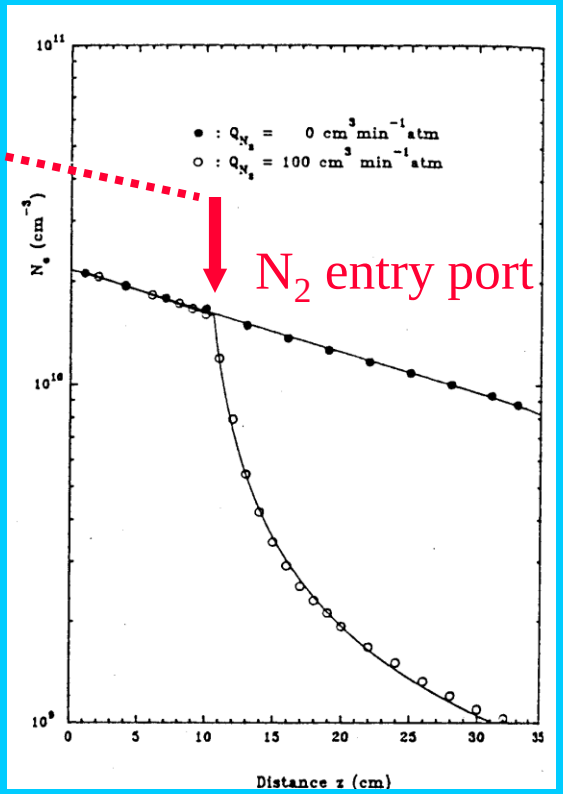

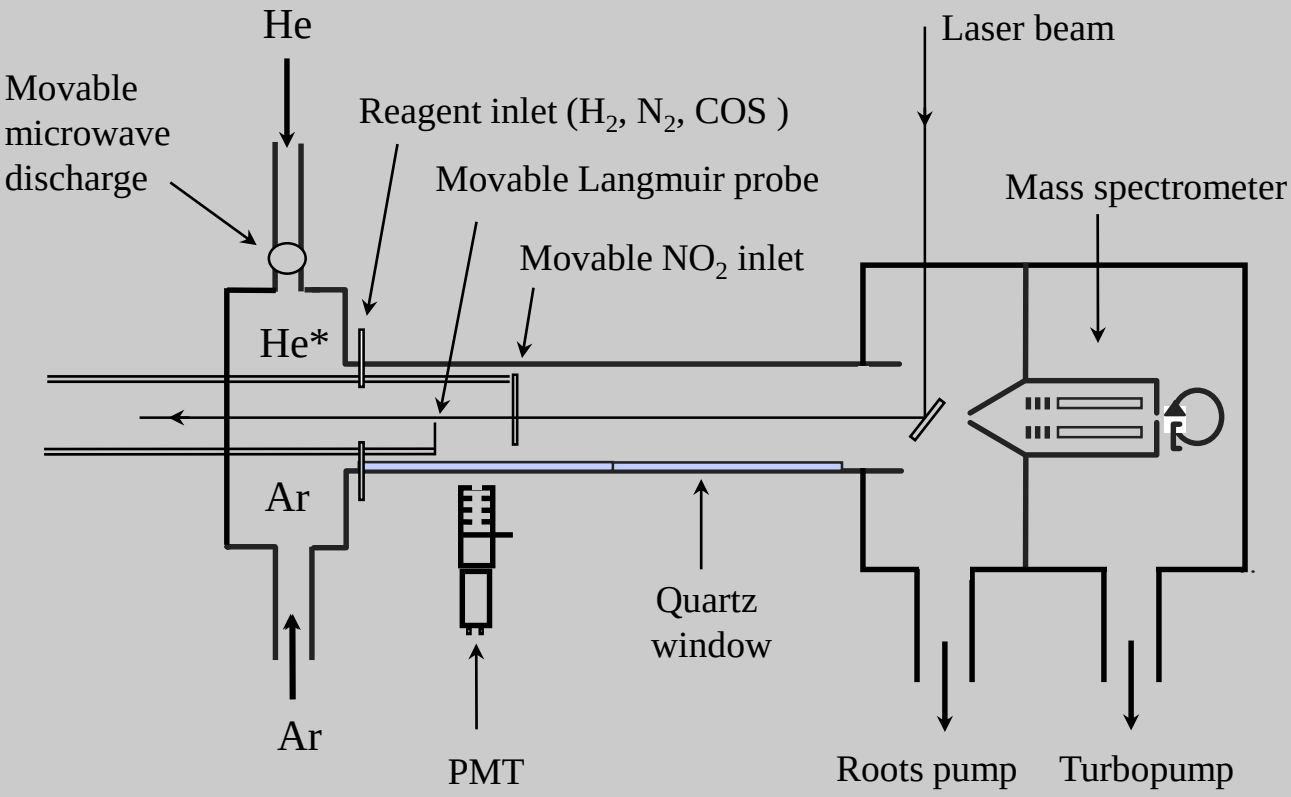
He
Movable
microwave
discharge
Reagent inlet (H_2, N_2, COS)
Movable Langmuir probe
Movable NO_2 inlet
Laser beam
Mass spectrometer
He*
Ar
Ar
PMT
Quartz
window
Roots pump
Turbopump

Pittsburg Rainer Johnsen FALP

Emission spectroscopy for identification products of recombination

collisional radiative recombination of argon ions

$Ar^+ + e^- + e^- \rightarrow Ar + e^-$

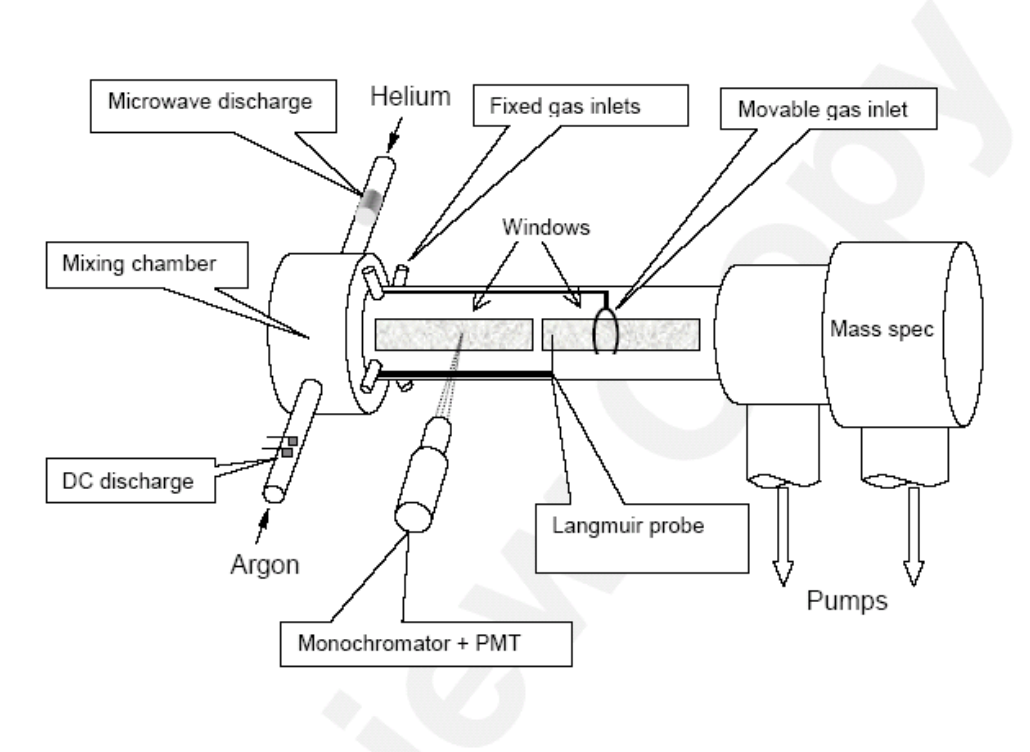

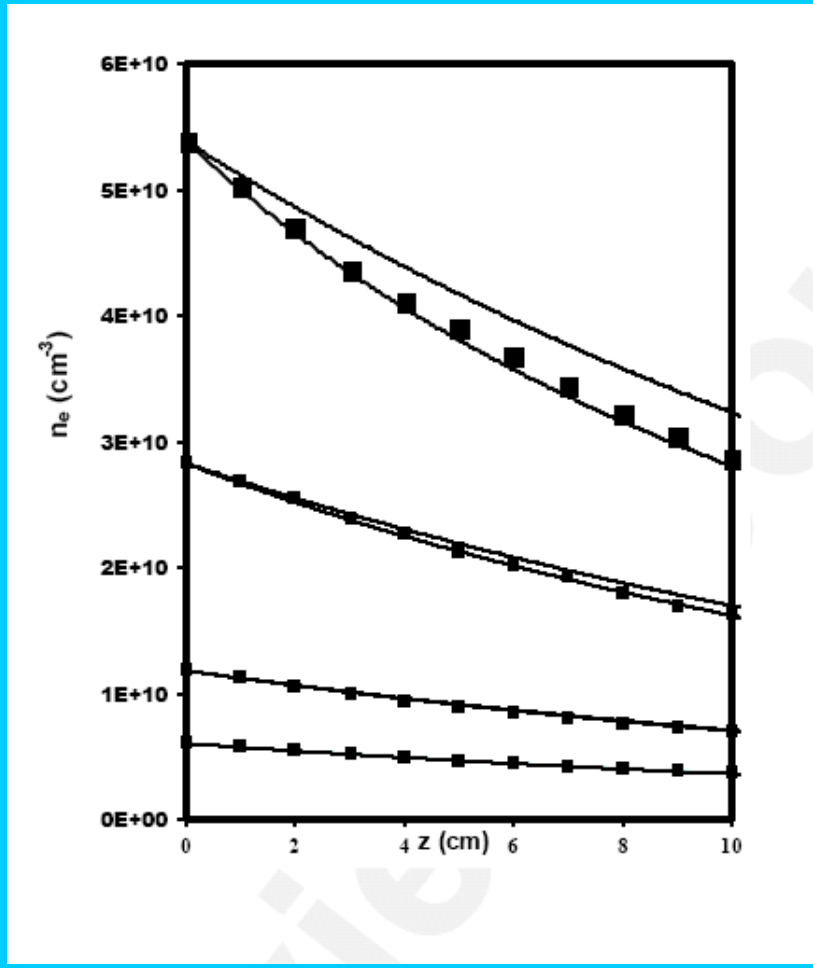

The Pittsburgh flow tube

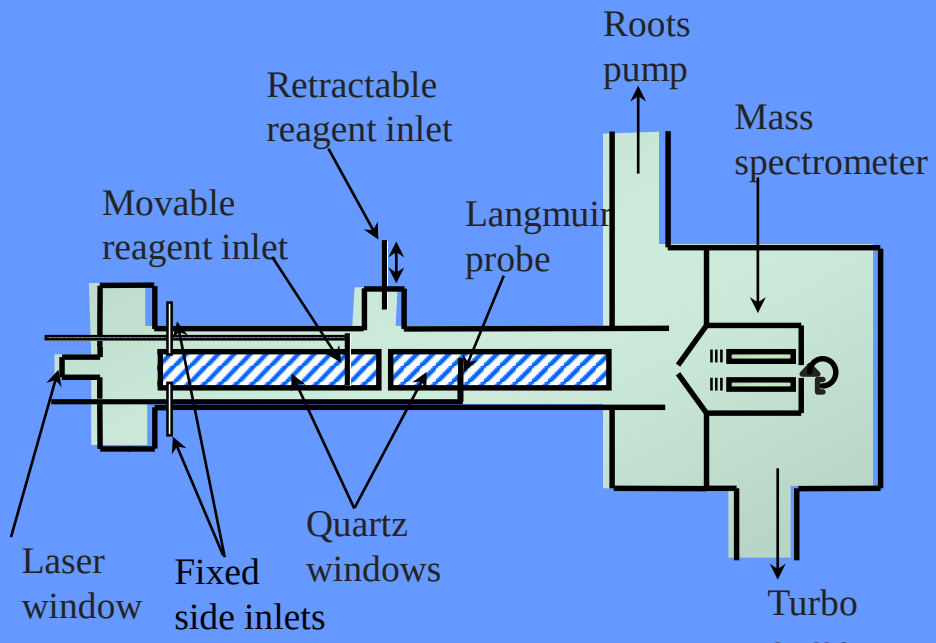

FLOW TUBE (side view)

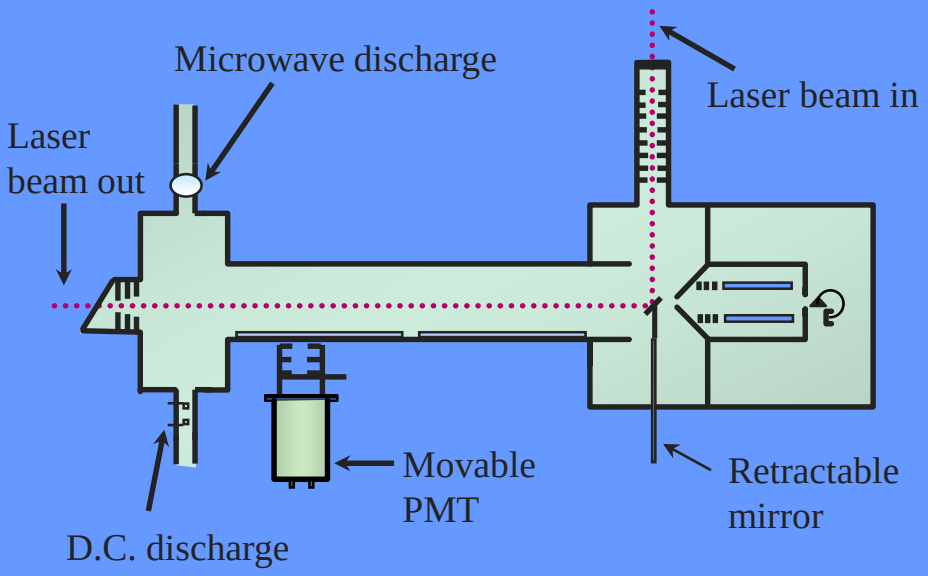

FLOW TUBE (top view)

$$Ar^+ + H_2 \rightarrow ArH^+ + H \quad (+ 1.53eV)$$

$$ArH^+ + H_2 \rightarrow Ar + H_3^+ \quad (+ 0.57\ eV)$$

N.G.ADAMS University of Georgia, Viktoria Poterya

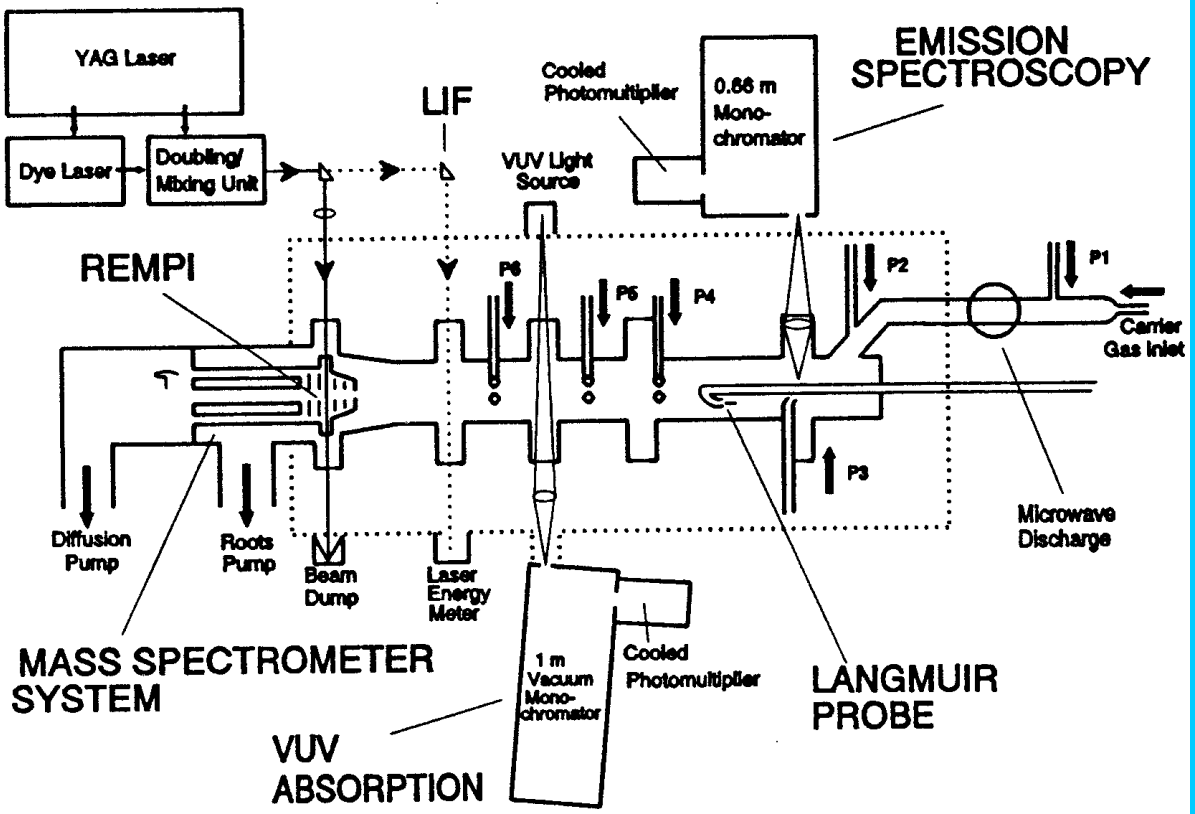

Figure 1. A schematic of the University of Georgia flowing afterglow. Illustrated are the axially movable Langmuir probe, the downstream mass spectrometer, a 0.66 m monochromator with red sensitive photomultiplier for emission studies, a vuv light source and 1 m vacuum monochromator with uv enhanced photomultiplier for detection of atoms and a YAG pumped dye laser with doubling and mixing capabilities for detection of radical species by LIF and REMPI. All photomultipliers are cooled to reduce the background noise and photon counting is used throughout. Further details of this apparatus are described in a separate review.[27]

FA– Flowing Afterglow 2005

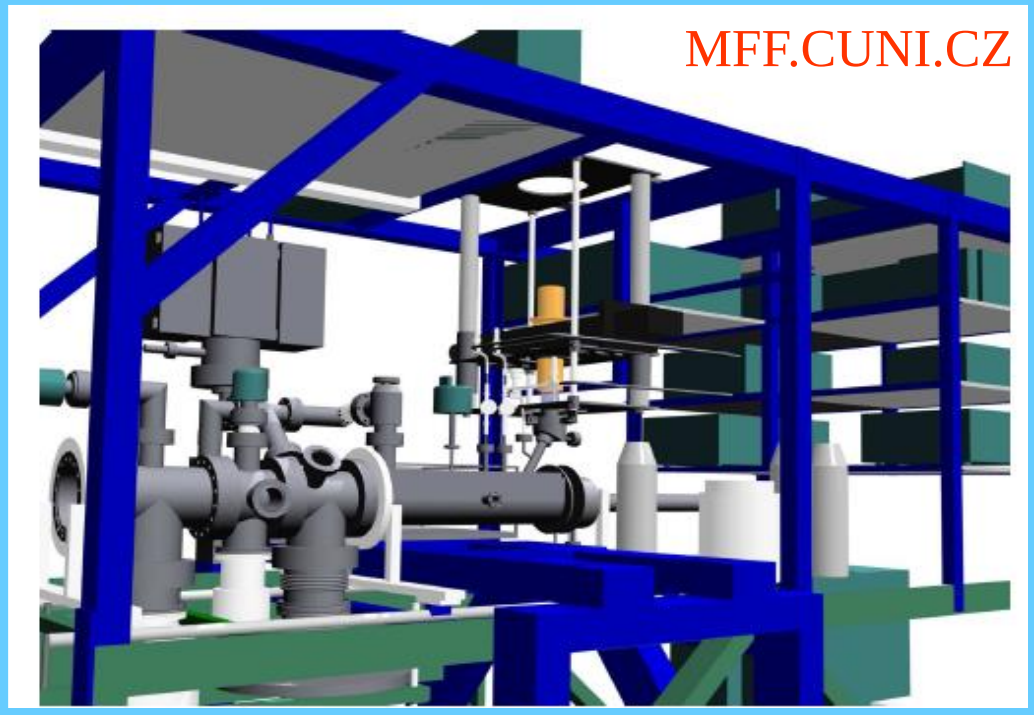

FA– Flowing Afterglow 2005

MFF.CUNI.CZ

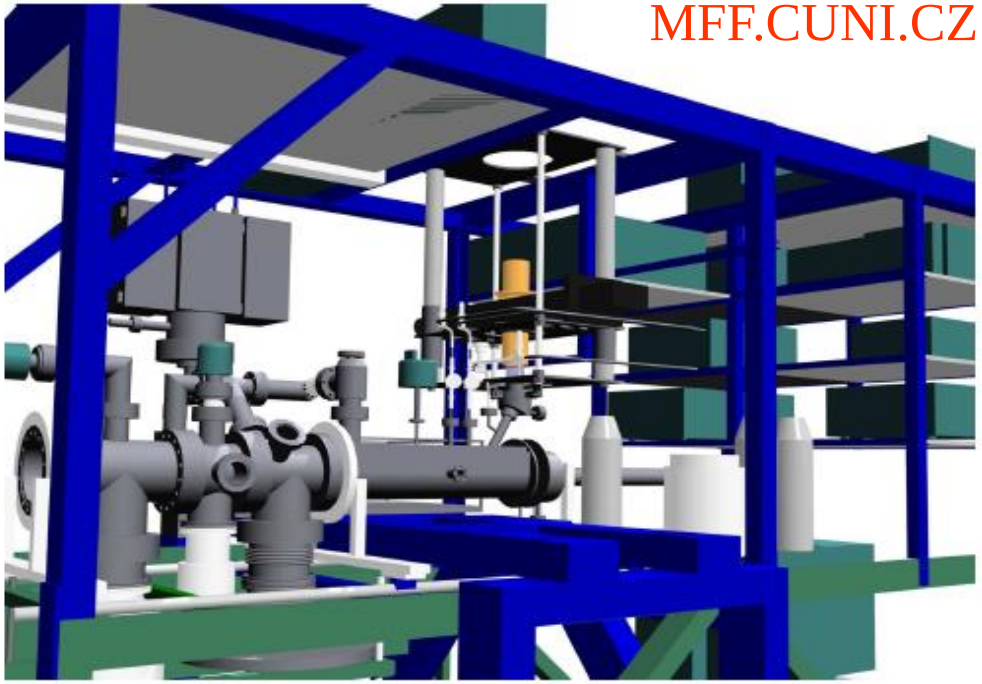

FA– Flowing Afterglow 1965 -2006

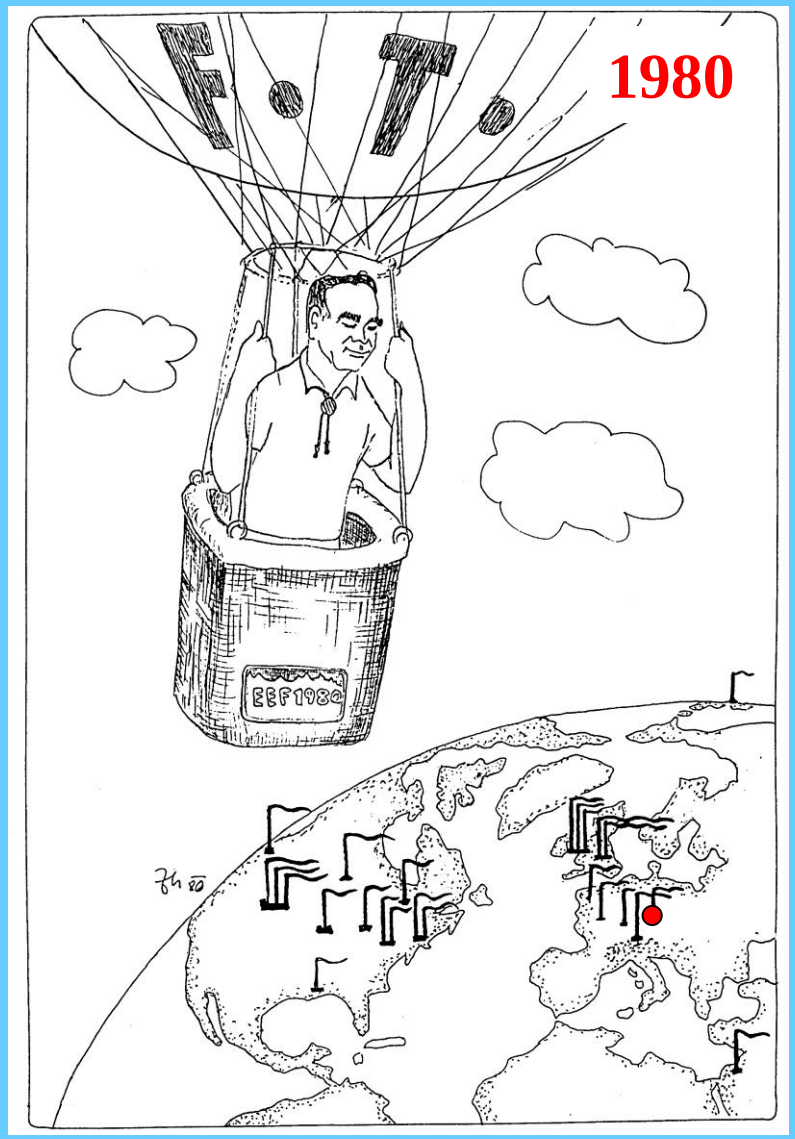

CU – Chemistry 1980:
Eldon Ferguson watching the flow-tube centers

MFF.CUNI.CZ

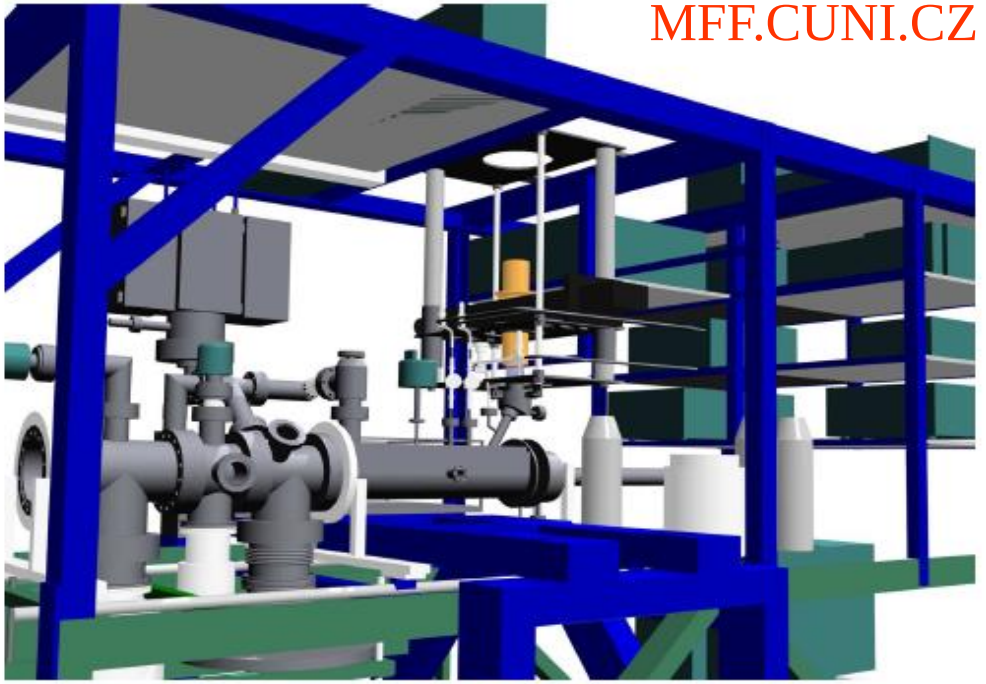

FALP – MFF.CUNI.CZ

Plasma, IMR, Recombination Diagnostics

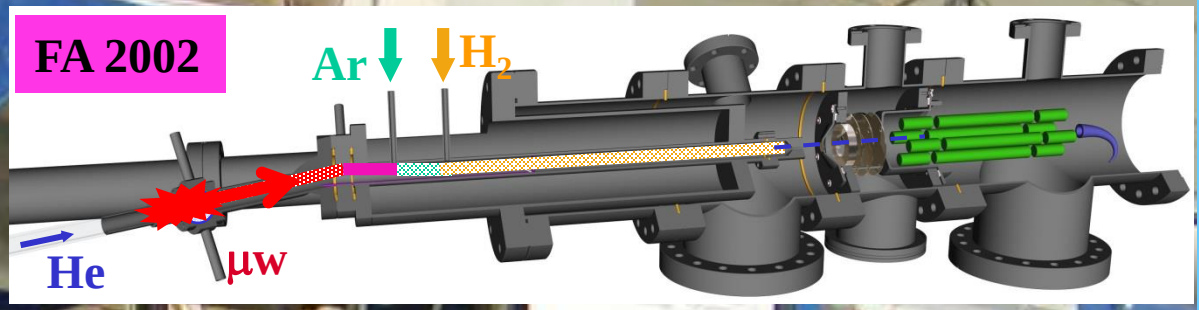

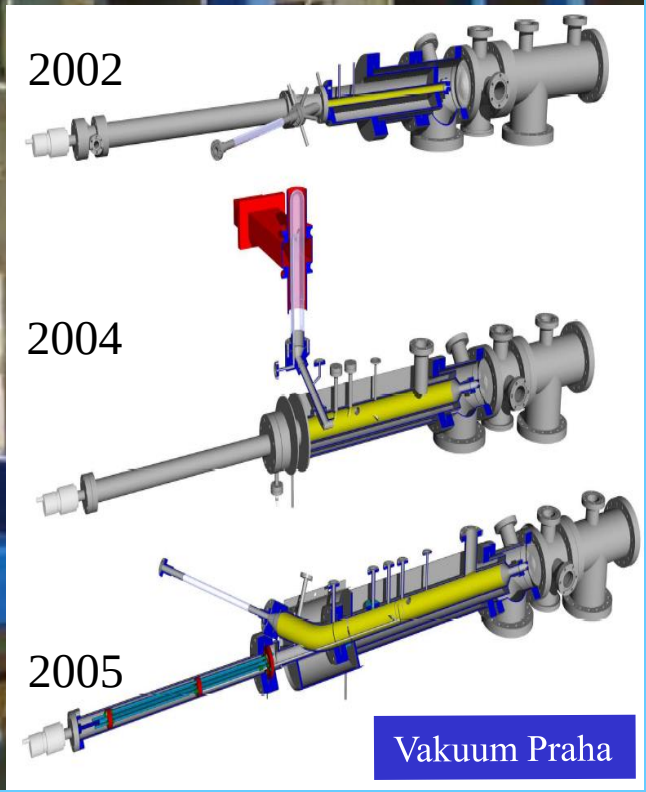

Vakuum Praha

O.Novotný

14th August 2002

Our LAB

FACULTY OF MATHEMATICS AND PHYSICS

TROJA, Praha 8

2002 - 2004

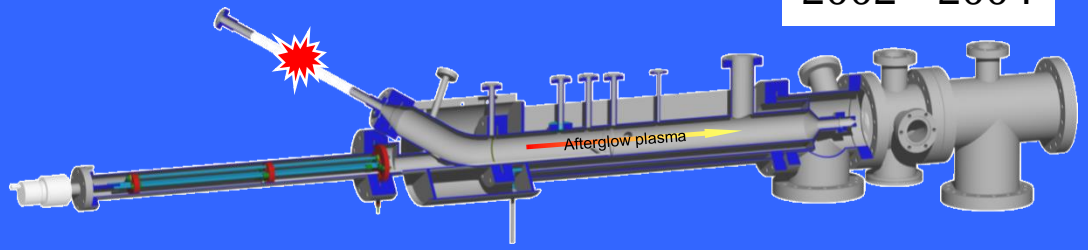

Principle of Flowing Afterglow Langmuir Probe - FALP

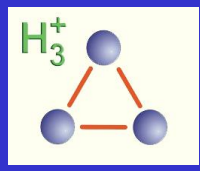

microwave discharge

Formation of H_3^+ in He/Ar/H_2 mixture (10 Torr)

He^+
He^m
e^-
He_2^+

Ar → Ar^+ → H_2 → ArH^+, H_2^+ → H_2 → H_3^+ +

H_2 → H_5^+ +

μw

Ar

H_2

He → **He** → **RECOMBINATION**

T_e ~2eV

$T_e = T_i = T_G$ = 170 - 260K

Apparatus -FALP

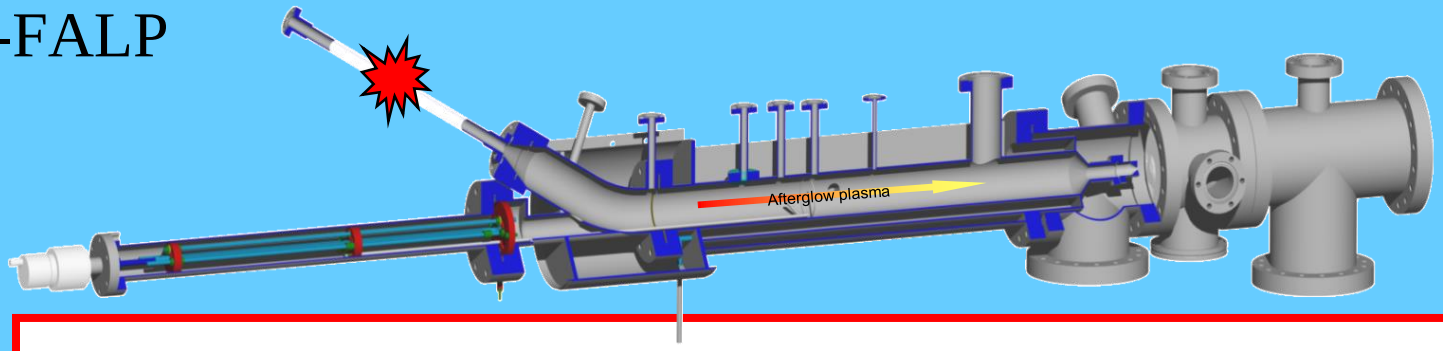

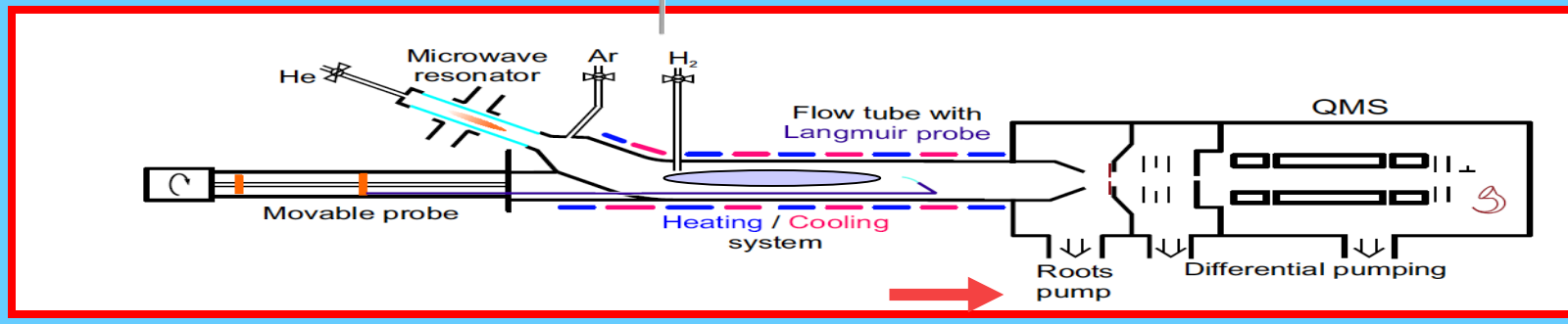

Kinetics

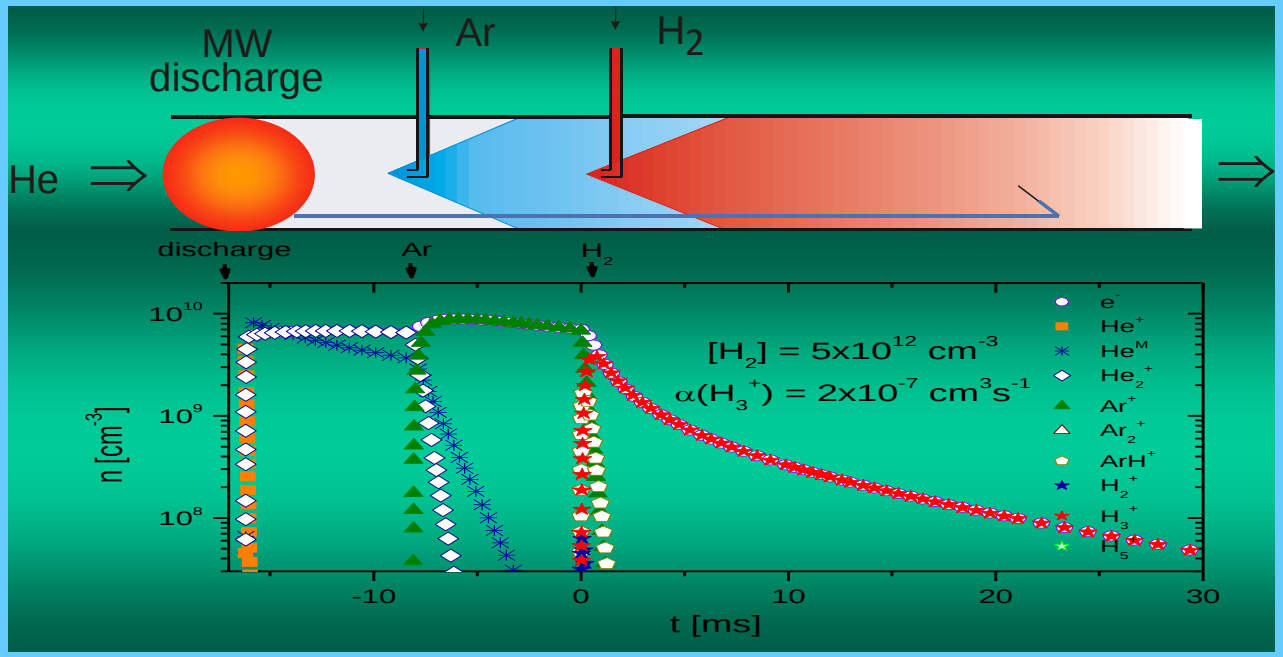

$\alpha \sim 5x10^{-9}$ cm^{3}s^{-1}

Plasma decay can be monitored up to 35 cm ➔ 65 ms, Temperature – 130 - 300 K Pressure up to 12 Torr

Evolution along the flow tube

$$[A^+]_L = [A^+]_{L=0} \cdot e^{-DL/\lambda^2 v}$$

$$[A^+]_L = [A^+]_{L=0} \cdot e^{-const_1 . D_0 p_0 L/Q} = [A^+]_{L=0} \cdot e^{-const_2 . L/Q}$$

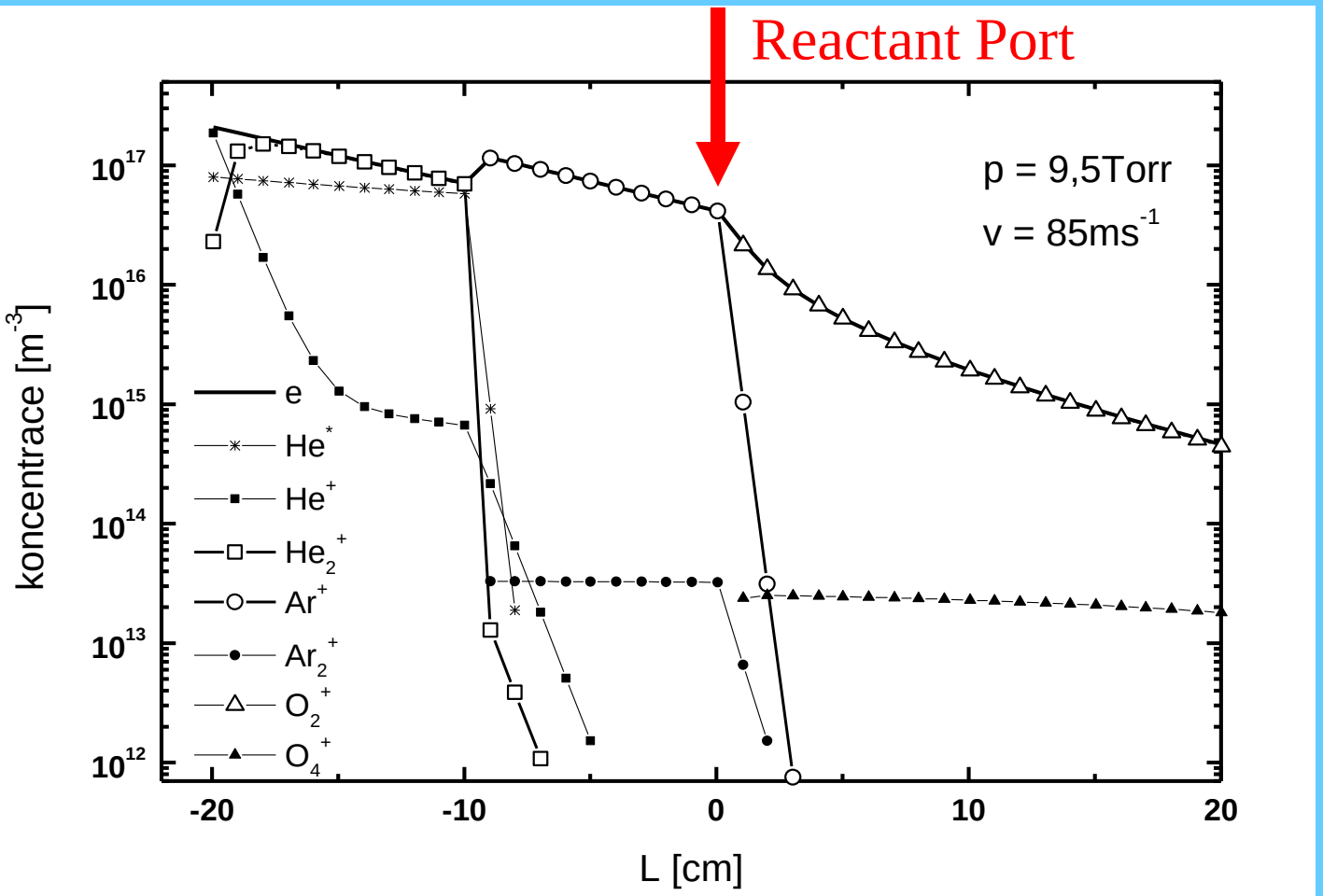

Ion-molecule reactions

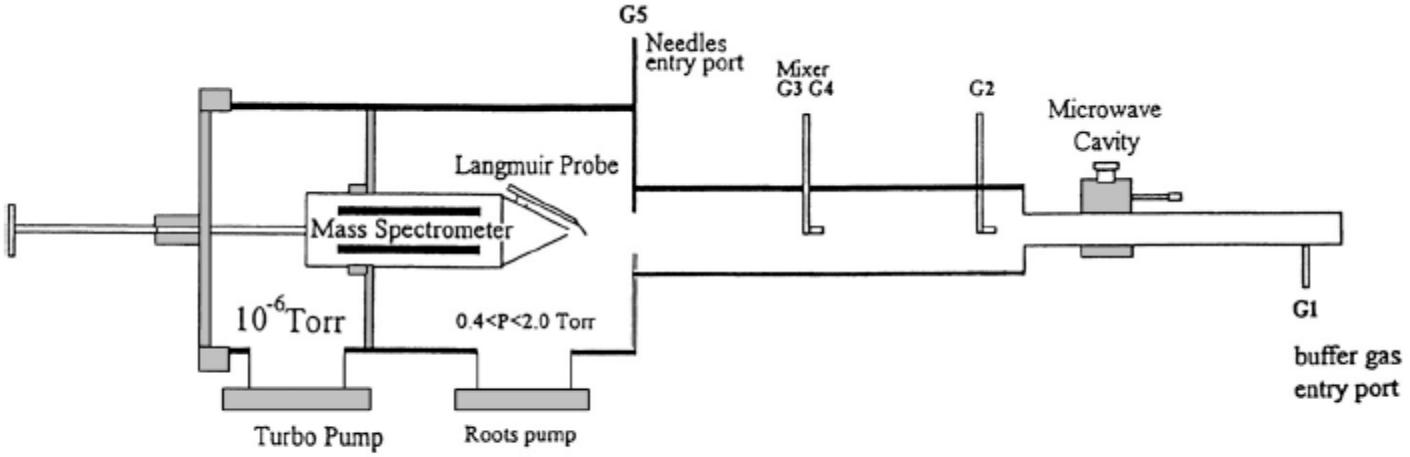

Fig. 12. Schematic view of the Rennes FALP-MS [164]

2. EXPERIMENTAL TECHNIQUE

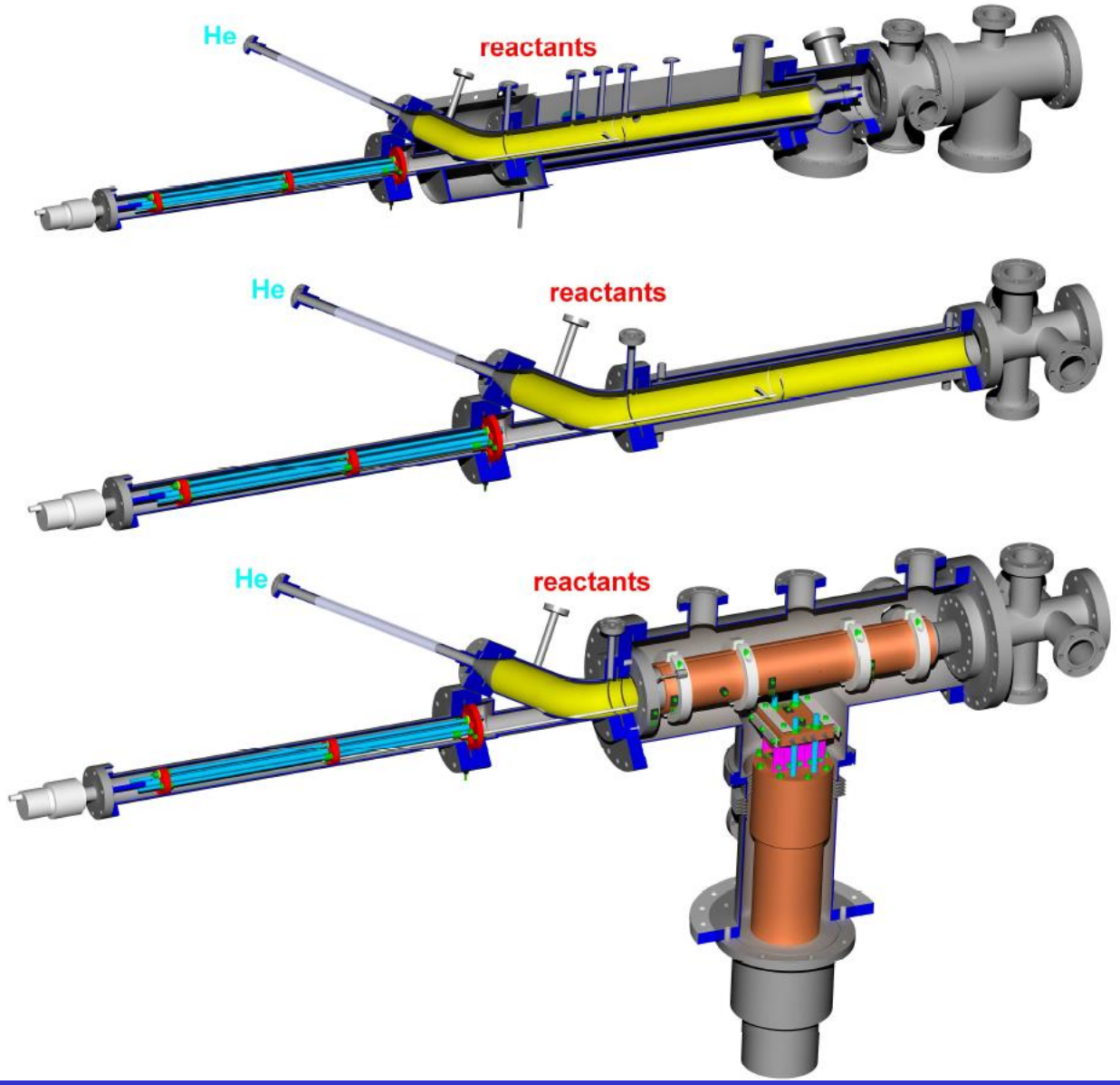

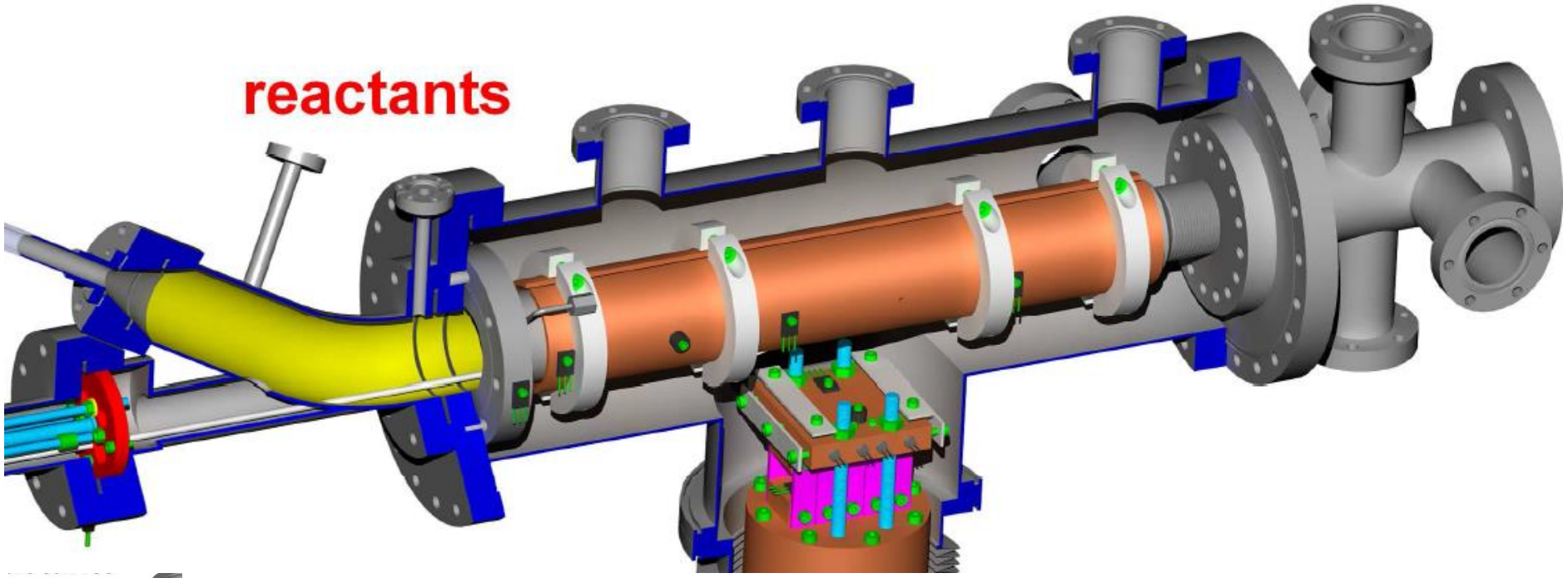
reactants

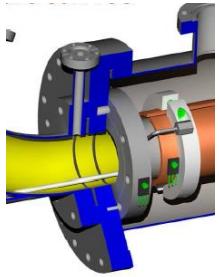

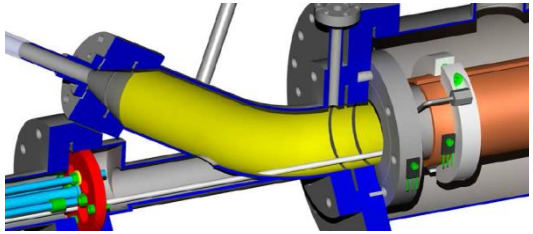

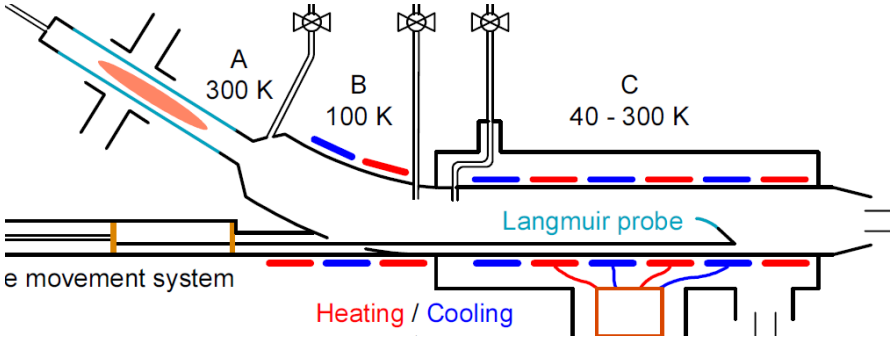
A
300 K
B
100 K
C
40 - 300 K
Langmuir probe
e movement system
Heating / Cooling

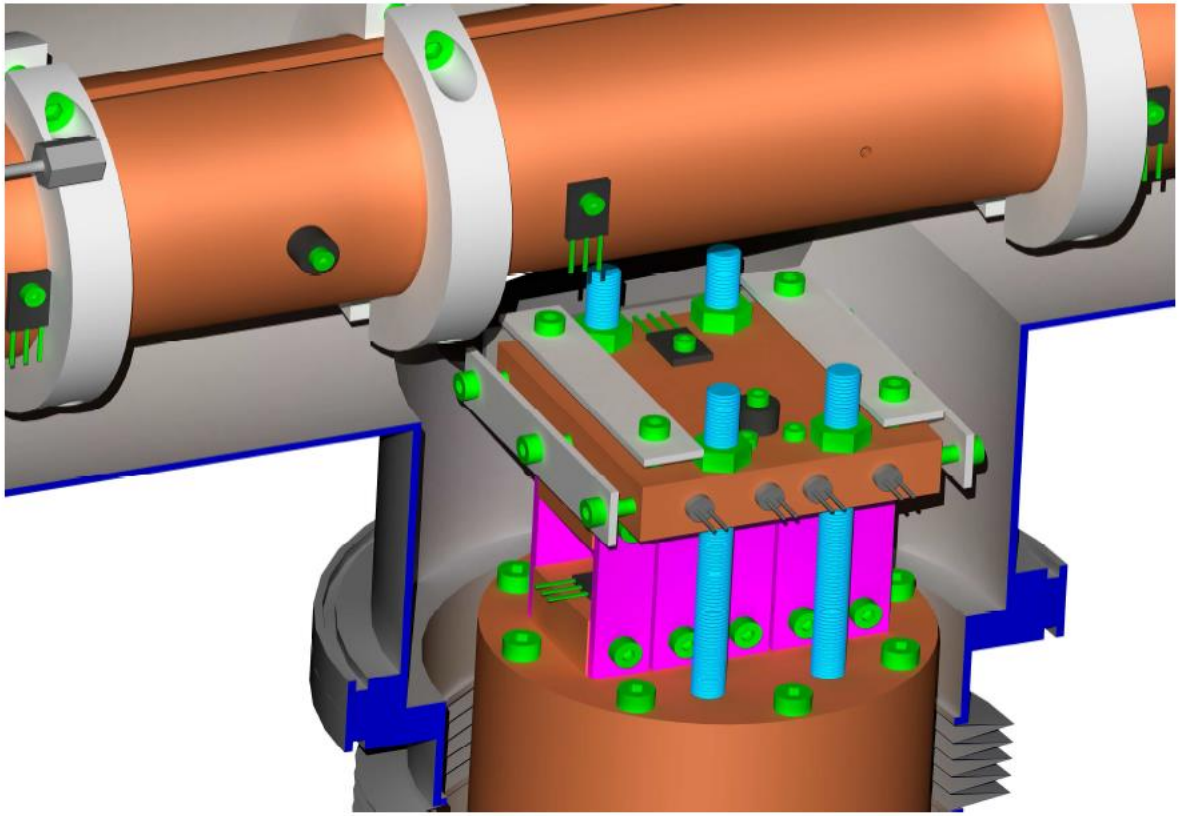

Figure 2.6 The detail of a 3D model of the Cryo-FALP II cooling system. The main copper parts are coldhead, platform and two half-cylinders pressing the copper braids (not shown in the figure) wound on the flow tube against the flow tube wall. The interconnecting removable copper blocks are colored magenta, the temperature sensors are black and the heating elements are dark grey cylinders embedded in the platform block. Other construction elements are colored green and cyan.

Techniques for study of IMR – reality

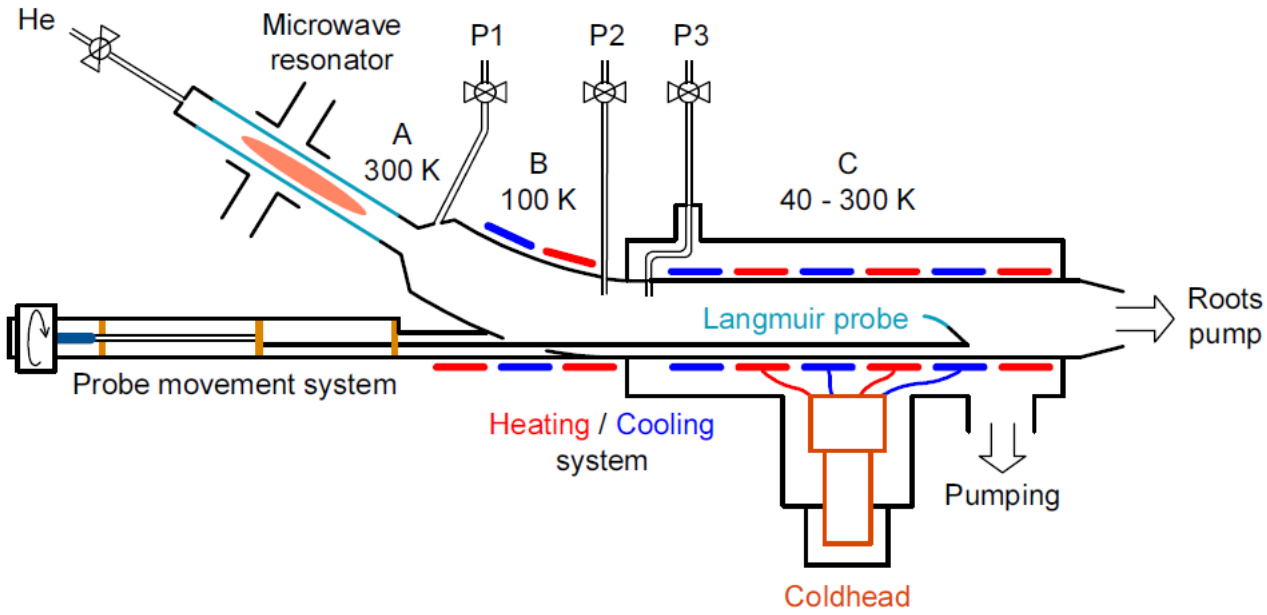

Figure 2.3 The scheme of the novel Cryo-FALP II apparatus.

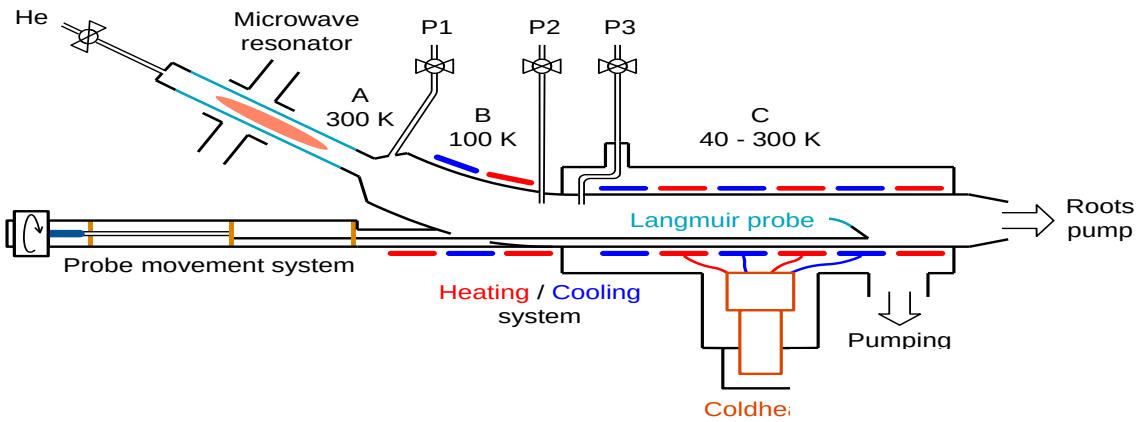
He
Microwave resonator
P1
P2
P3
A
300 K
B
100 K
C
40 - 300 K
Roots pump
Langmuir probe
Probe movement system
Heating / Cooling system
Pumping
Coldhe

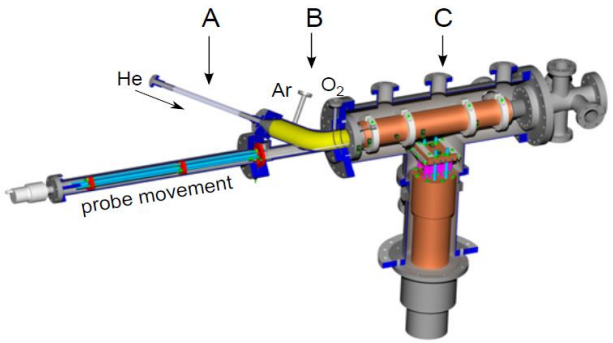
A
B
C
He
Ar
O_2
probe movement

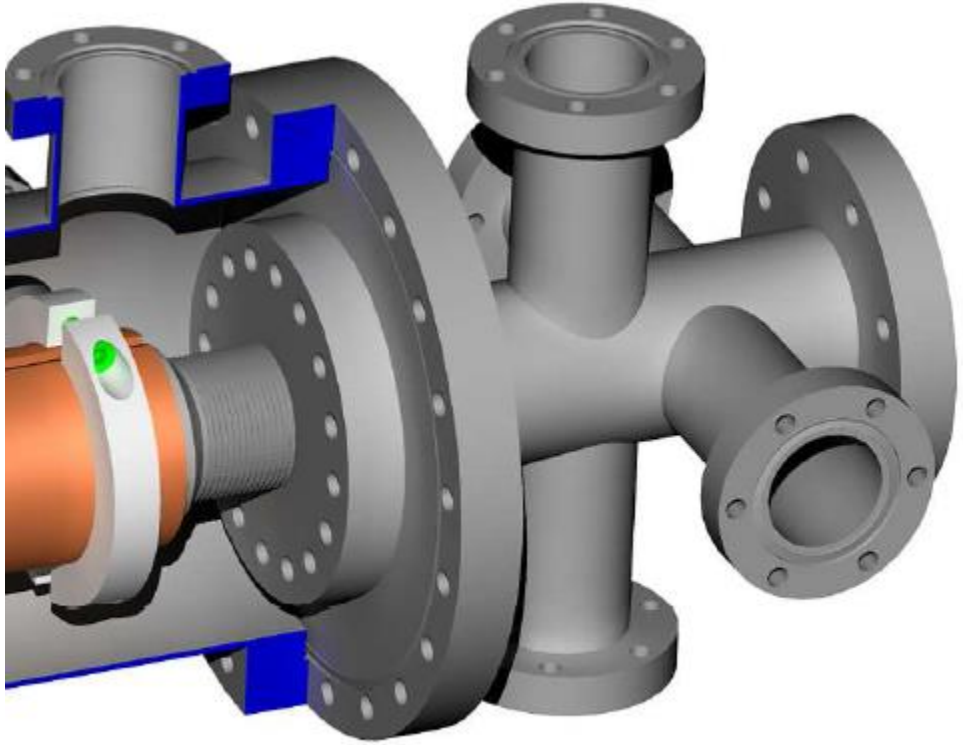

Fig. 1

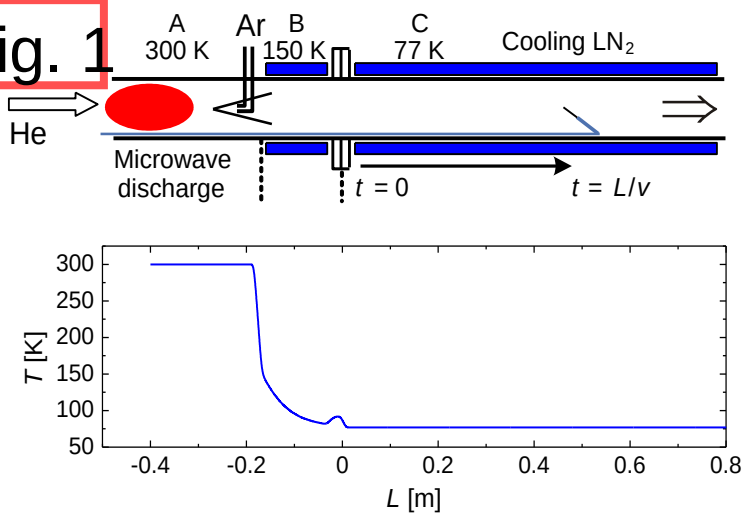
A
300 K
Ar
B
150 K
C
77 K
Cooling LN2
He
Microwave
discharge
t = 0
t = L/v
T [K]
300
250
200
150
100
50
-0.4
-0.2
0
0.2
0.4
0.6
0.8
L [m]

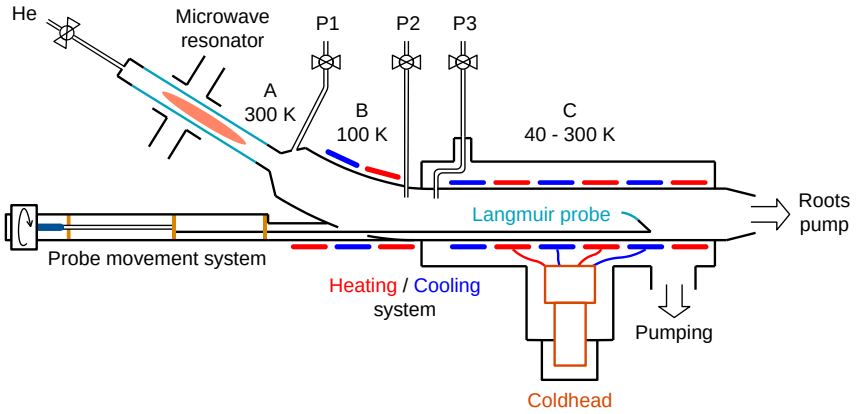
He
Microwave
resonator
P1
P2
P3
A
300 K
B
100 K
C
40 - 300 K
Roots
pump
Langmuir probe
Probe movement system
Heating / Cooling
system
Pumping
Coldhead

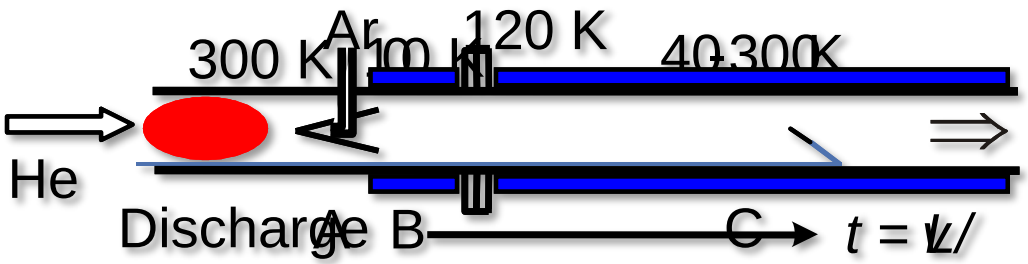
300 K
Ar
120 K
40-300K
He
Discharge
A
B
C
t = L/v

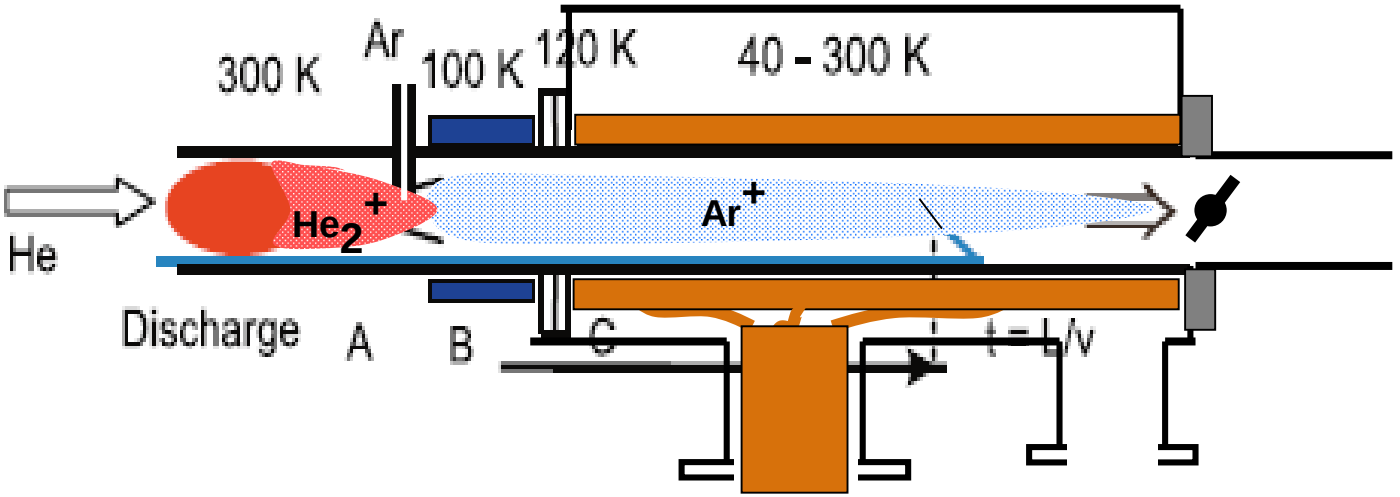
300 K
Ar
100 K
120 K
40 - 300 K
He
He2+
Ar+
Discharge
A
B
C
t = L/v

Recombination in He/Ar Afterglow Plasma at Low Temperatures

P. Dohnal, P. Rubovič, T. Kotrík, R. Plašil, and J. Glosík

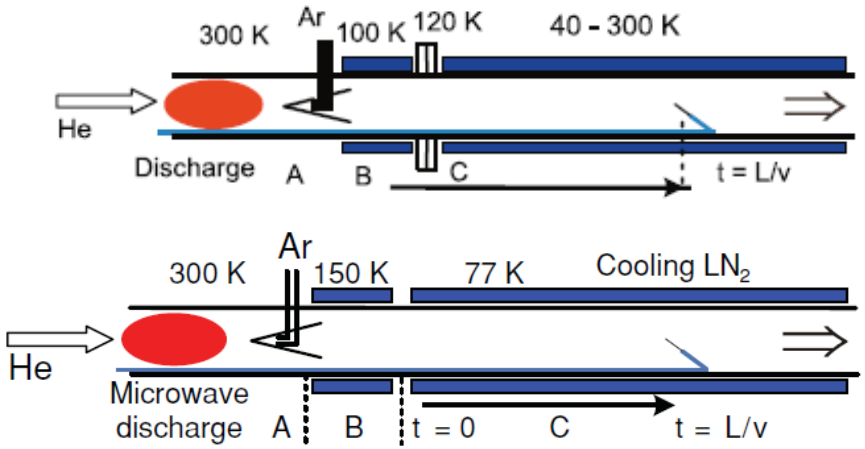

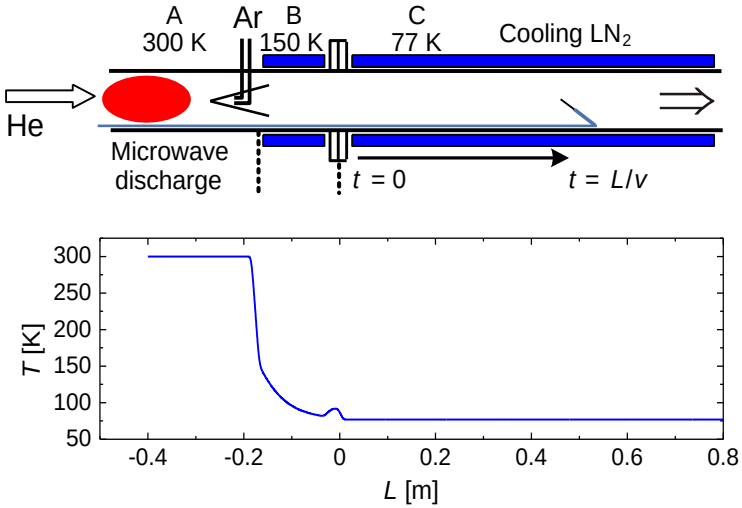

FIG. 1. (Color online) Simplified diagram of the Cryo-FALP apparatus (see text in Sec. II).

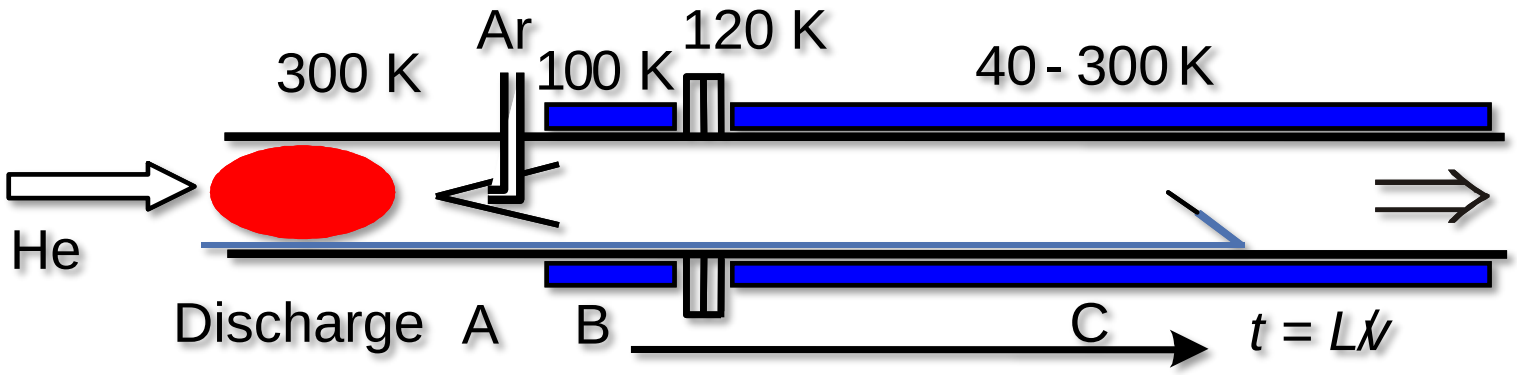

Techniques for study of IMR – reality

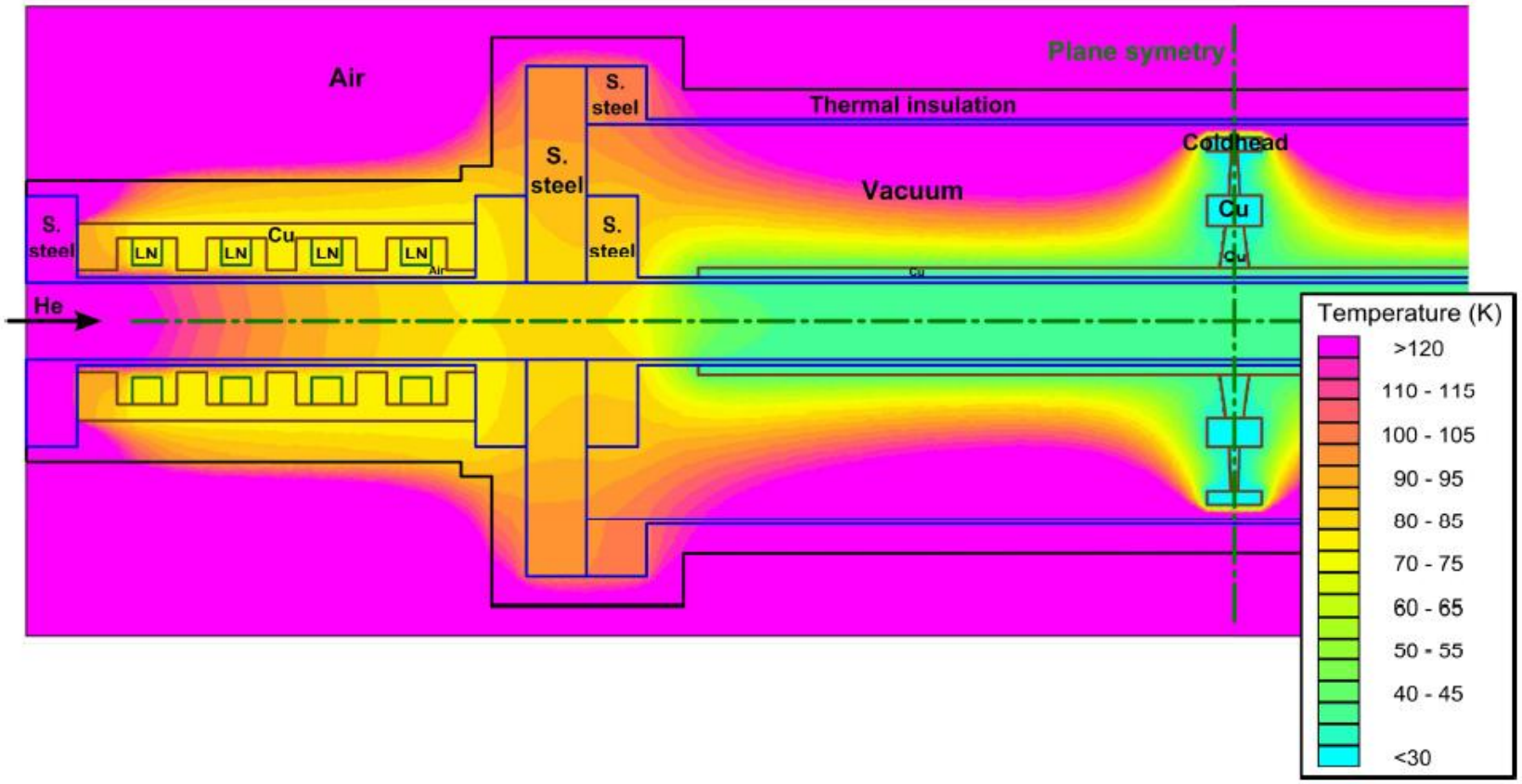

CRYO-FALP

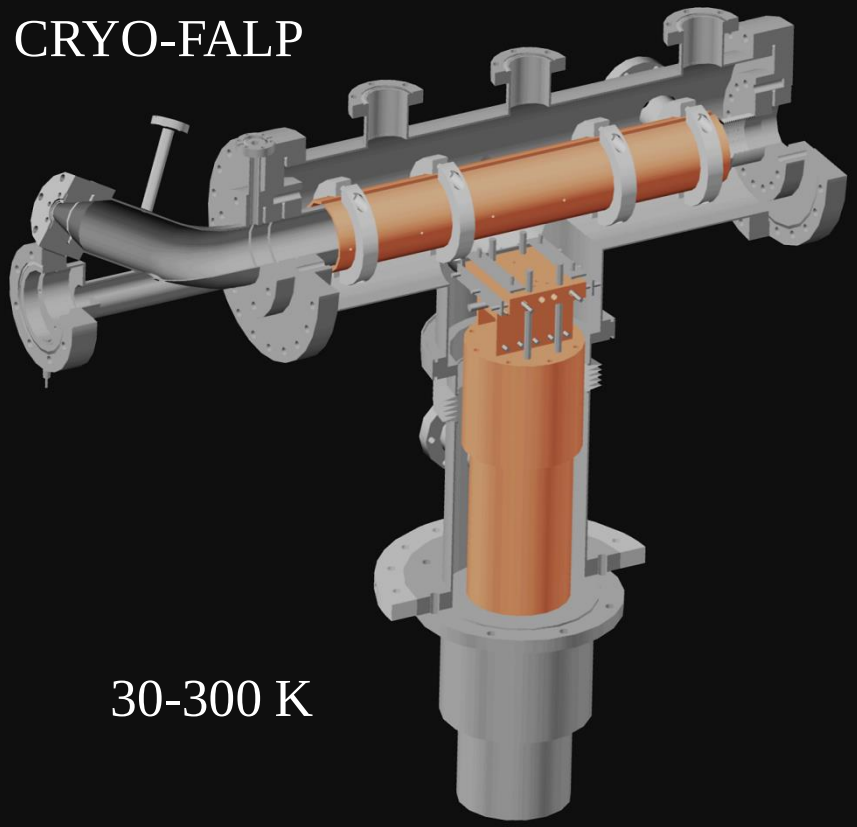

30-300 K

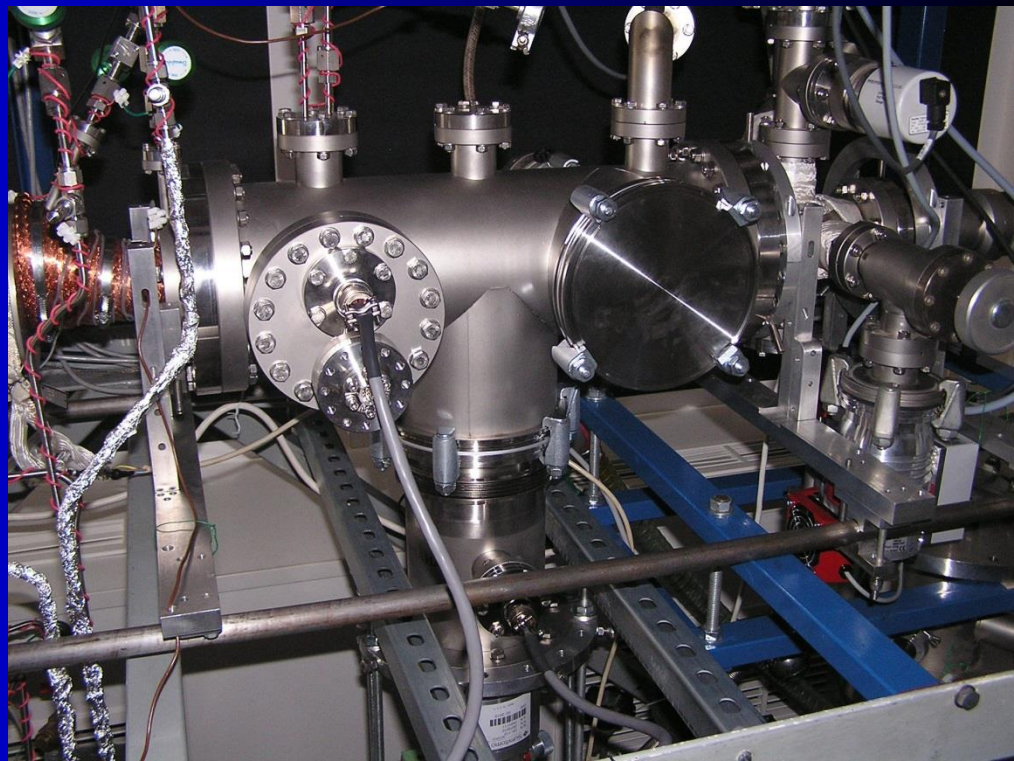

Low Temperature Collisions in Flow Systems and Traps

(state-of-the-art experiments)

50-100 l/min carrier gas (He, Ar) + reagent + precursor

chamber pressure 0.1 – 0.25 mbar
max pumping speed ~ 30000 $m^3\ h^{-1}$

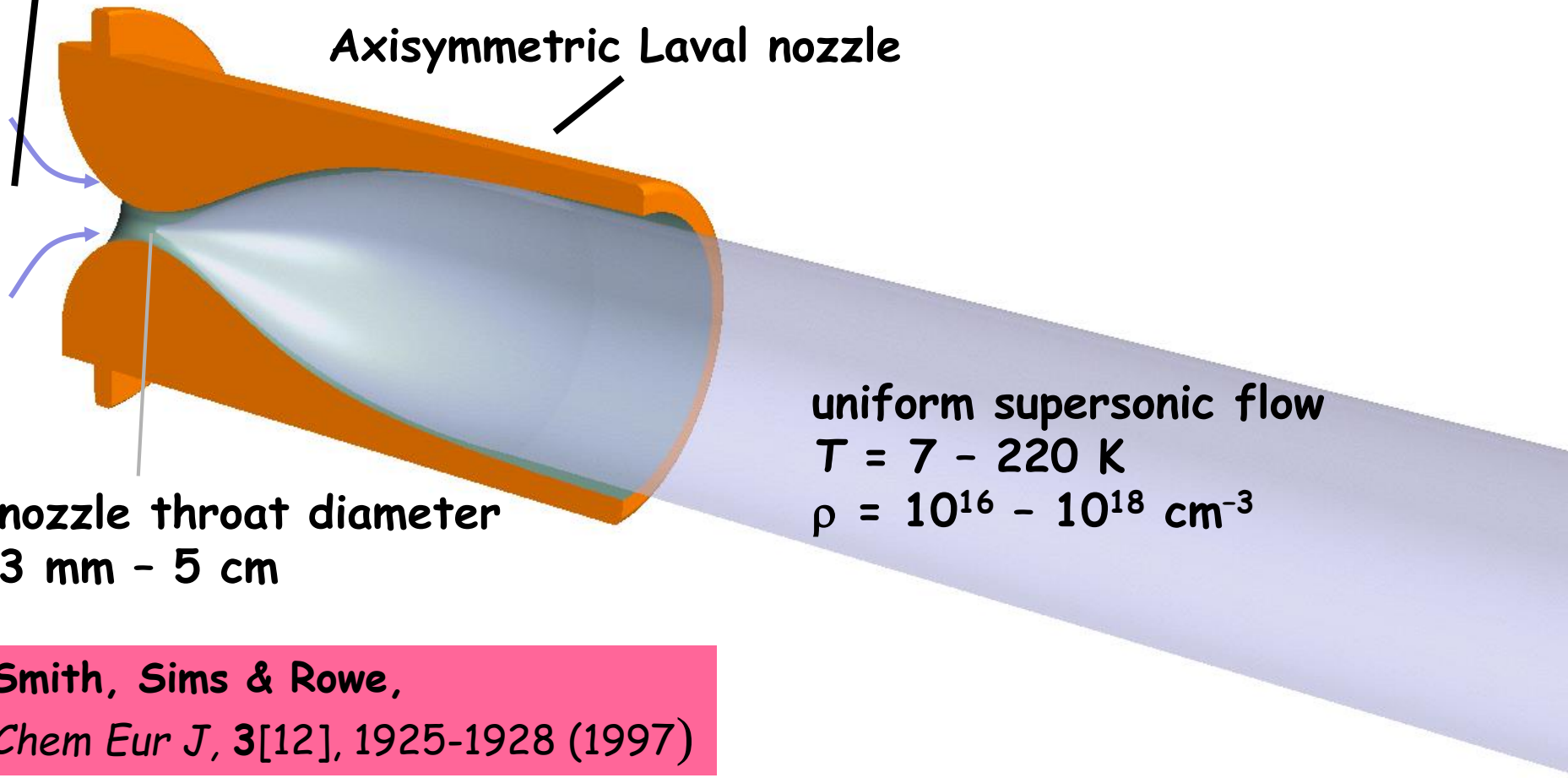

Smith, Sims & Rowe,
Chem Eur J, **3**[12], 1925-1928 (1997)

Laval nozzle and isentropic flow

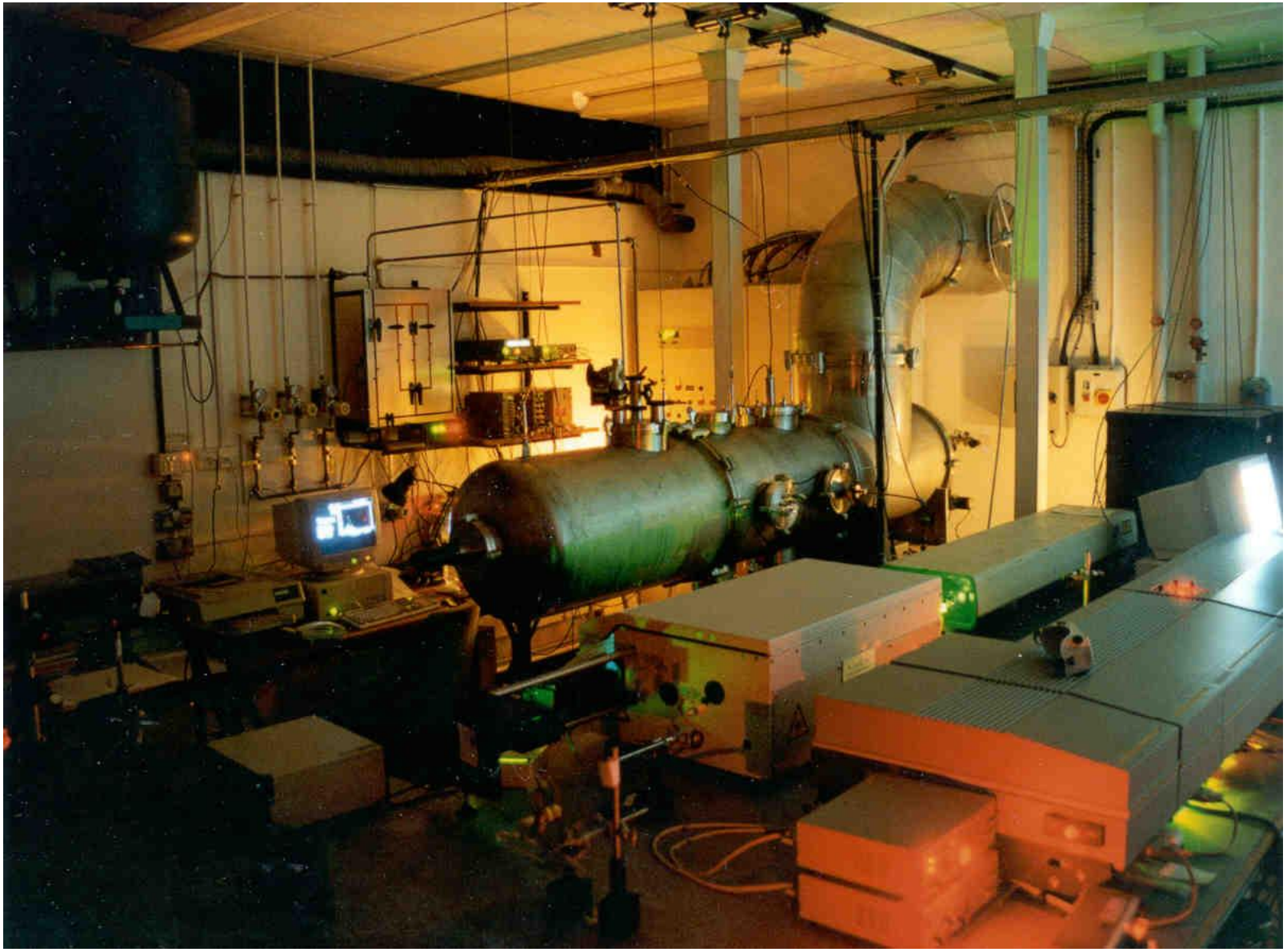

Schematic of the CRESU apparatus devoted to the measurement of ion/molecule reactions at low temperatures

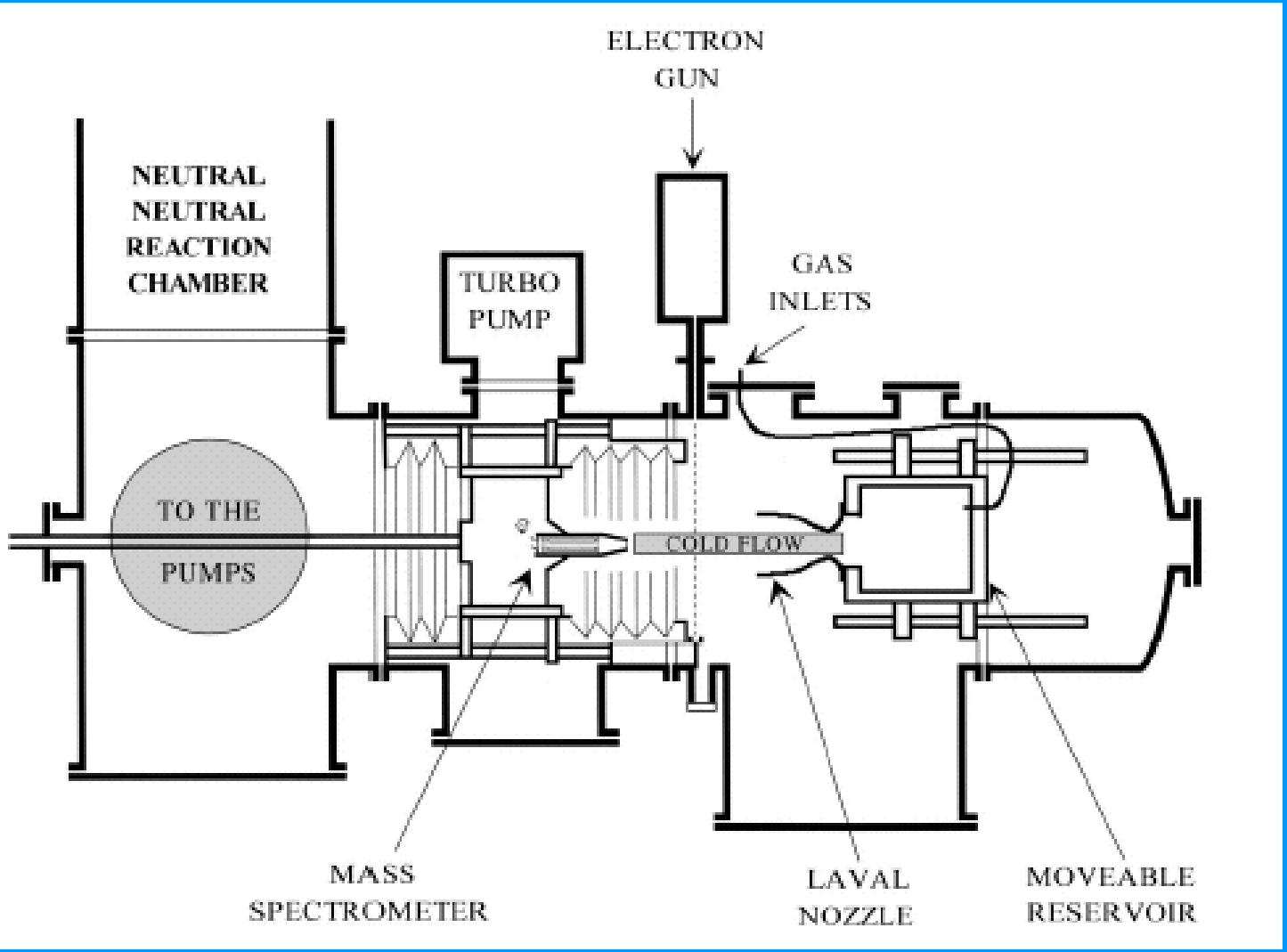

CRESU apparatus
Variation of the rate coefficient with temperature
N+ NH_3

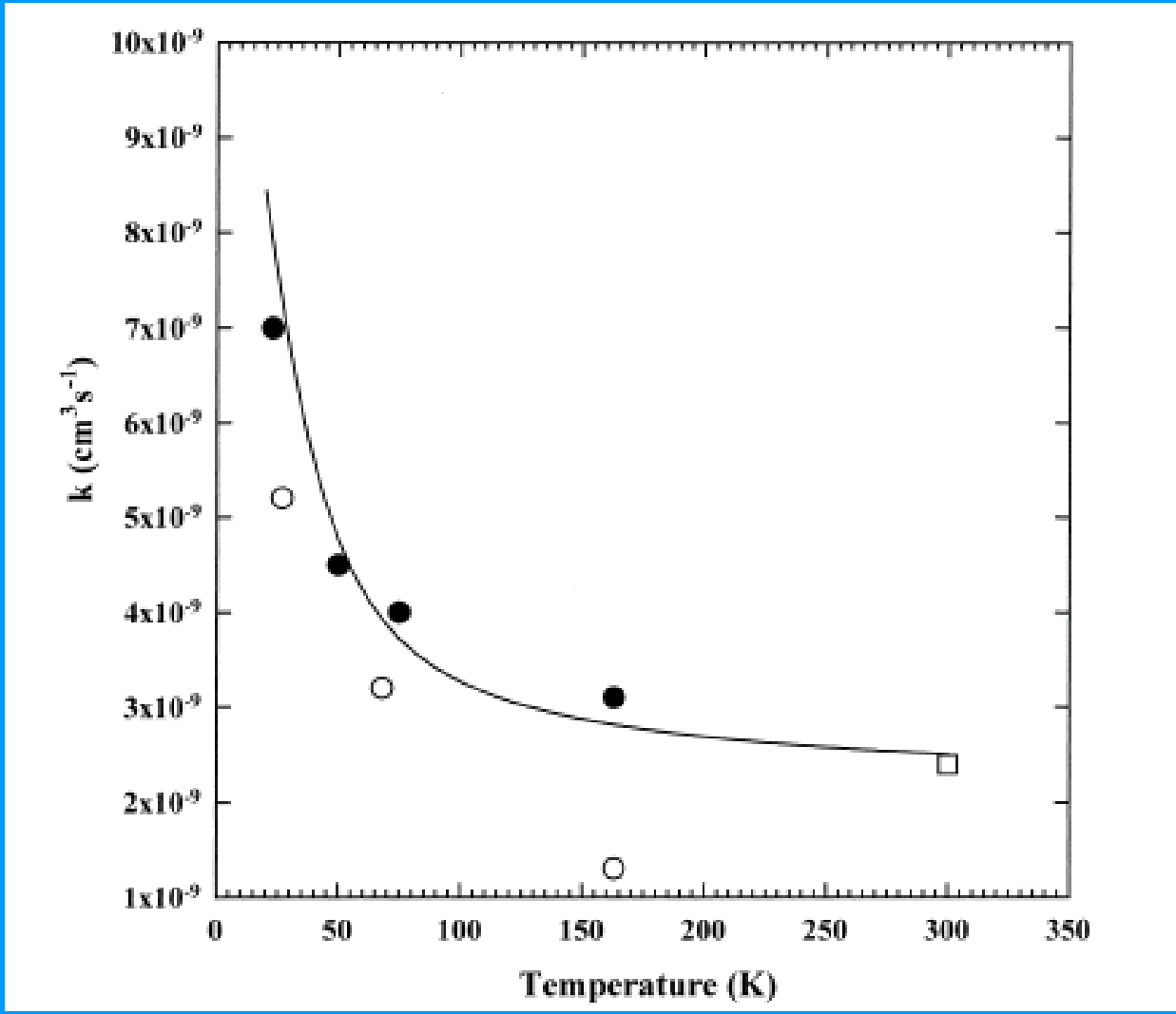

Pulsed Uniform Supersonic Expansion

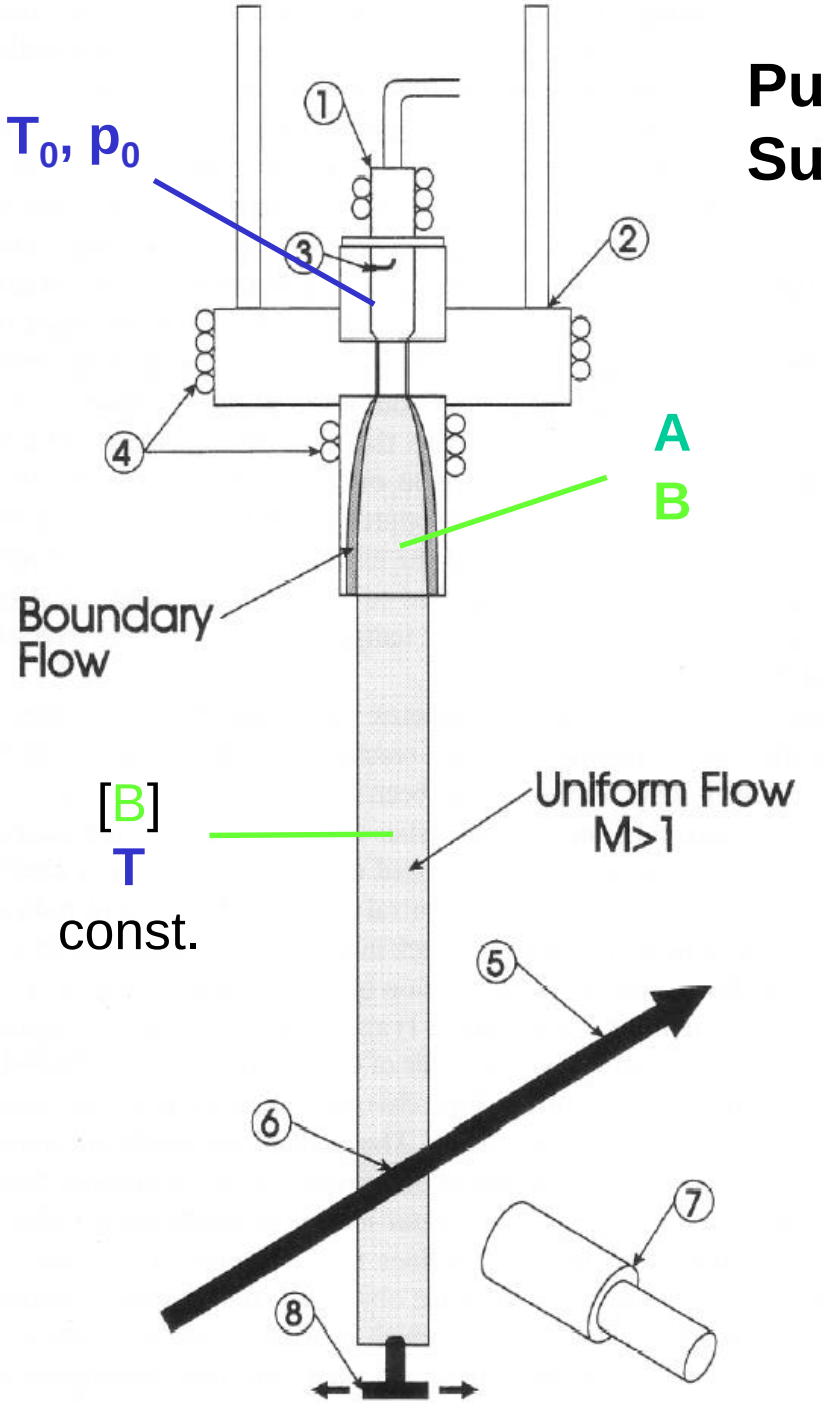

k(T)

$A + B \rightarrow Products$

$k = (\tau [B])^{-1}$

Free jet flow reactor

Mark Smith

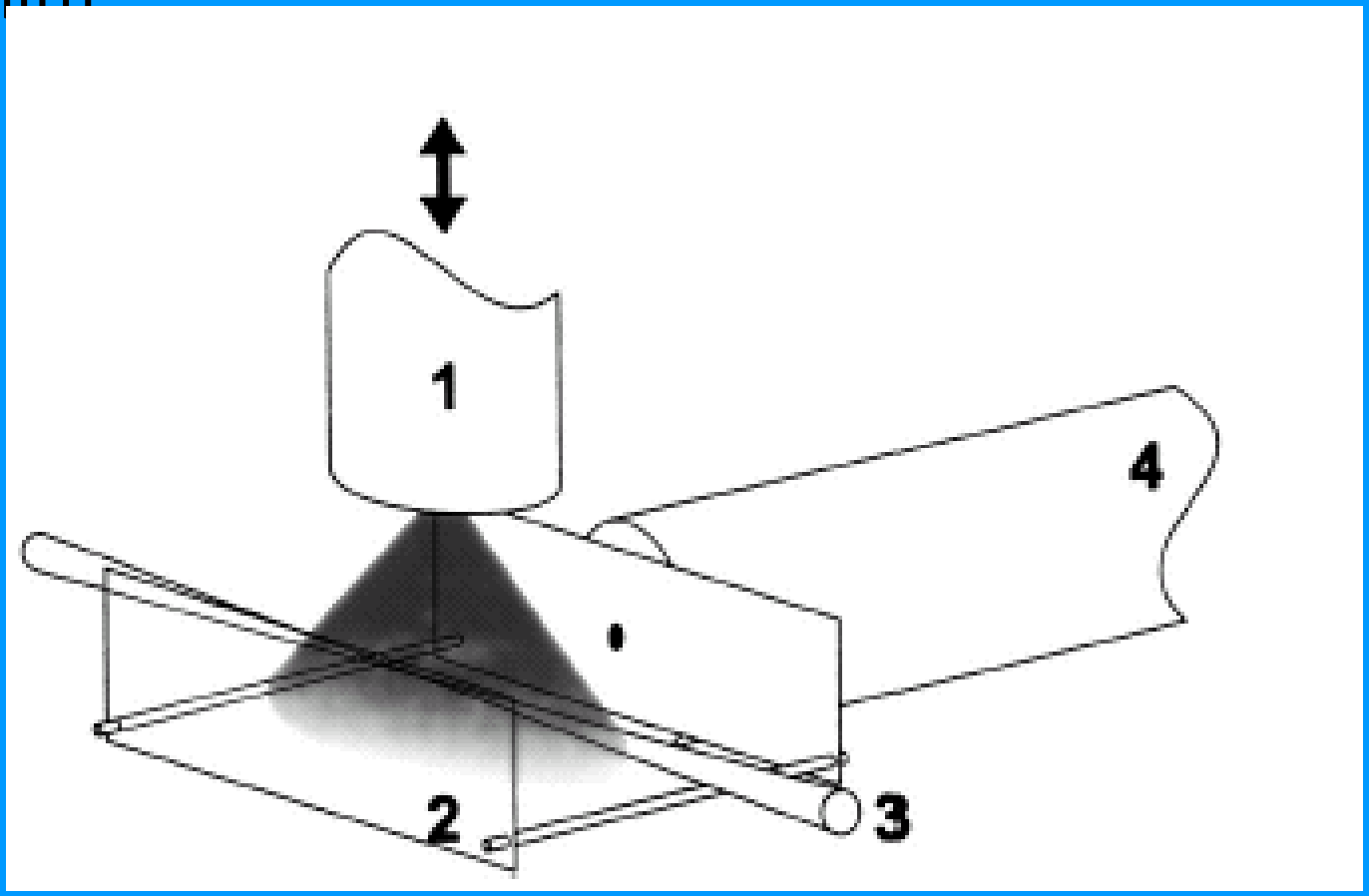

The jet originates from a pulsed beam valve **1**, and ions are produced by REMPI using a focused pulsed laser. The reaction zone is bounded by a repeller plate **2** and an endplate **3**:
ions are propelled, by a pulsed voltage on the repeller, towards a sampling aperture in the endplate which leads to a TOF-MS **4**

Energies experiments